



Argonne
NATIONAL
LABORATORY

... for a brighter future



U.S. Department
of Energy



THE UNIVERSITY OF
CHICAGO

A U.S. Department of Energy laboratory
managed by The University of Chicago

Materials science and SAS techniques

Jan Ilavsky & Pete R. Jemian
APS, ANL

Why small-angle scattering?

Premier method for size characterization of nano- to micro-scale density inhomogeneities

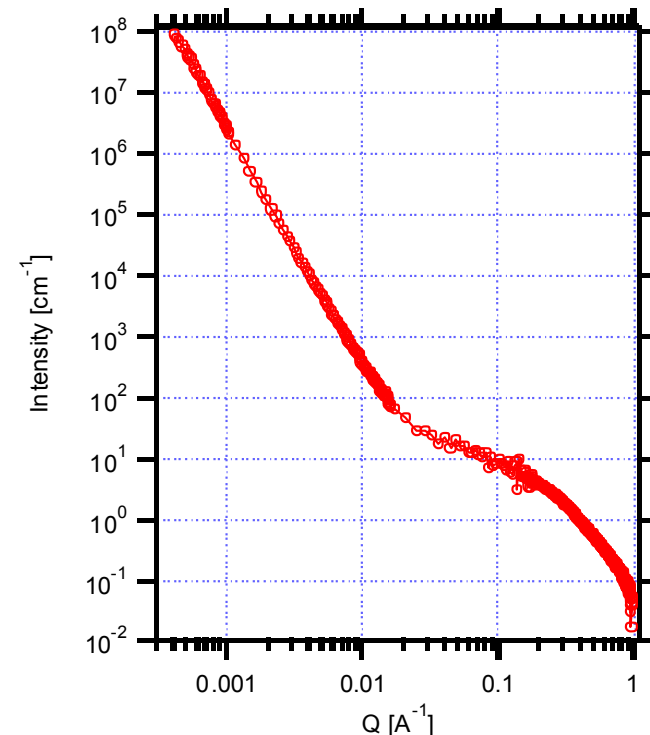
- Indirect measure of size, amount, or shape
 - If used without absolute intensity calibration... ---> size variations
 - Quantitative SAXS (absolute intensity calibration)?
 - *Determine volume fraction and number density = Much richer data.*
- Studies complement other methods
- Applicable to wide variety of technologically important materials
- Easy experiment, harder analysis
- Sample in transmission, $t=1/\mu$
- Monochromatic radiation ($\Delta\lambda/\lambda$ up to 25% is acceptable, common in SANS)

Outline

- Small-Angle Scattering Primer
- Quantitative Small-Angle Scattering
- Instrumentation
- Examples
- Summary

What can be learned from a Small-Angle Scattering Experiment?

- Size of scatterer
- Amount of scatterers
- Polydispersity
- Distribution of scatterers
- Shape of scatterers
- Morphology of scatterers
- Composition of scatterers



- There is *strong* dependence between some of these terms.
- SAS experiments, *complemented by other measurements*, can yield rich information about the microstructure.

Need for complementary methods

The richness of an integrated approach to materials characterization is dependent on the availability of complementary methods.

*The more you know
the more you can learn.*

Example: M_2C in AF1410 Steel

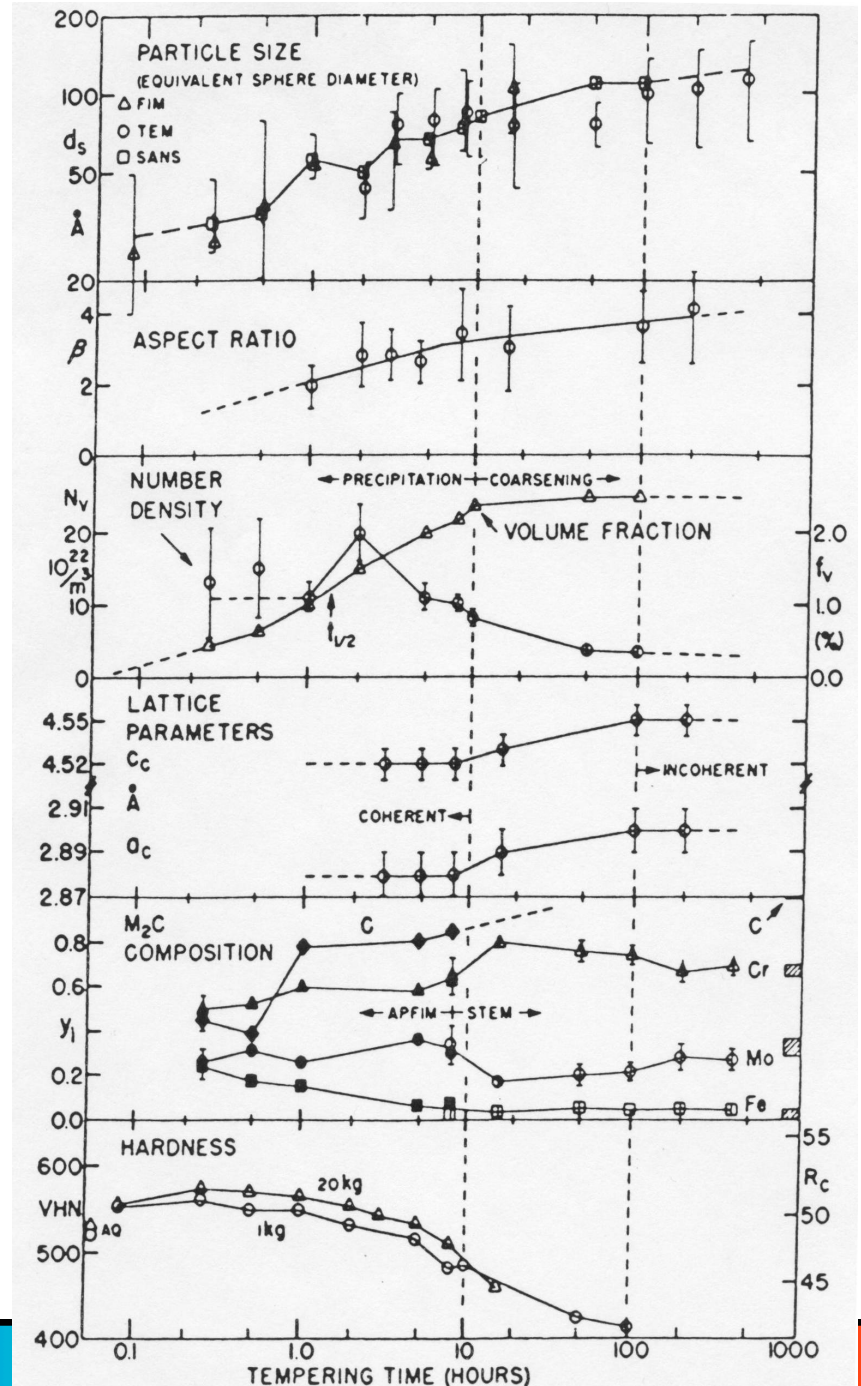
Complementary Methods:
XRD, TEM, AP/FIM, SANS,
mechanical properties,
thermodynamics calculations

SANS results bridged gap between
TEM & AP/FIM size data
Also provided new information of
volume fraction and number density

J.S. Montgomery, 1990,
Ph. D. Thesis, Northwestern University.

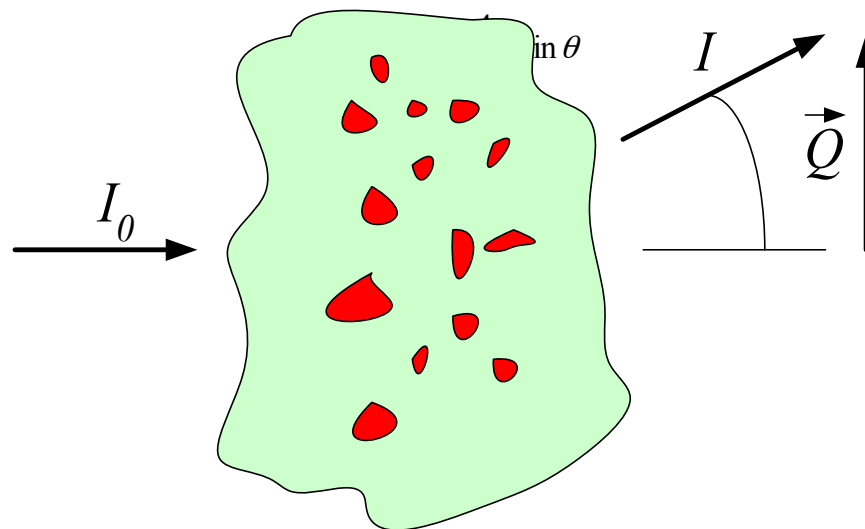
A.J. Allen, D. Gavillet, and J.R. Weertman;
Acta Metall 41 (1993) 1869-1884.

Innovations in Ultrahigh-Strength Steel Technology;
edited by G.B. Olson, M. Azrin, and E. S. Wright
Proceedings of the 34th Sagamore Conference,
August 30 - September 3, 1987, Lake George, NY, 1987



Origin of scattering

- Scattering is due to inhomogeneities in scattering length density, ρ
- When scatterers are
 - Homogeneous
 - Dilute (non-interacting)
 - Randomly dispersed
 - Same morphology
 - Same contrast, $|\Delta\rho|^2$



Then.....

$$\frac{d\Sigma}{d\Omega}(Q) = \left| V_p^{-1} \int_{V_p^{-1}} \rho(r) e^{-Q \cdot r} d^3 r \right|^2$$

Basic measures from a Small-Angle Scattering experiment

Guinier law $\lim_{Q \rightarrow 0} I(Q) = I(0) \exp\left(-\frac{1}{3} R_G^2 Q^2\right)$

$$Q_{\max} R_G < 1.2$$

Porod law $\lim_{Q \rightarrow \infty} I(Q) = 2\pi S_V |\Delta\rho|^2 Q^{-4}$

$$Q_{\min} D > 3$$

invariant $2\pi^2 V_V (1 - V_V) |\Delta\rho|^2 = \int_0^{\infty} Q^2 I(Q) dQ$

Outline

- Small-Angle Scattering Primer
- Quantitative Small-Angle Scattering
 - Absolute calibration
 - Contrast variation techniques
 - Multiple scattering
- Instrumentation
- Examples
- Summary

Advantages of Quantitative SAS

- Sampling volume large compared to features investigated: Statistically Significant Sampling
 - Sample volume typically 10^{-12} - 10^{-10} m^3
 - Scatterer size typically 10^{-9} - 10^{-6} m
 - 10^3 - 10^{13} scatterers in a single sample volume
- SAS probes through bulk material, not limited to surface or open porosity
- X-ray or neutron radiation sources can probe optically opaque substances
- Can separate different components in multi-component system (in some cases)
- SAS can often address anisotropy
- Local SAS can address inhomogeneities

Information Obtained from Quantitative Small-Angle Scattering

volume fraction

$$V_V = \sum_i f_i(D) \Delta D_i$$

number density

$$N_V = \sum_i \frac{f_i(D) \Delta D_i}{\left(\frac{\pi}{6}\right) D_i^3}$$

Radius of gyration

$$R_G = \sqrt{\frac{\langle r^8 \rangle}{\langle r^6 \rangle}}$$

specific surface

$$S_V = 6 \sum_i f_i(D) \frac{\Delta D_i}{D_i}$$

mean spacing

$$\Lambda = (N_V)^{-1/3}$$

volume-weighted

mean diameter

$$\bar{D}_V = V_V^{-1} \left[\sum_i D_i f_i(D) \Delta D_i \right]$$

number-weighted

$$\bar{D}_N = N_V^{-1} \left[\sum_i D_i \frac{f_i(D) \Delta D_i}{\left(\frac{\pi}{6}\right) D_i^3} \right]$$

standard deviation

$$\sigma(\bar{D}_V) = \sqrt{V_V^{-1} \left[\sum_i D_i^2 f_i(D) \Delta D_i \right] - (\bar{D}_V)^2}$$

$$\sigma(\bar{D}_N) = \sqrt{N_V^{-1} \left[\sum_i D_i^2 \frac{f_i(D) \Delta D_i}{\left(\frac{\pi}{6}\right) D_i^3} \right] - (\bar{D}_N)^2}$$

Absolute SAS Cross-Section $d\Sigma/d\Omega$

J Appl Cryst **5** (1972) 315-324, **16** (1983) 473-478
Acta Metall Mater **39.11** (1991) 2477-2487

$$I(Q) = I_0 \Omega t e^{-\mu t} \frac{d\Sigma}{d\Omega}(Q)$$

$I(Q)$: intensity, arbitrary units

I_0 : apparent source intensity, arbitrary units

Ω : solid angle subtended by detector

t : sample thickness

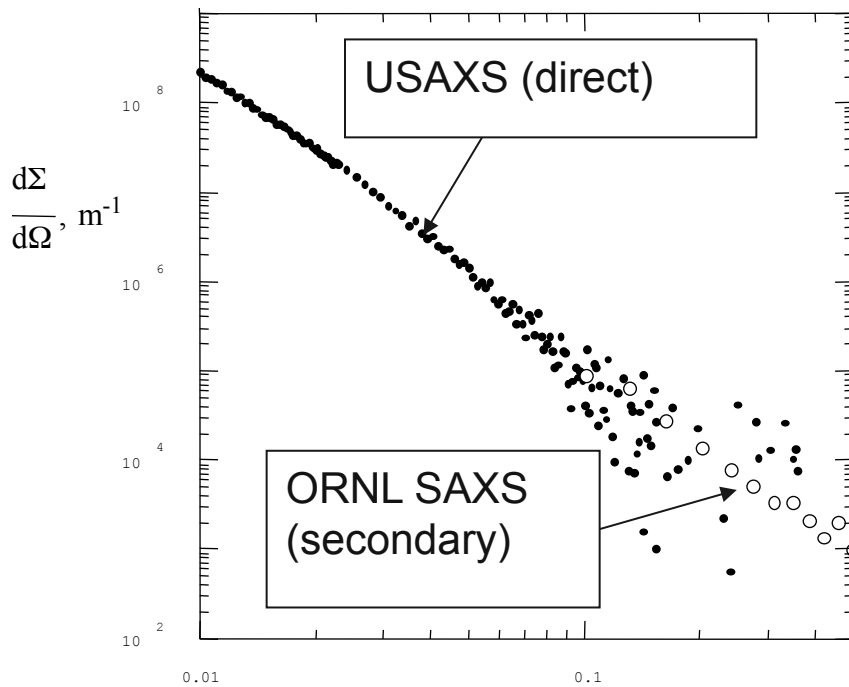
μ : absorption coefficient

$d\Sigma(Q)/d\Omega$: differential scattering cross-section
per unit volume per unit solid angle

Methods to obtain $d\Sigma/d\Omega$

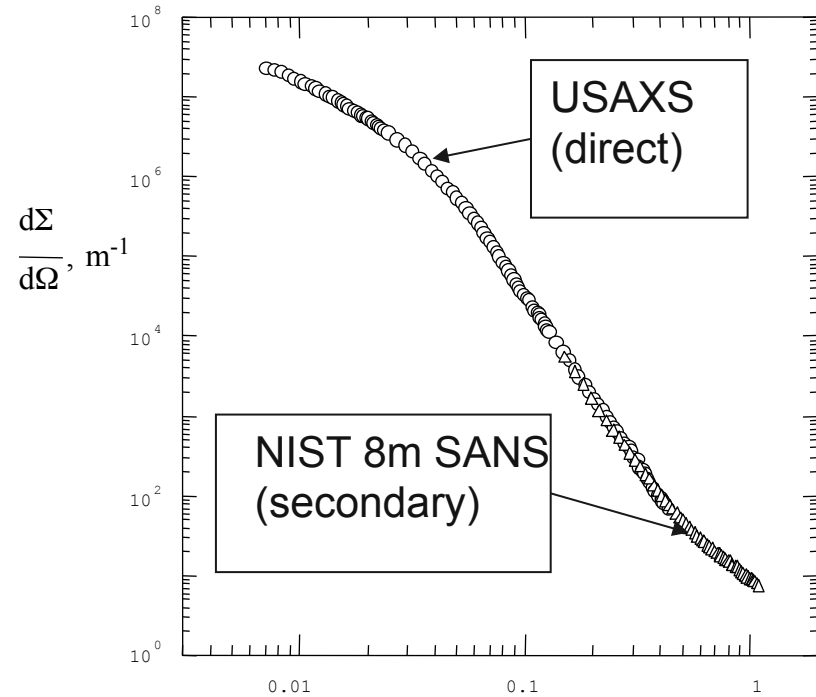
Comparison of USAXS: Direct Intensity Scaling with secondary standard

- Direct measurement of all parameters
- Calibration against secondary standard



$$Q = \left(\frac{4\pi}{\lambda} \right) \sin \theta, \text{nm}^{-1}$$

Jemian, Ph.D. Thesis, 1990, Northwestern



$$Q = \left(\frac{4\pi}{\lambda} \right) \sin \theta, \text{nm}^{-1}$$

Long, et al., *J Appl Cryst* **23.6** (1990) 535

Size Distribution Determination – scatterers same shape and chemistry, size varies

$$\frac{d\Sigma}{d\Omega}(Q) = \int_0^{\infty} |\Delta\rho F(Q, r) V(r)|^2 N(r) dr$$

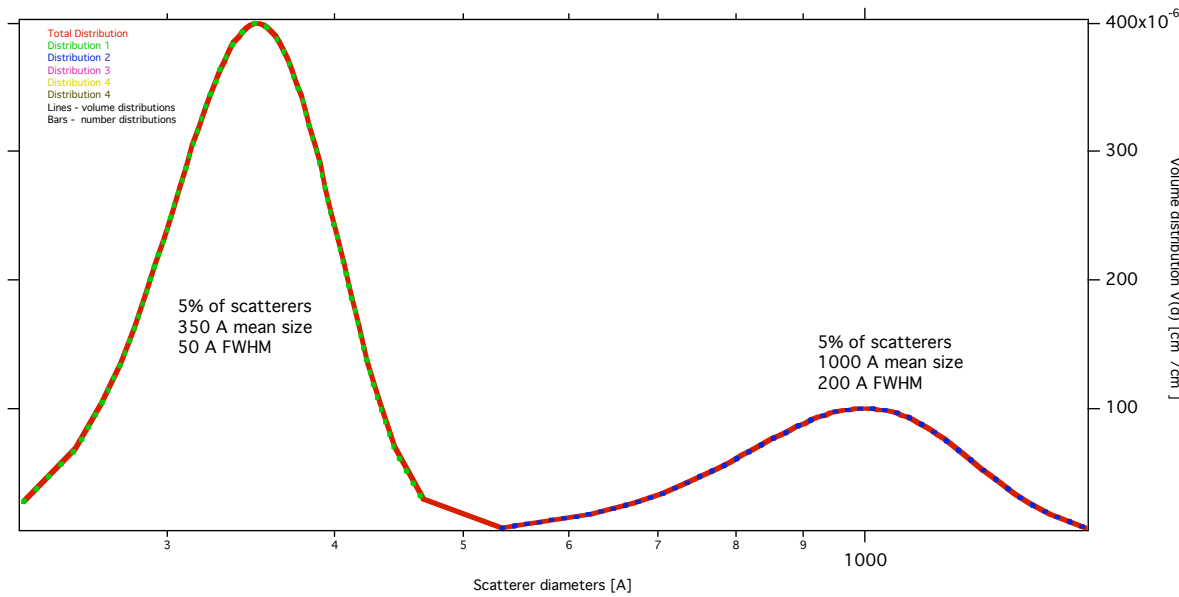
$$\frac{d\Sigma}{d\Omega}(Q) = |\Delta\rho|^2 \int_0^{\infty} |F(Q, r)|^2 V(r) f(r) dr$$

Solve for $f(r) dr$ by a regularization method such as:

- enforcing only positive values of $f(r) dr$
- maximizing smoothness of $f(r) dr$

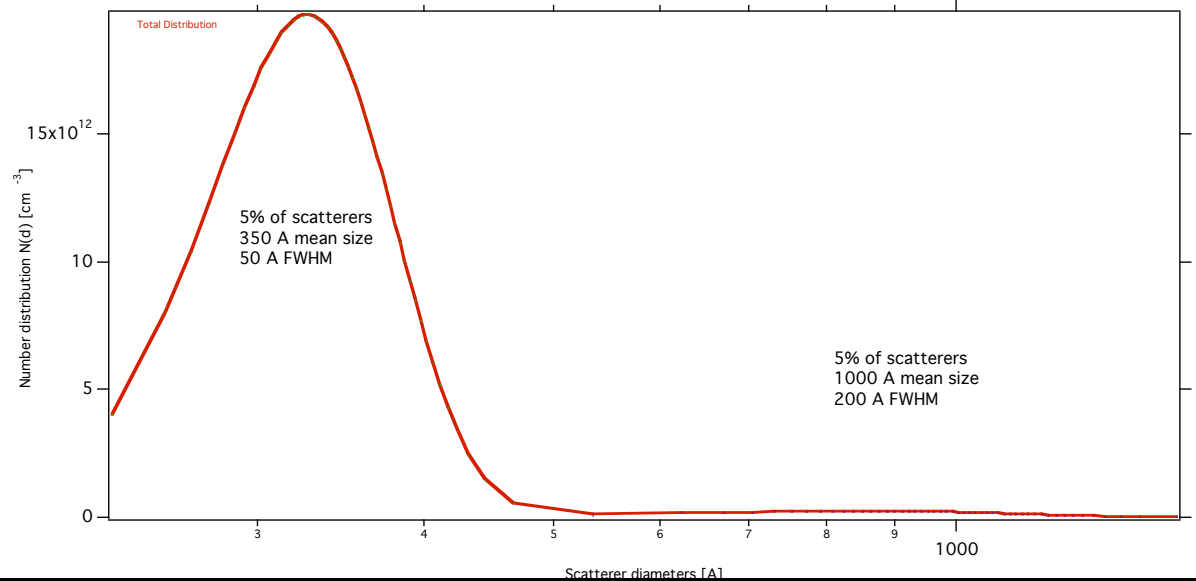
Spheres: $F(Q, r) = 3(Qr)^{-3} [\sin(Qr) - (Qr)\cos(Qr)]$

Size Distribution Determination – volume & number distributions?



Volume distribution:
 How much volume is in given size interval
 Area under the curve = volume (fraction)

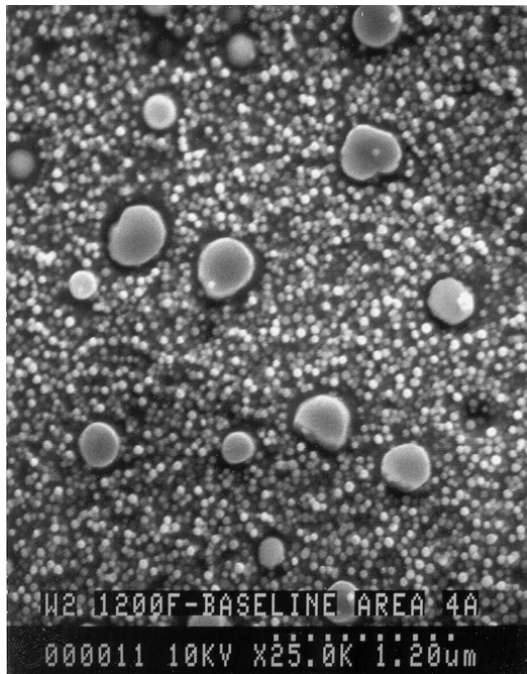
Number distribution:
 How many particles are in given size interval
 Area under the curve = number of particles
 (per unit of volume)



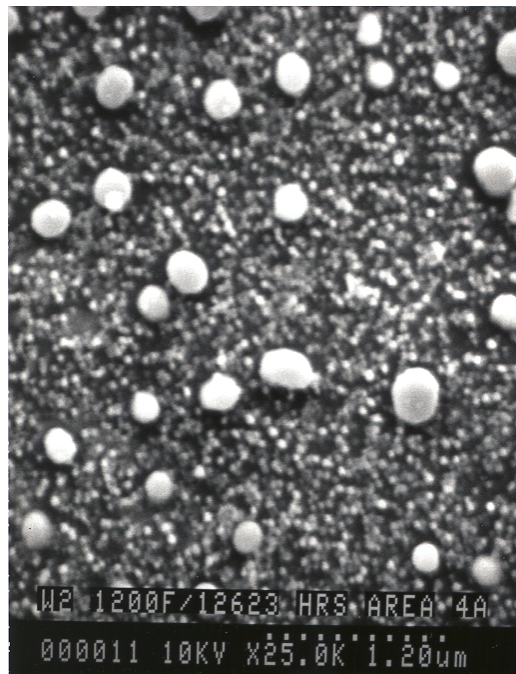
Complicated systems...

What can we do for more complex samples, such as γ' precipitation in WaspaloyTM ?

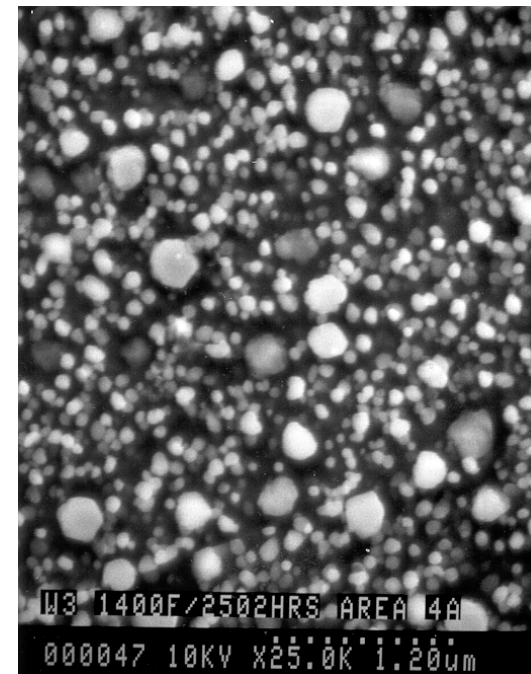
GerhardtI, private communications, 2000



base microstructure



12623 h, 1200° F



2502 h, 1400 ° F

Simple contrast variation example



When the monster came, Lola, like the peppered moth and the arctic hare, remained motionless and undetected. Harold, of course, was immediately devoured.

When the monster came, Lola, like the peppered moth and the arctic hare, remained motionless and undetected. Harold, of course, was immediately devoured.

Contrast Variation Methods

- Needed when more than one type of scatterer is present
- Vary $|\Delta\rho|^2$ of one type, holding others constant

- Anomalous scattering (X-ray & neutron)
- Isotope substitution (neutron)
- Isomorphous replacement
- Magnetic scattering (neutron)
- Concentration variation (X-ray & neutron)

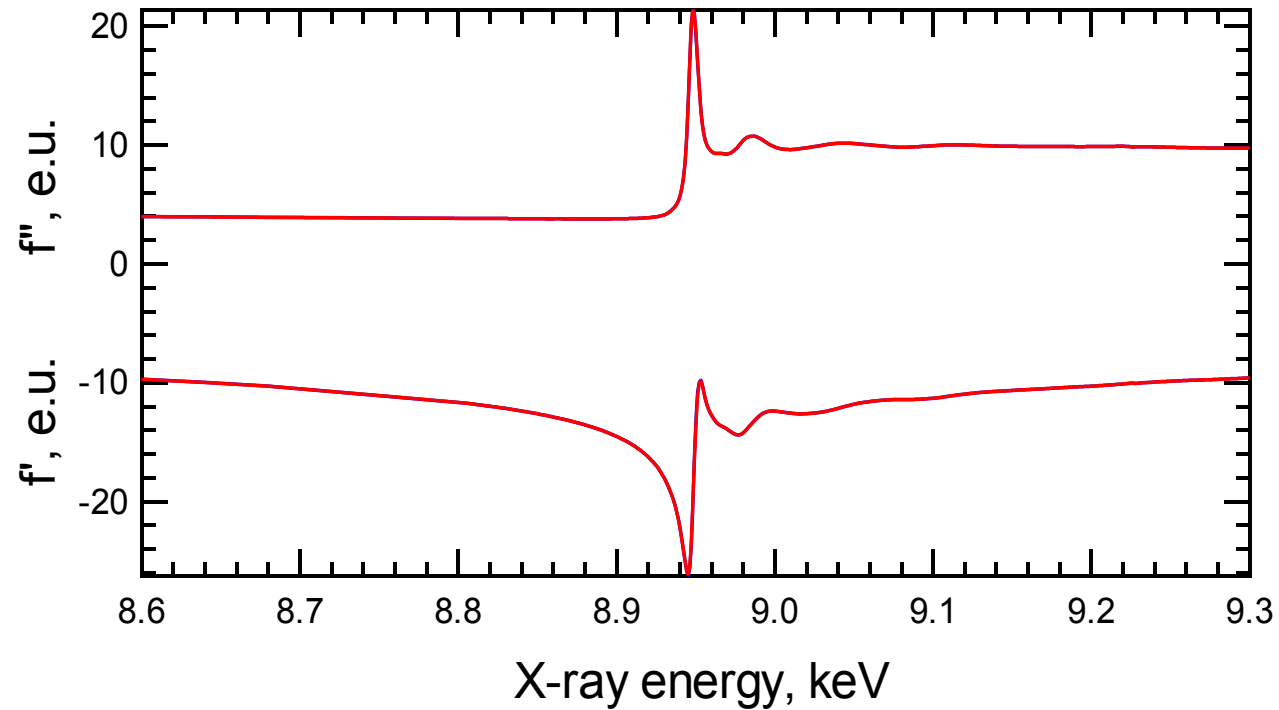
- ...

Anomalous Small-Angle X-ray Scattering

- Why anomalous SAXS?
 - Element-specific contrast variation
 - Use to separate population distributions of scatterers
- Will ASAXS solve every problem?
 - Not even close
 - The easy problems are already taken

Calculated $f'(E)$ and $f''(E)$

Anomalous dispersion terms of
Yb in SN-88 near the Yb L_{III} edge (8.939 keV)



Calculation of $f'(E)$ and $f''(E)$

- The anomalous dispersion terms are calculated from the absorption spectrum:
 - *Z Phys* **48** (1928) 174-179, *J Appl Cryst* **17** (1984) 344-351

Beer's Law $\frac{I}{I_0} = \exp[-\mu_l(E)t]$

optical theorem $f''(E) = \frac{E}{2r_e ch} \frac{A}{N_A} \frac{\mu_l(E)}{\rho_m} = \frac{E}{2r_e ch} \frac{A}{N_A} \mu_m(E)$

Kramers-Kronig integral $f'(E) = \frac{2}{\pi} \int_0^{\infty} f''(\varepsilon) \frac{\varepsilon}{E^2 - \varepsilon^2} d\varepsilon$

ASAXS Analytical Method

- Absorption spectrum
 - Energy selection
 - Determine anomalous scattering factors
 - Calculate scattering contrasts
- SAXS measurements
 - Sample and blank at each energy
 - Calculate transmission
 - Subtract blank
 - Apply corrections (e.g., desmearing)
 - Solve for size distribution
- ASAXS analysis
 - Extract size distribution for each scatterer using contrast gradient method
 - Assess integral, mode, mean, standard deviation, etc. for each size distribution

Useful (extremely) for analysis of SAS

- *a priori* information
 - Sample composition
 - TEM/STEM/AFM/AP-FIM
 - XRD
 - Porosimetry
 - Gas adsorption
 - ...
- Sample thickness
- Sample uniformity
- Sample absorption spectrum
- Instrument absorption spectrum
- Sample (+instrument) SAXS
- Instrument SAXS profile
- Absolute SAXS cross-section $d\Sigma/d\Omega$

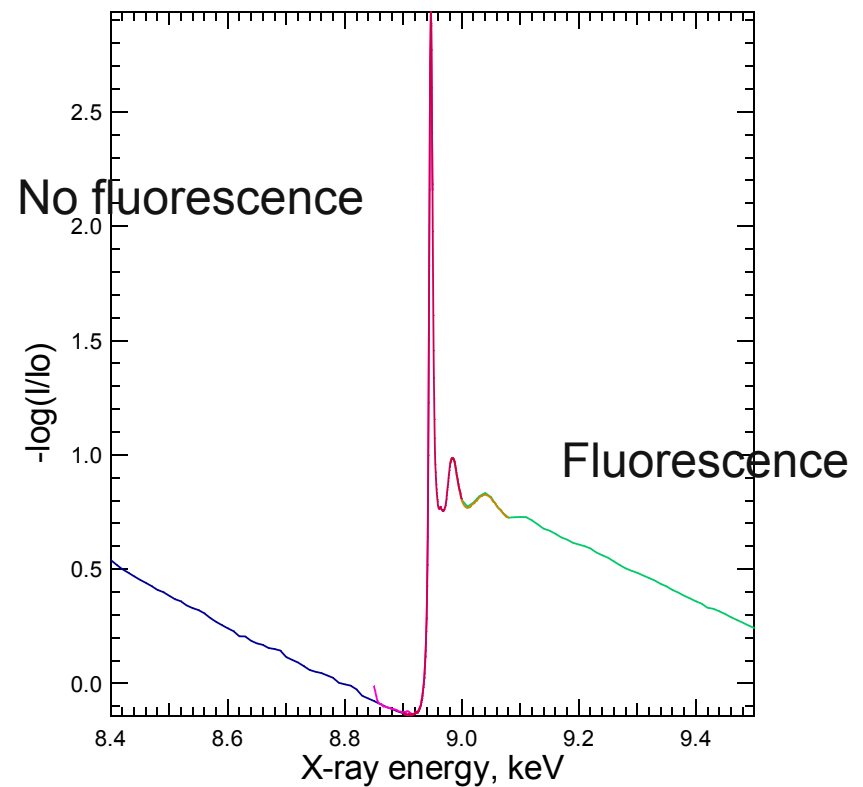
Sample Uniformity Measurement

- Illuminated area must be representative of sample
- Sample thickness must be uniform
- No pinholes
- Sample positioning must be *precise and reproducible*
 - How precise?
 - *Depends on beam size & sample uniformity*
 - *Precision (step size) ~ 20 μm*
 - *Reproducibility < 50 μm*
 - Achieve with a X-Y translation stage
- Verify using *radiography and USAXS imaging*

Absorption Spectrum Measurement

- Use to determine position of absorption edge
- Calibrate energy for experiment
- Derive anomalous dispersion corrections

X-ray absorption spectrum of SN-88 near the Yb L_{III} edge (8.939 keV)



ASAXS Energy Selection Criteria

- Maximize contrast change of target population, work near absorption edge
- Minimize the energy range to be covered, 200-300 eV sufficient
- Avoid X-ray fluorescence, stay below absorption edge
- Avoid Resonant Raman Scattering, stay away from absorption
- Consider monochromator energy tails, measure absorption spectrum from SAXS sample!
- Maximize the number of energies
- Use all available beam time

Multiple scattering issues....

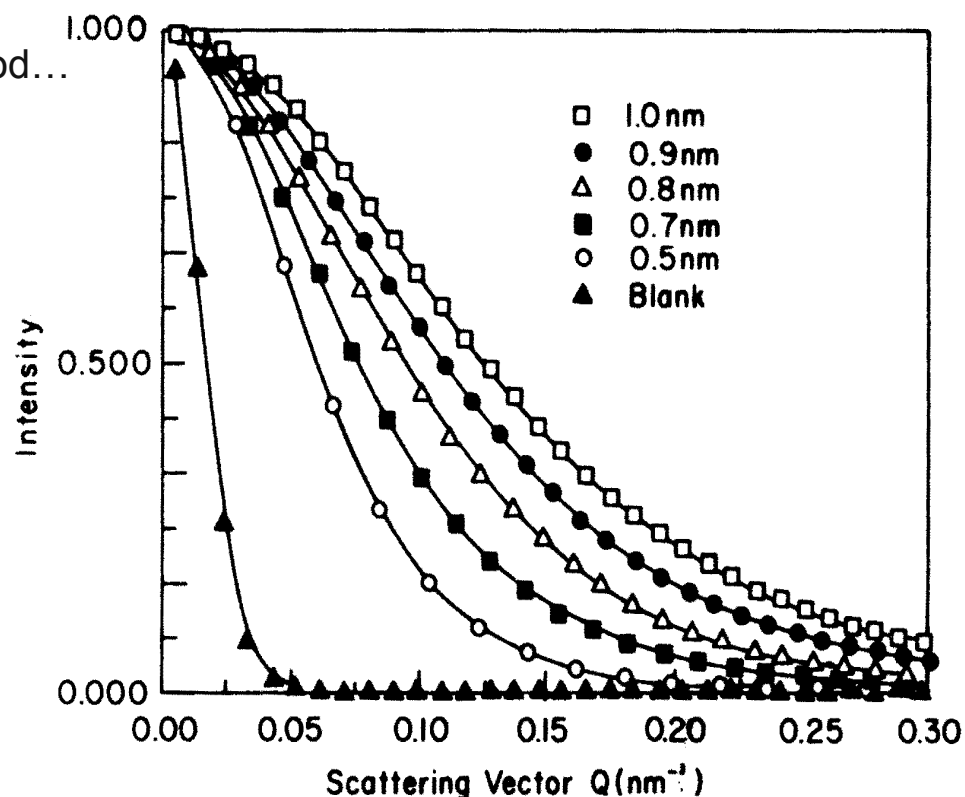
- When scattering probability high enough that each photon (neutron) is scattered more than one time while passing the sample
 - mean free path < sample thickness
- Major problem for data analysis – most theories assume mean free path >> sample thickness
- Depends on:
 - Wavelength (longer wavelength = smaller mean free path)
 - Scattering contrast of scatterers
 - Size of scatterers
 - Number of scatterers
- Theory to analyze “copious multiple scattering” (Hardman-Rhyne, K. A. and N. F. Berk (1985). "Characterization of Alumina Powder Using Multiple Small-Angle Neutron-Scattering .2. Experiment." Journal of Applied Crystallography **18(Dec): 473-479.**, Berk, N. F. and K. A. Hardman-Rhyne (1985). "Characterization of Alumina Powder Using Multiple Small-Angle Neutron-Scattering .1. Theory." Journal of Applied Crystallography **18(Dec): 467-472.**, Allen, A. J., N. F. Berk, et al. (2002). "Multiple small-angle neutron scattering studies of anisotropic materials." Applied Physics a-Materials Science & Processing **74: S937-S939.**)
- Most cases – avoid if you can. Reduce sample thickness, reduce wavelength...

Multiple small-angle scattering results

- Complicated, tedious measurement at number of different wavelengths
- Complicated theory
 - Each photon/neutron scattered copious time when passing through sample (5x or more)
 - This broadens the beam profile -> microstructure information
- Time consuming, model based data analysis
- Needs to be combined with Anisotropic Porod scattering & independent porosity volume measurement (intrusion)
- Simply – if not necessary, do not use this method...

However:

- Some samples scatter so strongly, that no other method is usable
- For anisotropic samples such as plasma sprayed deposits enables to:
 - Independently quantify different parts of the microstructure
 - Obtain both volume and mean size (model based)



Outline

- Small-Angle Scattering Primer
- Quantitative Small-Angle Scattering
- Instrumentation
 - Types of instruments
 - Q range selection
- Examples
- Summary

Instrumentation

The trick is to measure an intensity which varies by several decades *very* close to the intense transmitted beam. Must avoid damaging the detector with the transmitted beam!

Designs

- Slit cameras
- Pinhole cameras
- Ultra-Small-Angle (a.k.a, USAS or Bonse-Hart)
- Grazing incidence (reflection, not transmission)

Sources

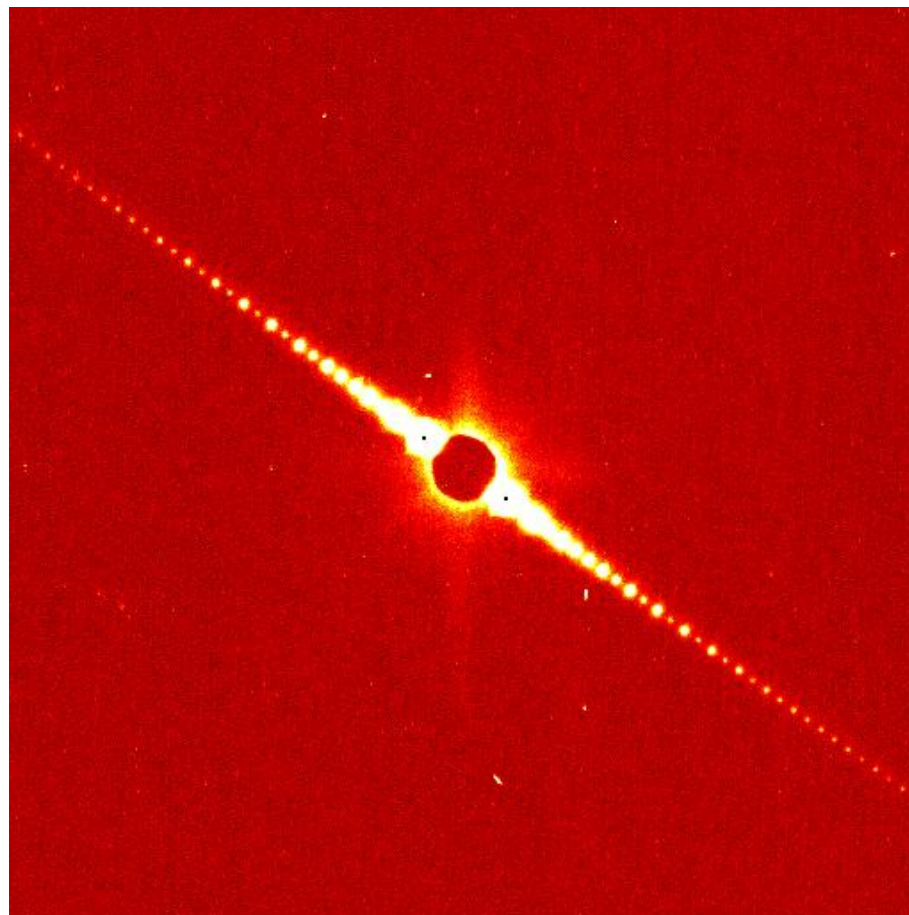
- X-ray tube
- Rotating anode
- Synchrotron X-ray source
- Reactor
- Pulsed neutron source

Beam stop limits largest size resolved

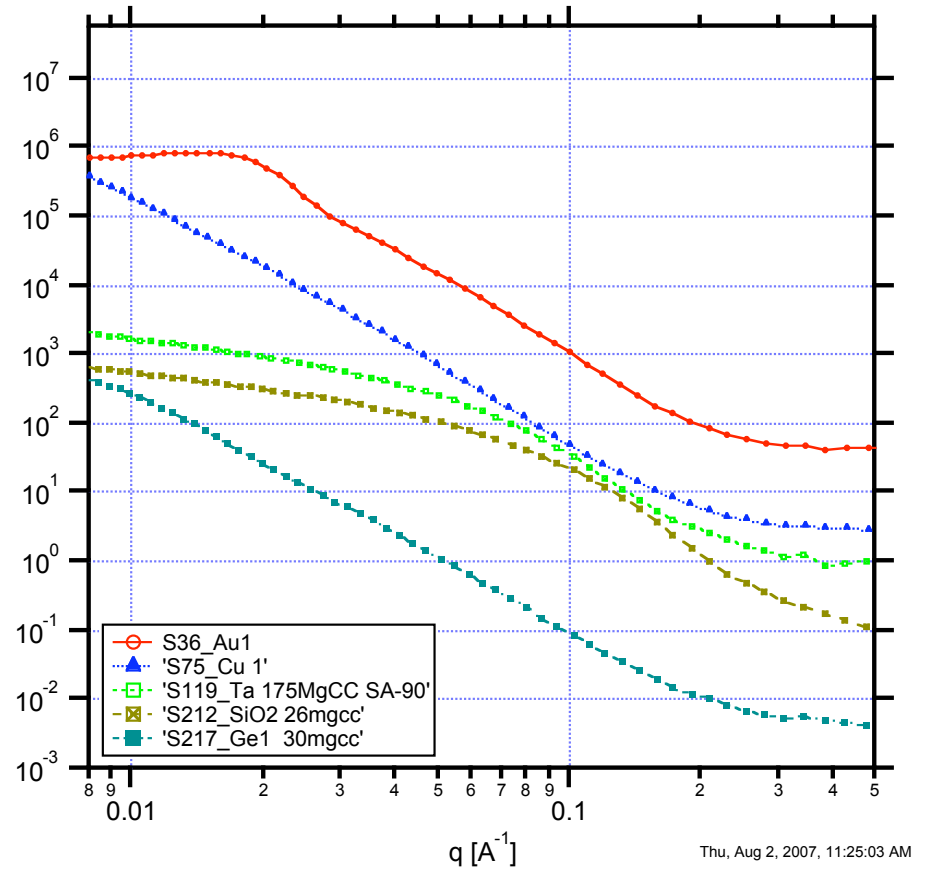
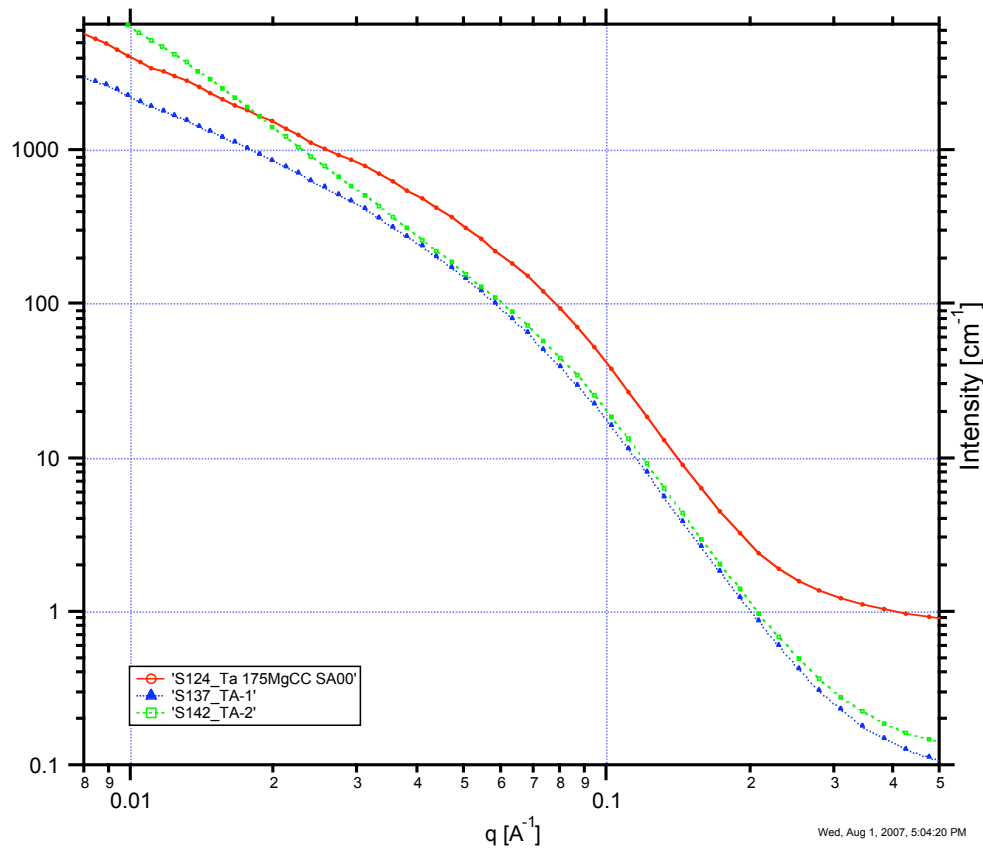
Beam stop

- Needed to protect detector
- Limits minimum Q ,
typical $Q_{\min} \sim 10^{-3} \text{ \AA}^{-1}$,
($d_{\max} \sim 200\text{-}600 \text{ nm}$)

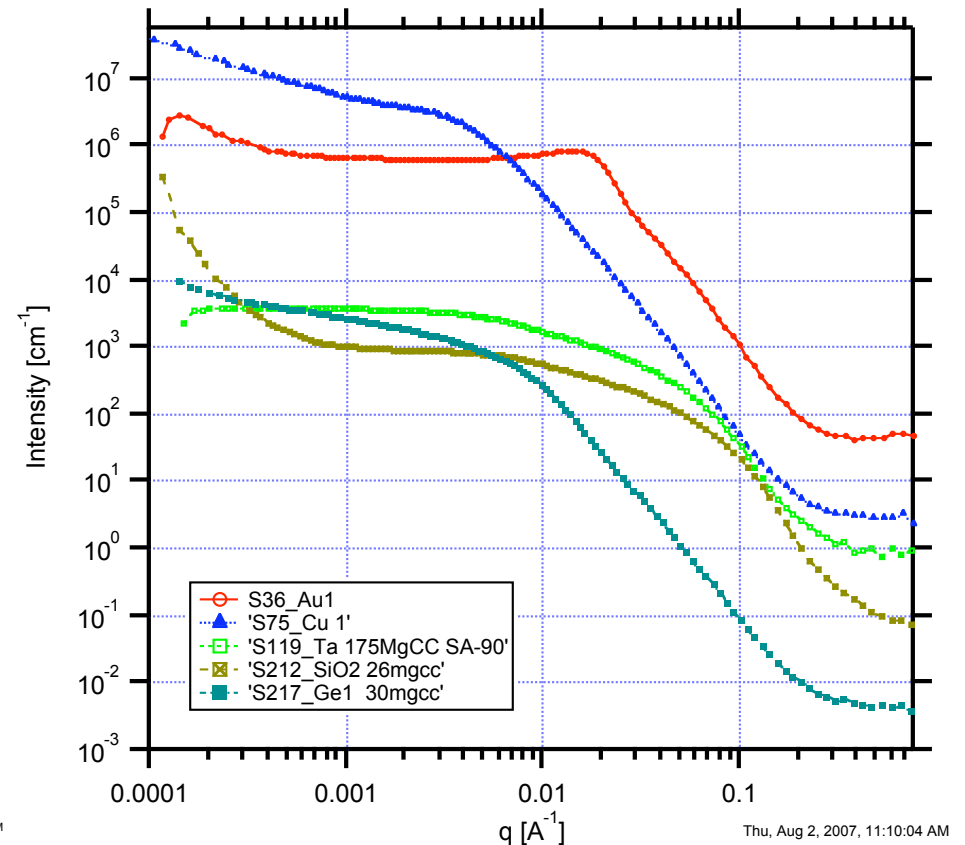
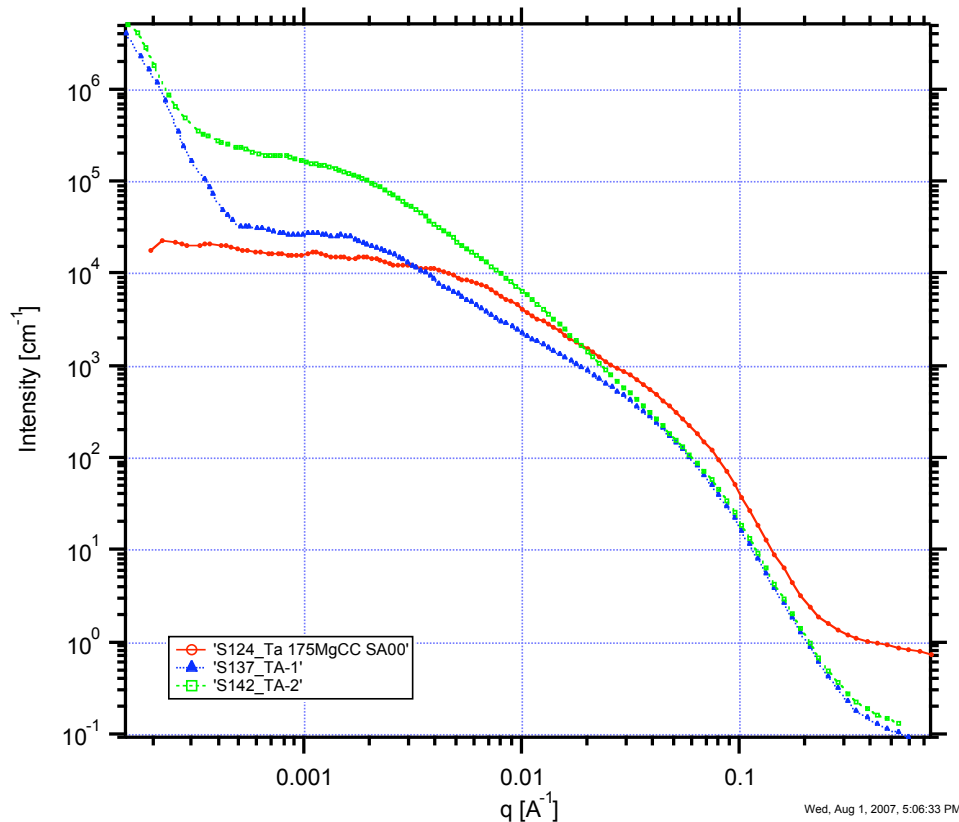
$$Q_{\min} d_{\max} \sim 2\pi$$



Instrument q range selection: Aerogels - this is what pinhole camera is likely going to look like:

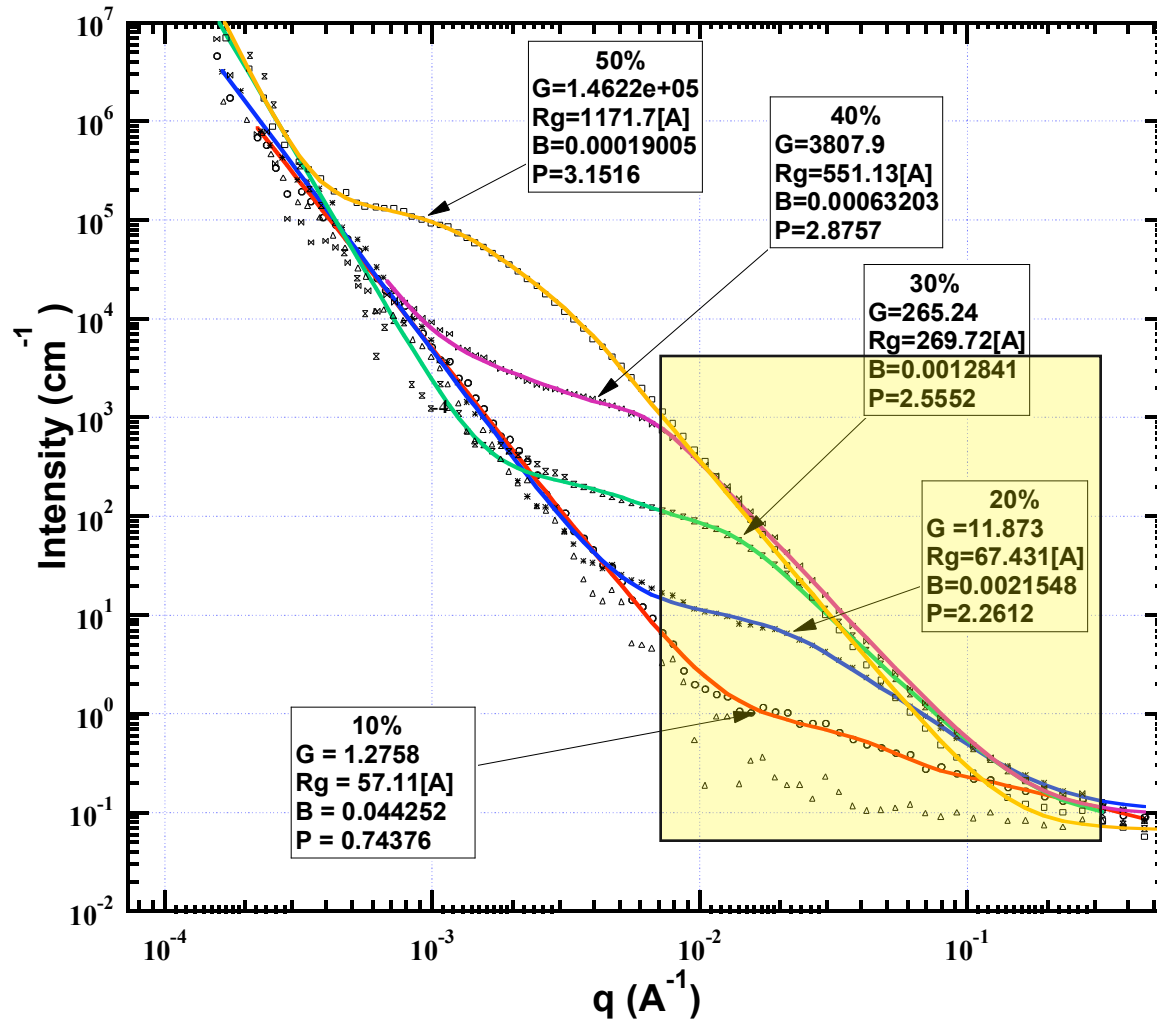


Aerogels - this is how USAXS data look like:



Example of small angle scattering from Ta aerogels. Slit smeared data left graph, same data desmeared right graph. Aerogels are unique materials with very low density which are considered for many applications in aerospace industry. Graphs from work by Ted Baumann, Joe Satcher, Trevor Willey, and Tony Van Buuren, LLNL.

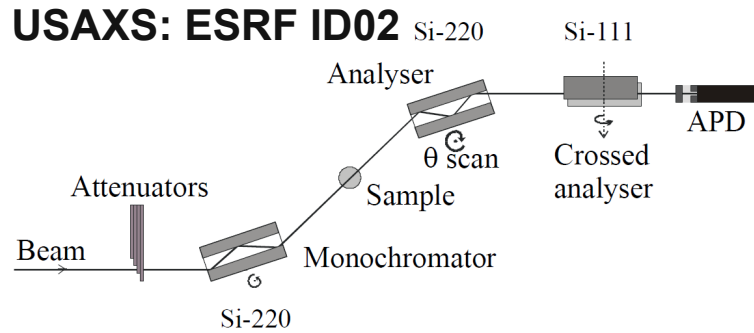
Liquid crystals dispersed in polymers



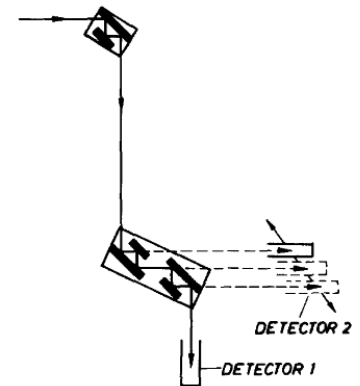
USAXS data from Polymer-dispersed liquid crystals. The loading of liquid crystals in polymer changes the structure over wide size range accessible only by USAXS. Polymer-dispersed liquid crystals (PDLCs) are of technological importance for electro-optic applications such as privacy windows, electro-optic shutters, and large area flat-panel displays. Graph from current work by Ryan S. Justice, Dale Schaefer, Richard Vaia, David Tomlin, and Timothy Bunning, “*Interface morphology and phase separation in polymer-dispersed liquid crystal composites*”, accepted to *Polymer*. Authors are from University of Cincinnati, Air Force research Lab, and UES Incorporated.

Yellow box is estimate of pinhole camera range

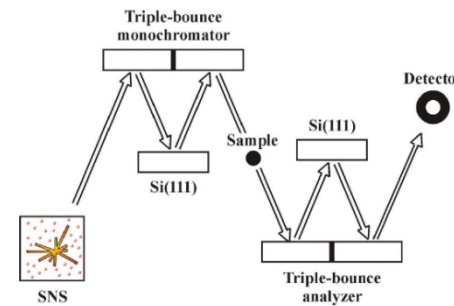
Example B&H instruments for USANS and USAXS



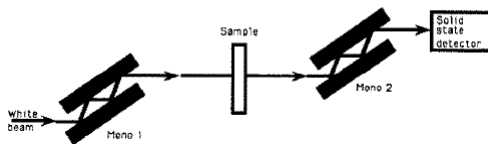
USANS: FRJ-2, Jülic



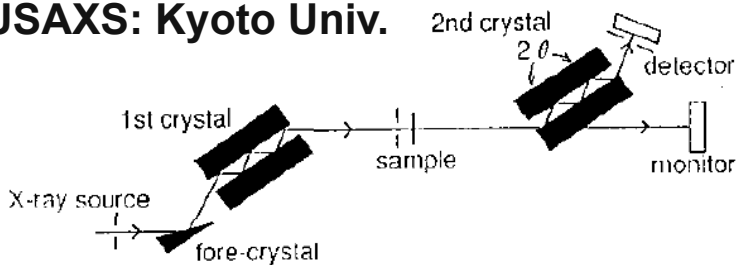
TOF-USANS: SNS (planned)



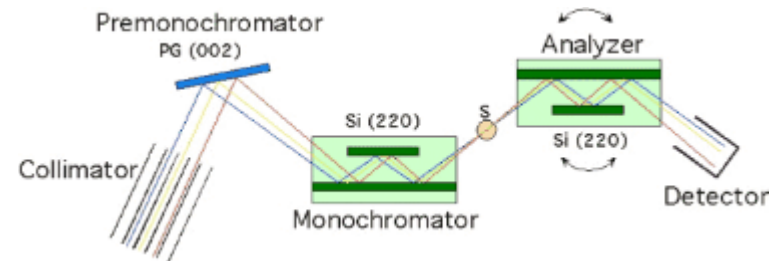
USAXS: Daresbury



USAXS: Kyoto Univ.



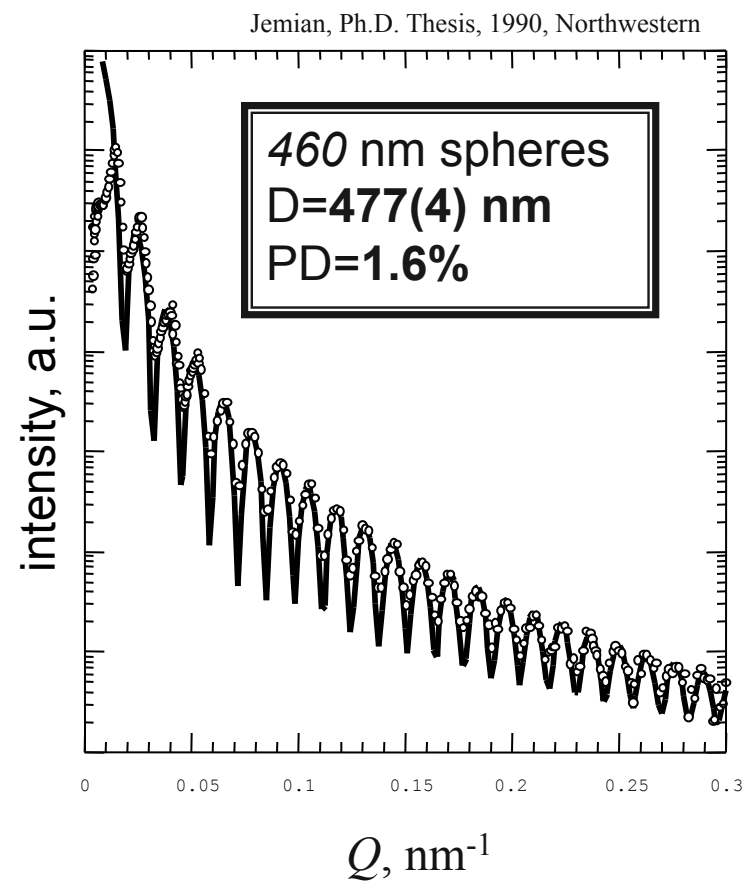
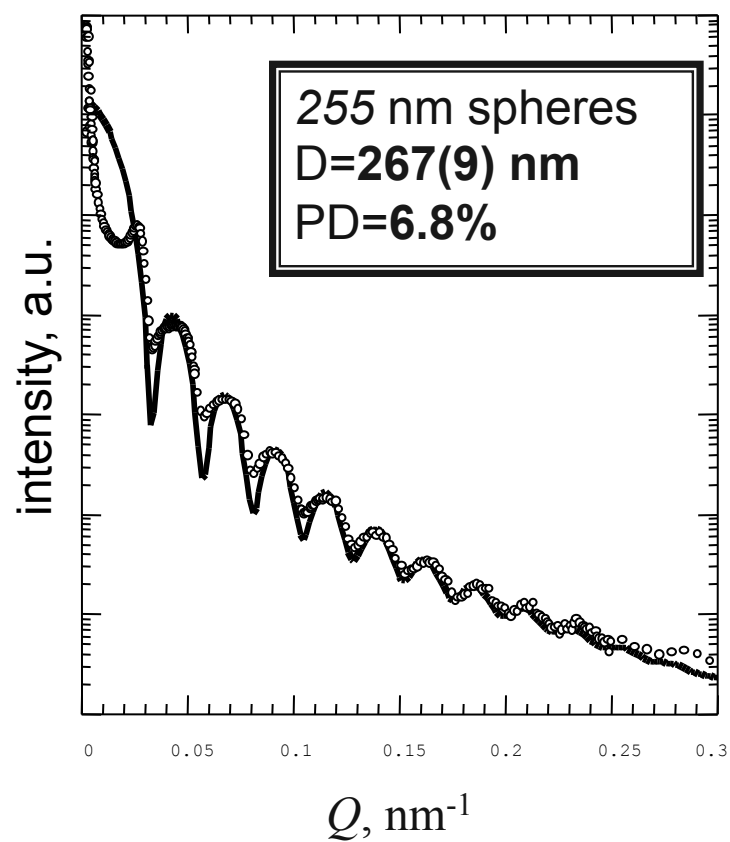
USANS: NIST PCD



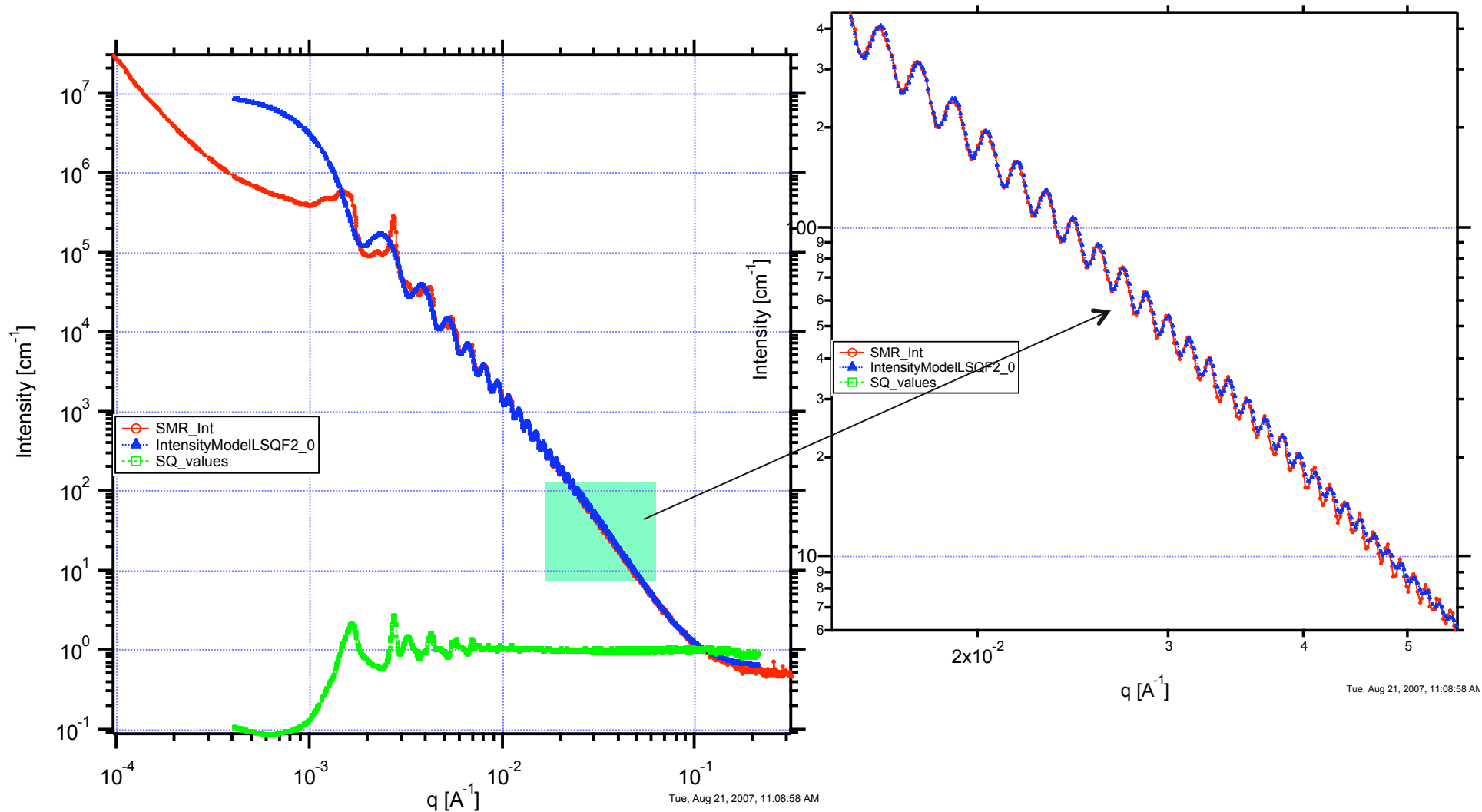
Outline

- Small-Angle Scattering Primer
- Quantitative Small-Angle Scattering
- Instrumentation
- Examples, including
 - Nanoparticle Colloidal Haloing effect
 - Colloidal silica porosity
 - Bone cements
 - Anomalous techniques (steels, SiN)
 - Time resolved SAXS (precipitation of CeO)
 - Anisotropic Porod scattering
 - Anisotropic USAXS
 - Local area SAXS
 - Carbon gas storage materials
- Summary

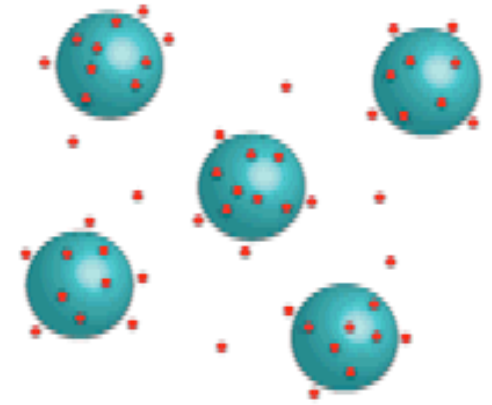
Polystyrene spheres: Determination of Size & Polydispersity



Real World materials – mono sized distribution of spheres, powder

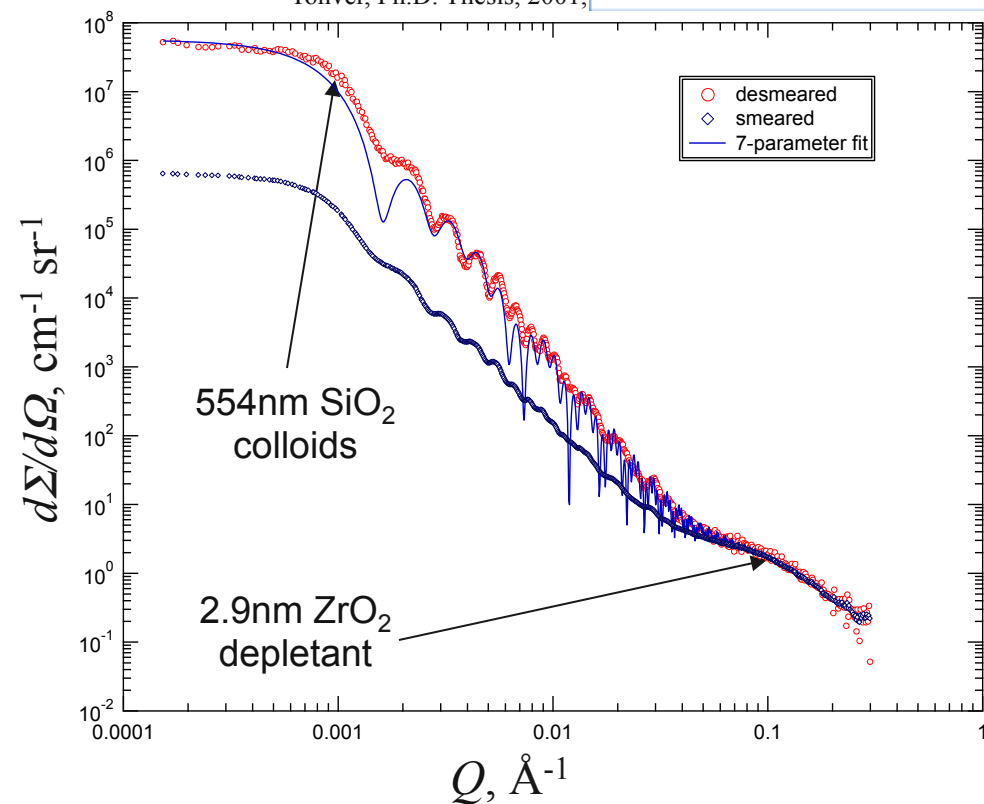


Colloidal silica with zirconia additive – nanoparticle haloing



Tohver, Ph.D. Thesis, 2001,

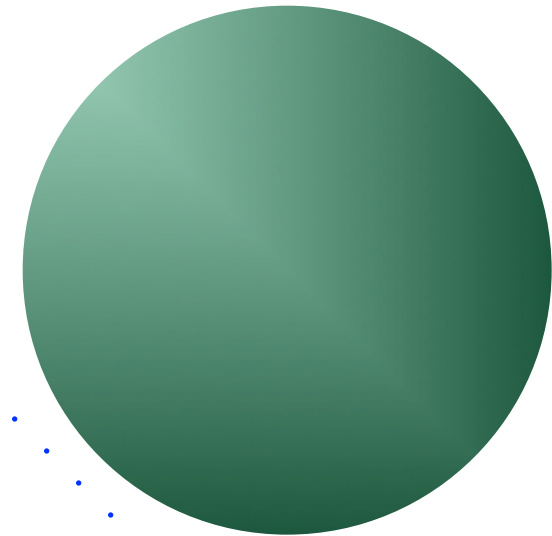
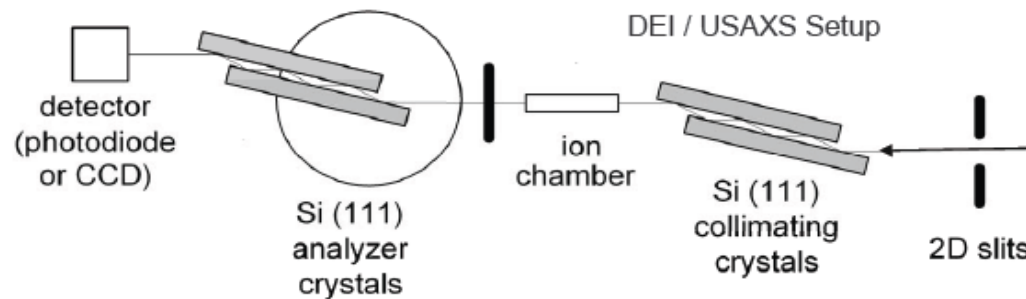
- Nonadsorbing (depletant) zirconia colloids added to disperse silica colloids
- SAS can be used to characterize these sizes



F. Zhang, G.G. Long, P.R. Jemian, J. Ilavsky, V.T. Milam, J.A. Lewis, "Quantitative Measurement of Nanoparticle Halo Formation around Colloidal Microspheres in Binary Mixtures," *Langmuir* 2008; ASAP Article. DOI: 10.1021/la702968n

USAXS could be useful!

The difficulty lies upon that great charge and size asymmetry



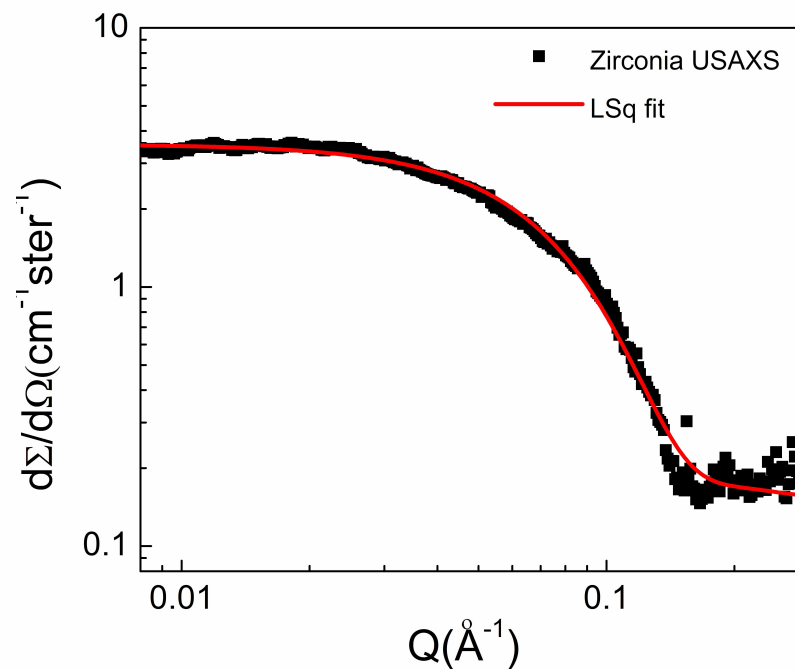
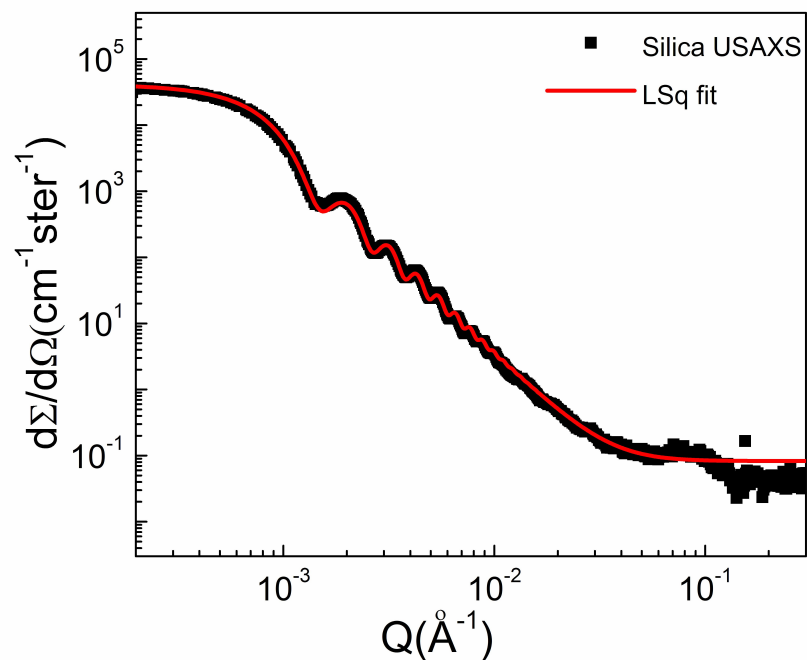
Size ratio: 100:1

- Bonse-Hart instrument with highly polished Si (220) crystals at analyzers and collimators
- Six reflections on both sets of crystals
- Q range: 0.0001 \AA^{-1} -- 1 \AA^{-1} .
- Q resolution: 0.00015 \AA^{-1} .
- Absolute determination of $d\Sigma/d\Omega$.

USAXS of SiO₂ and ZrO₂ dispersions

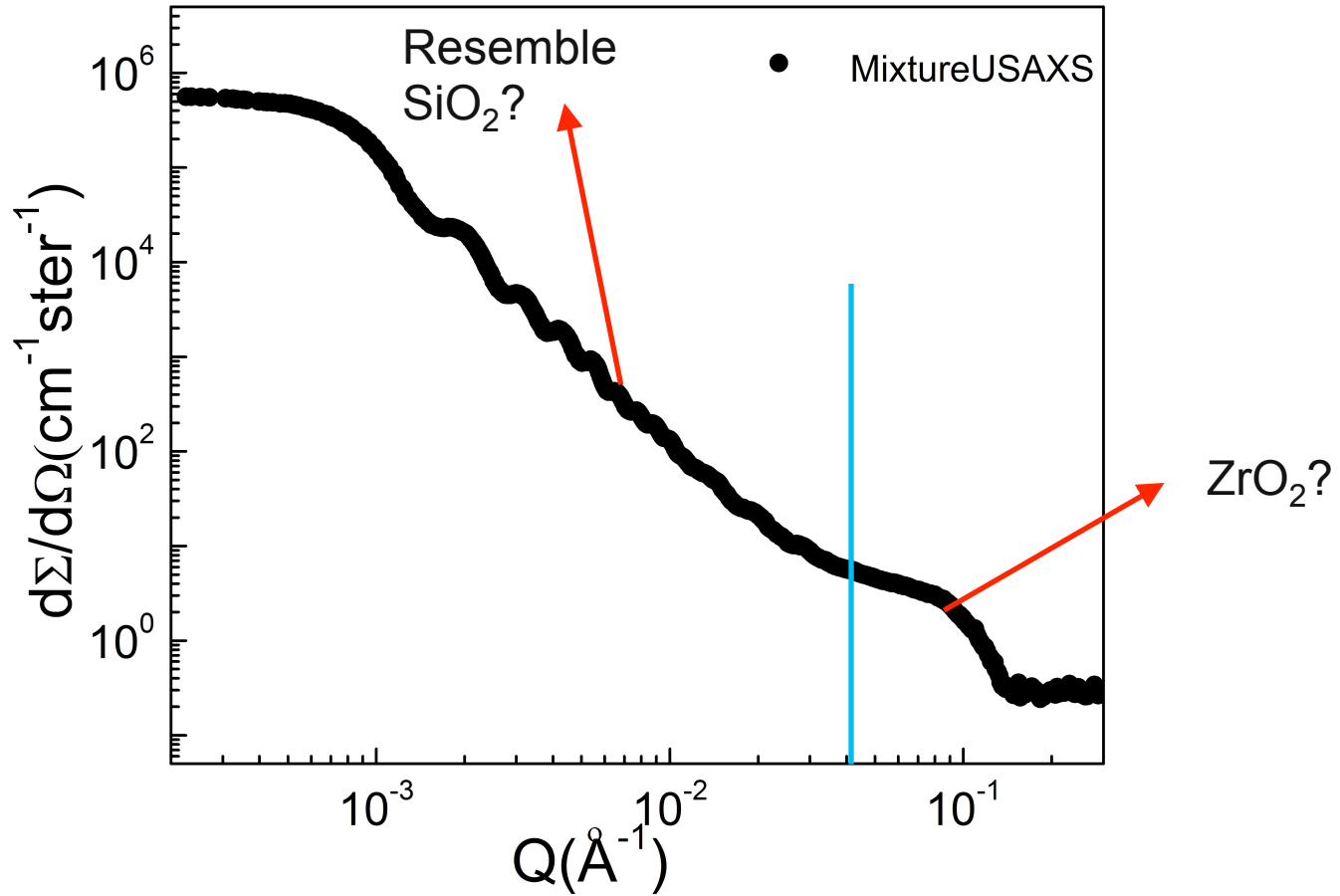
Assume both possess spherical geometry.

$$I(q) = (\Delta\rho)^2 V^2 \left[3 \frac{\sin qr - qr \cos qr}{(qr)^3} \right]^2$$

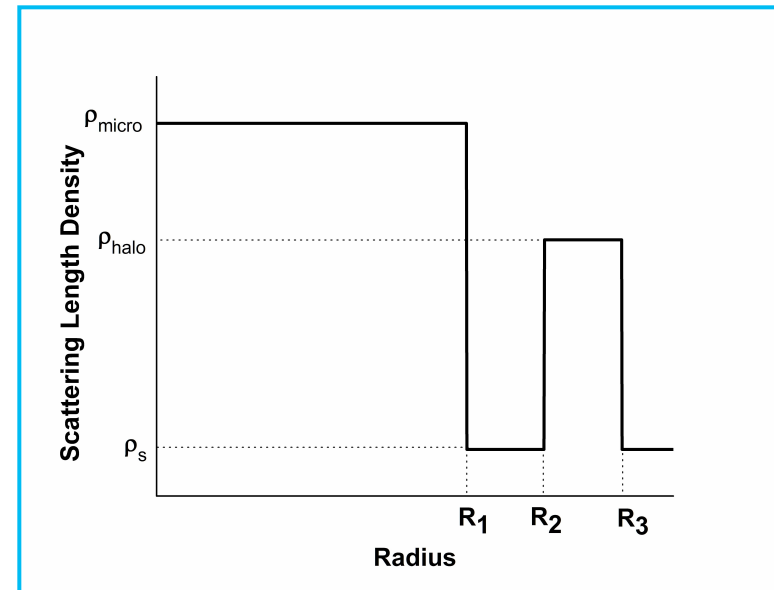
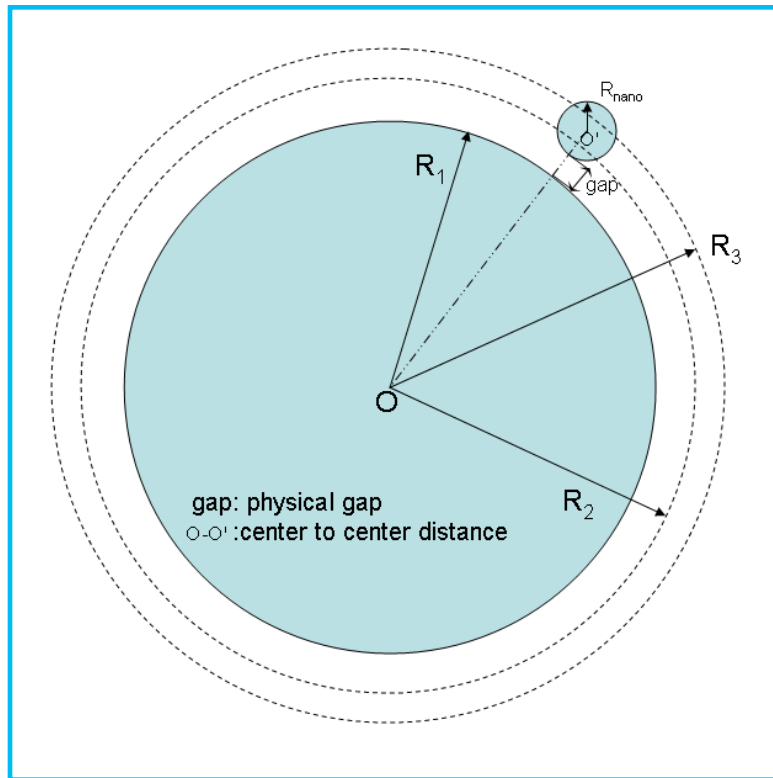


	Relative Scattering Volume	Mean Radius (nm)	FWHM (nm)
silica microspheres	0.34×10^{-2}	280.11	9.718
zirconia nanoparticles	0.42×10^{-2}	2.57	0.46

USAXS of SiO_2 and ZrO_2 mixtures



Our model



Scattering Form Factor:

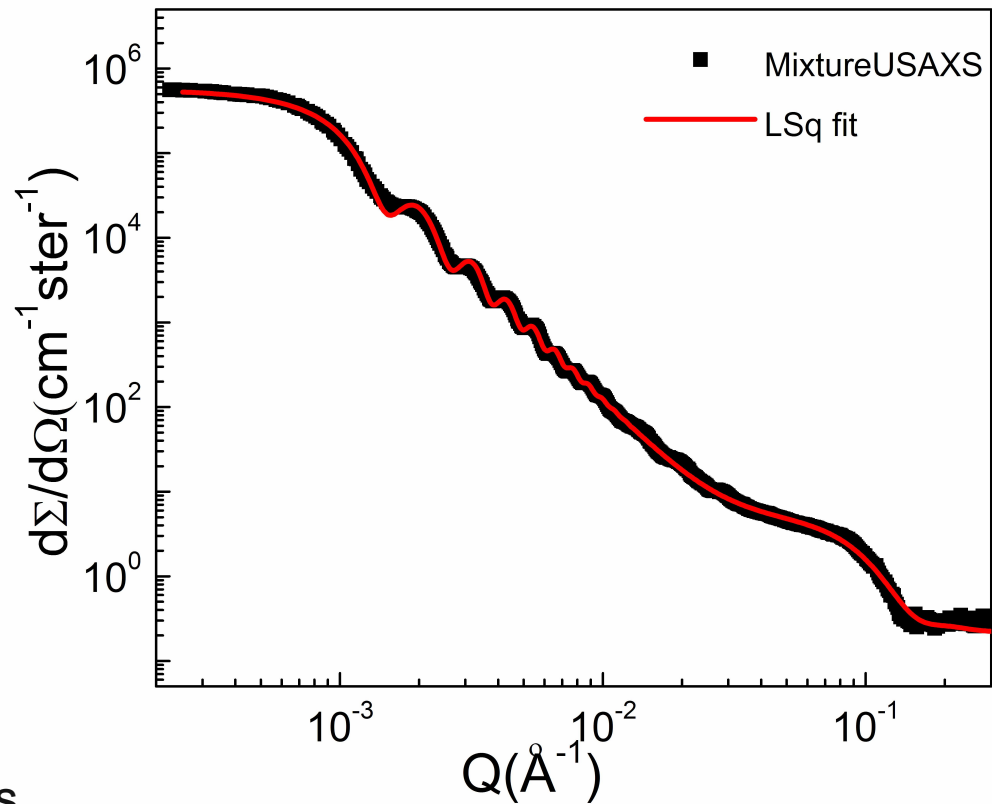
$$F(q) = \frac{3V_1(\rho_{\text{micro}} - \rho_s)J_1(qR_1)}{qR_1} + (\rho_{\text{halo}} - \rho_s) \left[\frac{3V_3J_1(qR_3)}{qR_3} - \frac{3V_2J_1(qR_2)}{qR_2} \right]$$

Why it's legit

- R_1 fixed, from microsphere USAXS analysis.
- R_2 and R_3 allowed to go to R_1 during fitting.
- Considered the halo as a shell with a constant scattering length density nanoparticle
 - a) interference term (np-np) can be neglected from previous study
 - b) dynamic nature of the nanoparticle halo ensures the validity of a mean-field approach.
- Percus-Yevick pair-distribution function between haloed-microspheres
 - a) P-V applies to monodisperse particle with hard-wall potentials
 - b) Silica microspheres have a very narrow size distribution \rightarrow monodisperse
 - c) concentration of microsphere is low to ensure that interpenetration of halo can be neglected.

	Density (g/cm ³)	X-ray Scattering length density (10 ¹⁰ cm ⁻²)	Scattering contrast relative to solvent (10 ²⁰ cm ⁻⁴)
silica microspheres	2.25	18.94	91.77
zirconia nanoparticles	3.65	27.97	346.3
solvent	1.00	9.36	0

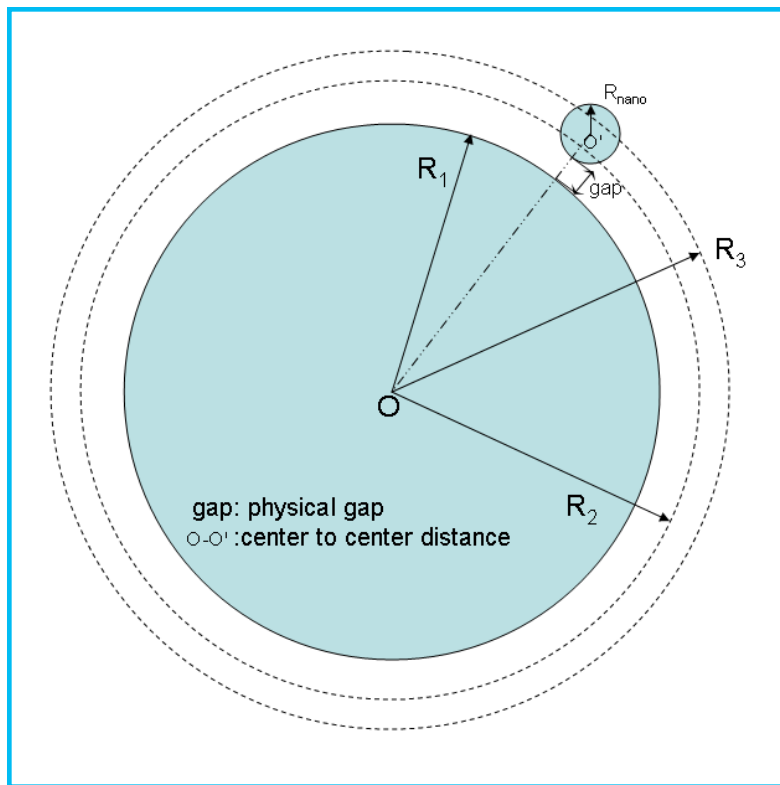
Least Square fit



Results

	R_1 (nm)	R_2 (nm)	R_3 (nm)	Halo Scattering Length Density (10^{10}cm^{-2})
silica microspheres	280.11	NA	NA	NA
binary mixture	280.11	284.02	285.63	10.92

The physical gap between nanoparticle and microsphere



$$\text{gap} = [\frac{1}{2}(R_2 + R_3) - R_{\text{micro}} - R_{\text{nano}}] = 2.15 \text{ nm}$$

Debye screening length

$$\kappa^{-1} = \sqrt{\frac{\epsilon_0 \epsilon_r kT}{2N_A e^2 I}} = 1.8 \text{ nm}$$

κ^{-1} is particle independent.

Physical gap \sim Debye length!!
This suggests that the electron cloud is partially intact.

Arrangement of nanoparticles in the halo

1. Number of nanoparticles in the halo

$$N_{nano} = L_{halo} / L_{nano} = \frac{(\rho_{halo} - \rho_{solv}) \frac{4}{3} \pi (R_3^3 - R_2^3)}{(\rho_{nano} - \rho_{solv}) \frac{4}{3} \pi R_{nano}^3} = 1935.$$

2. 2D volume fraction of nanoparticles in the halo

$$\phi_{area} = \frac{N_{nano} \pi R_{nano}^2}{4\pi \left((R_2 + R_3) / 2 \right)^2} = 0.039.$$

3. Nanoparticle separation distance with the halo

$$D = \left(\frac{\pi R_{nano}^2}{\phi_{area}} \right)^{1/2} = 22.9 \text{ nm} \approx 8.9 R_{nano}$$

4. Absolute intensity \rightarrow 93% nanoparticles in the solution, 7% in the halo.
 \rightarrow weak interaction between nanoparticles and microsphere.

Conclusions

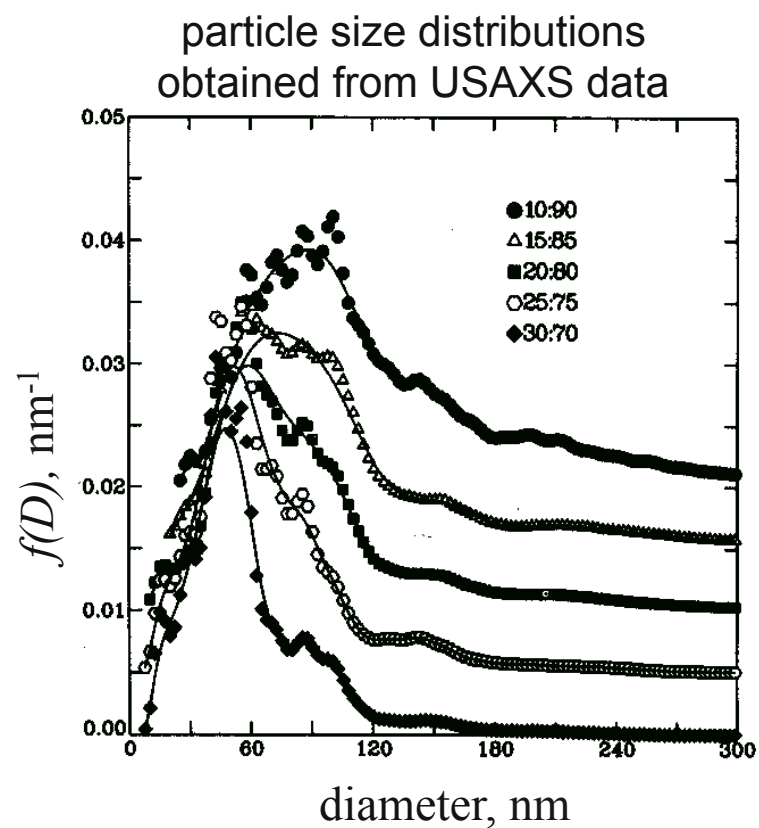
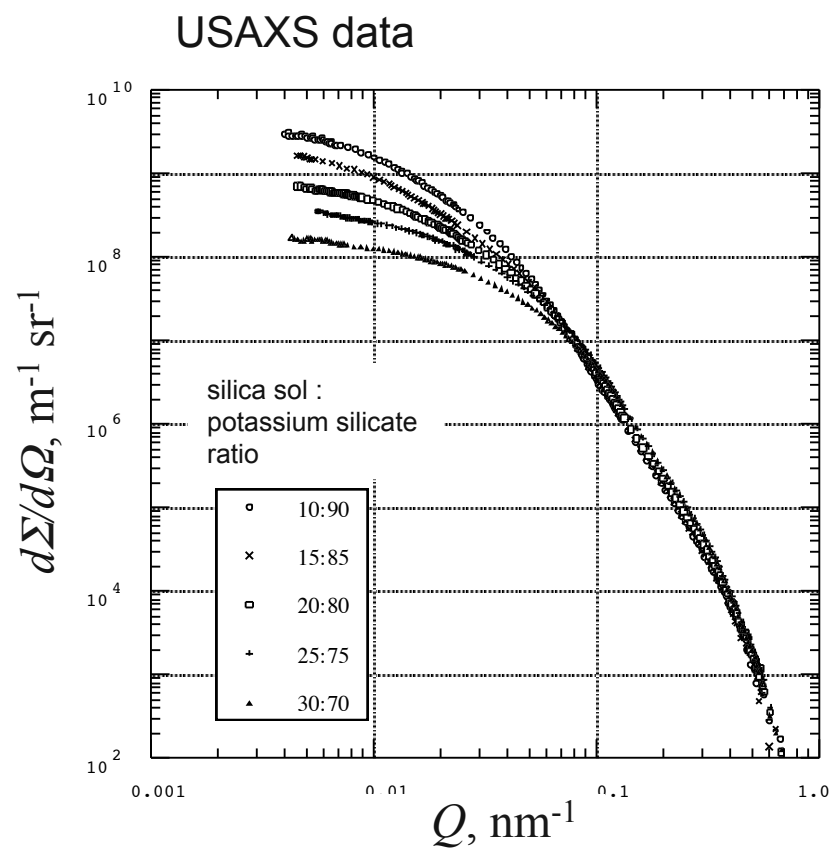
- The nanoparticles self-organize into a halo (or shell) that resides at a separation distance of ~ 2 nm from the microsphere surface, which is nearly equivalent to the Debye length of the solution.
- The nanoparticle concentration within this shell is significantly enriched relative to its bulk value in solution.
- The lateral separation distance between nanoparticles within each halo greatly exceeds their characteristic size .
- Most of the nanoparticles remain in the solution, which suggests that the attraction between nanoparticles and microsphere is weak.
- Offers better agreement with new theoretical insights than any other experimental methods. We believe that the advantage of SAXS is intrinsic.
- Dynamical scattering such as XPCS may shed more light.

Porous silica precursor bodies

- Prepared by sol-gel process
- Mixtures of colloidal silica and potassium silicate
- Microstructure: array of particles, small clusters, and aggregates of colloids
- USAXS and SANS to characterize polydisperse size distributions of particles in porous medium as function of mixture ratio

Long, et al., *J Appl Cryst* **23.6** (1990) 535

Microporous silica results



Long, et al., *J Appl Cryst* 23.6 (1990) 535

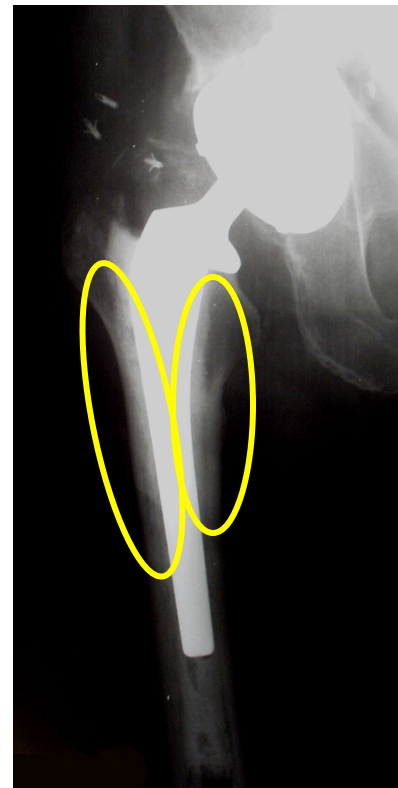
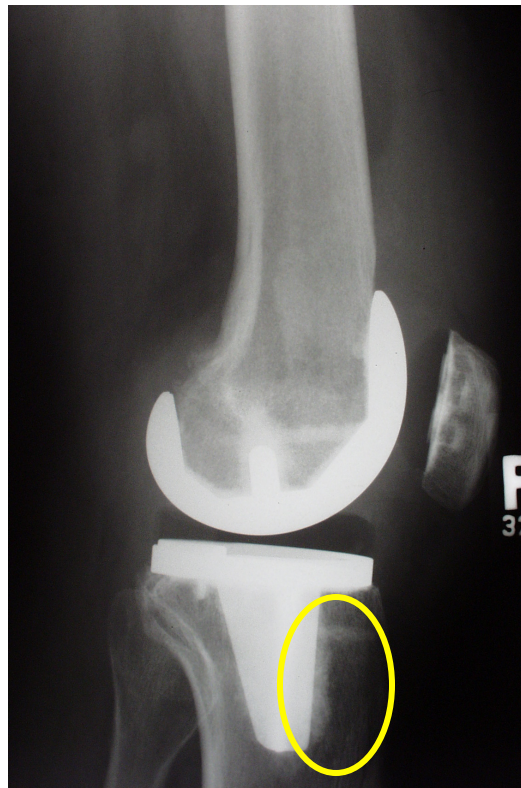
Fracture Toughness of PMMA Bone Cement Containing Particulate Fillers

Anuj Bellare, PhD, Wolfgang Fitz, MD, Andreas Gomoll, MD, Richard D. Scott, MD, Thomas S. Thornhill, MD,
Department of Orthopedic Surgery, Brigham and Women's Hospital, Harvard Medical School, Boston, MA

Total Knee and Hip Replacement Prostheses



Barium Sulfate Particulate added to PMMA as Radiopacifier



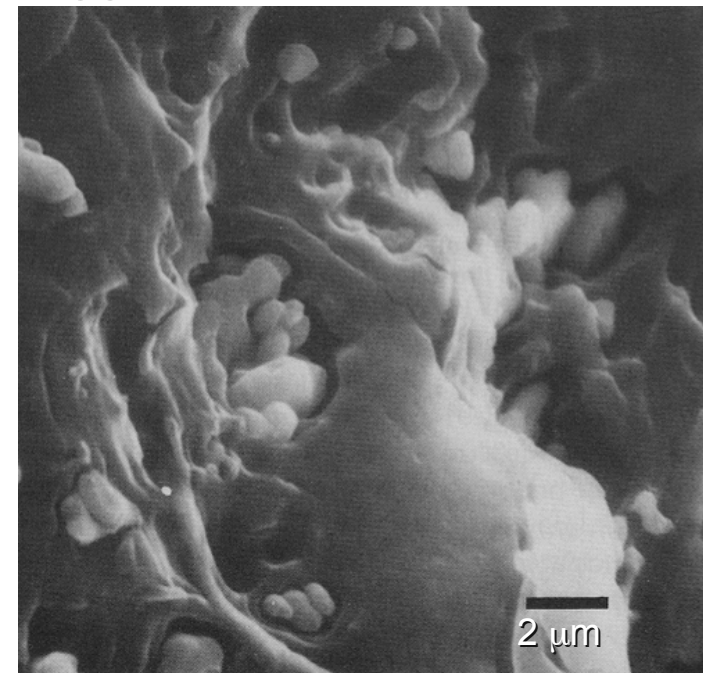
Bellare, private communications

Radiopacifier Weakens the Bone Cement

Various Bone Cements	Impact Strength (J)
Simplex	0.333± 0.02
Palacos R	0.402± 0.03
Palacos K	0.382± 0.03
CMW – 0	0.578± 0.06
CMW+4% BaSO ₄	0.323± 0.03
CMW+8% BaSO ₄	0.274± 0.03
CMW+4.2% Erythrocyne	0.461± 0.03
CMW+8% BaSO ₄ +4.2%Ery	0.372± 0.03

de Wijn et al, Acta Orthop Scand, 1975

agglomeration

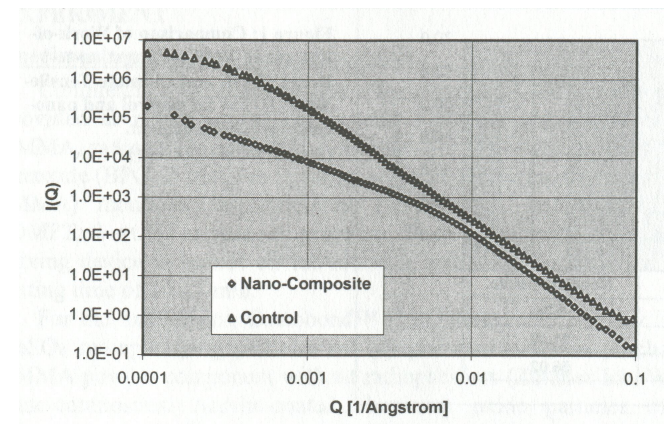
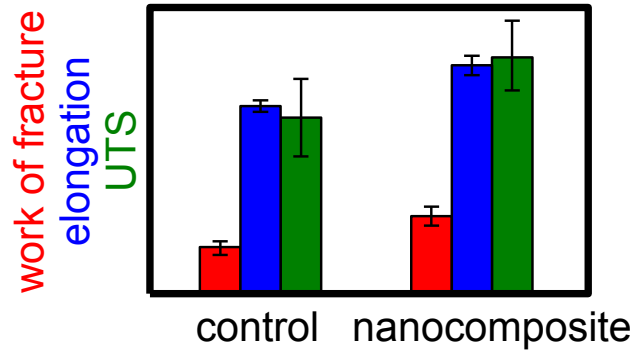
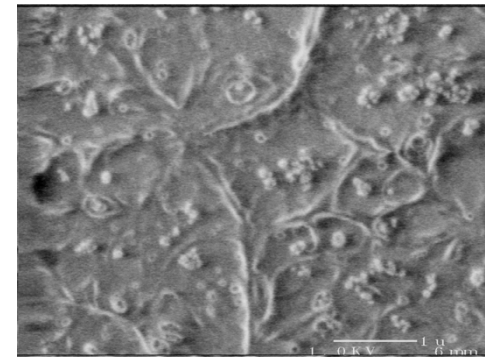
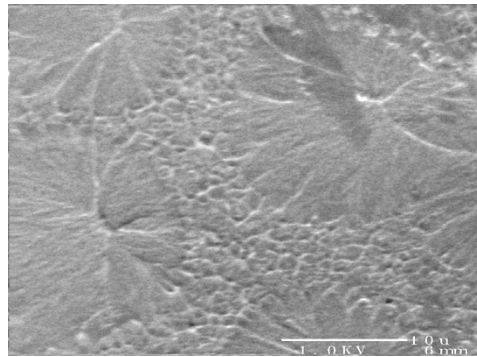


Topoleski et al, J. Biomed Mater. Res., 1990

Nanocomposite Bone Cement

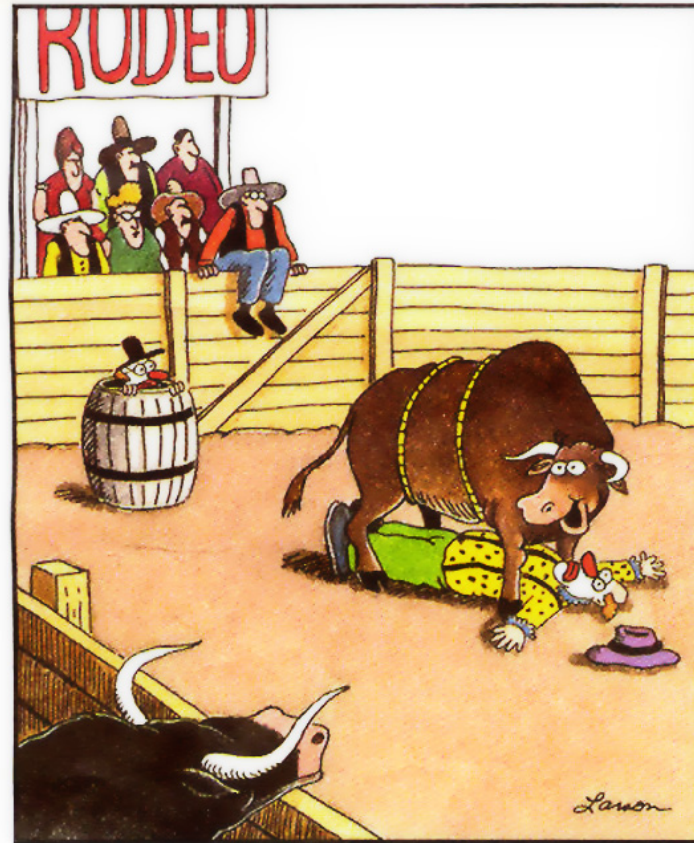
Gomoll, et al., MRS, Vol. 581, (2000) 399

Improved dispersion using nanoscale particulate and surfactant while maintaining radiopacity



Anomalous scattering – technique looking for a problem?

Hey!
I got one!
I got one!



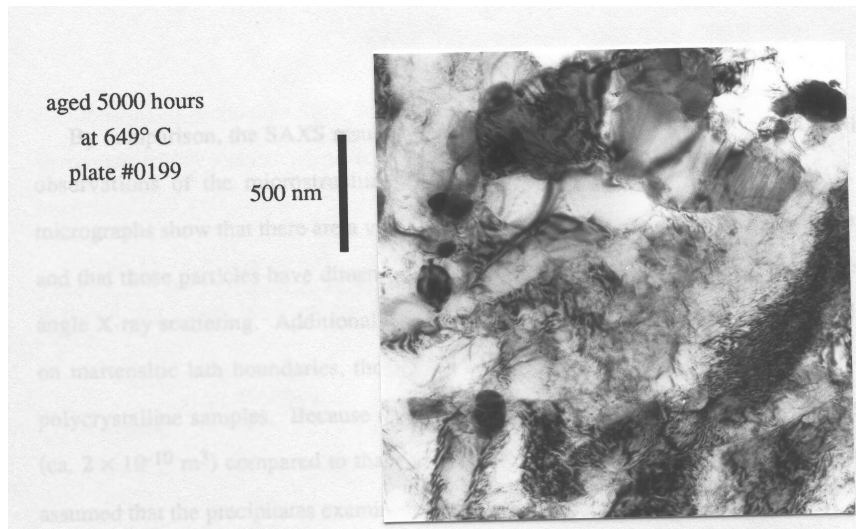
"Hey! I got one! I got one!"

Gary Larson, *The Far Side*

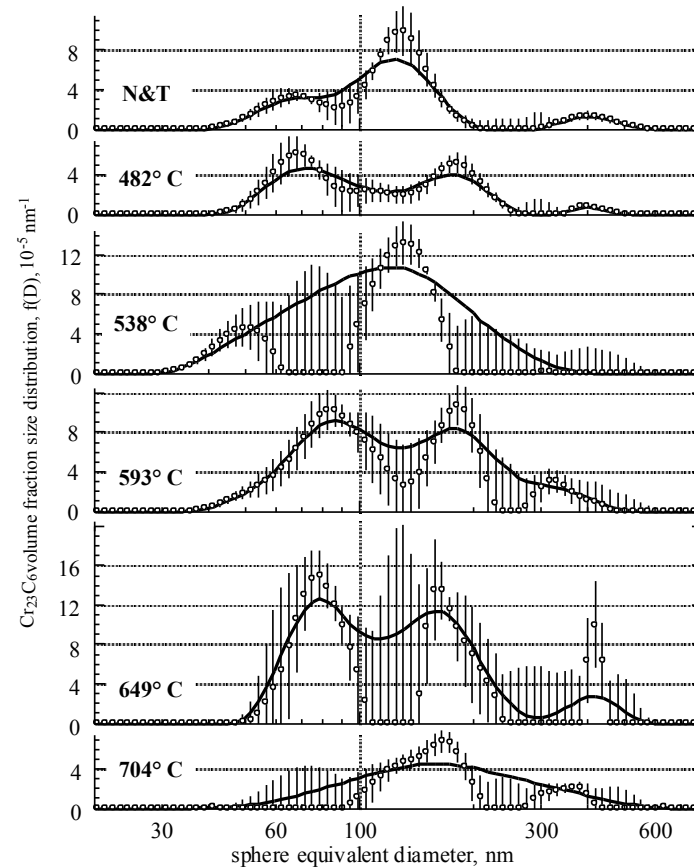
Stability of Modified Fe9Cr1Mo Steel at High Service Temperatures

- Ferritic steel developed at ORNL (1983), proposed for use in power-generation at elevated temperatures
- Attractive properties
 - High temperature use in corrosive environments
 - high rupture strength at both room and elevated temperatures
 - good weldability
 - low thermal expansion
 - resistance to radiation-induced void swelling
- Cr_{23}C_6 , VC, and NbC present

Chromium Carbide Distribution in Modified Fe9Cr1Mo steel by ASAXS



Volume-fraction size distributions of Cr_{23}C_6 in Modified Fe9Cr1Mo steel, determined by the ASAXS gradient method. The vertical bars represent the margin of error. The solid line is spline smoothed.



Jemian, Ph.D. Thesis, 1990, Northwestern

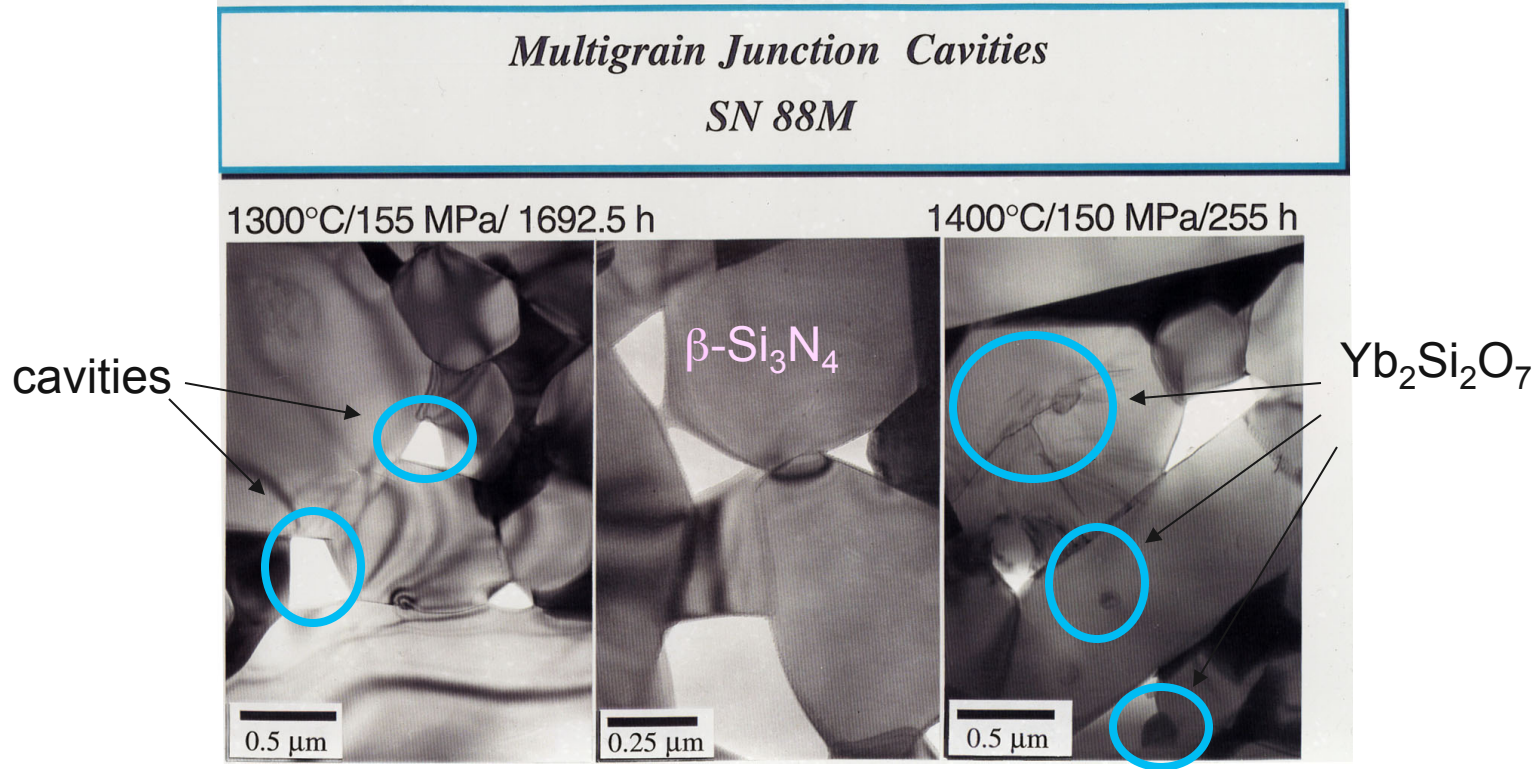
Tensile Creep Resistance of Commercial Silicon Nitride

- Prime candidate for structural components in advance gas turbines at high turbine inlet temperatures
- Creep compromises excellent high-temperature mechanical properties
- Cavitation possibly most important mechanism resulting in creep deformation
- Evolution of secondary phase pockets not previously studied due to lack of suitable technique
- Earlier USAXS showed deformation occurs via cavity accumulation at multigrain junctions
- Follow evolution of Yb-rich secondary phase pockets and voids as a function of creep testing using A-USAXS

Silicon Nitride Microstructure

- commercial grade of gas-pressure sintered silicon nitride (designated SN88)
- β - Si_3N_4 grains
- major crystalline secondary phase after heat treatment is ytterbium disilicate, $\text{Yb}_2\text{Si}_2\text{O}_7$
- minor phases include residual $\text{Yb}_4\text{Si}_2\text{N}_2\text{O}_7$, $\text{Y}_5\text{Si}_3\text{NO}_{12}$, residual SiO_2 glass, and porosity

Tensile Creep Resistance of Commercial Silicon Nitride

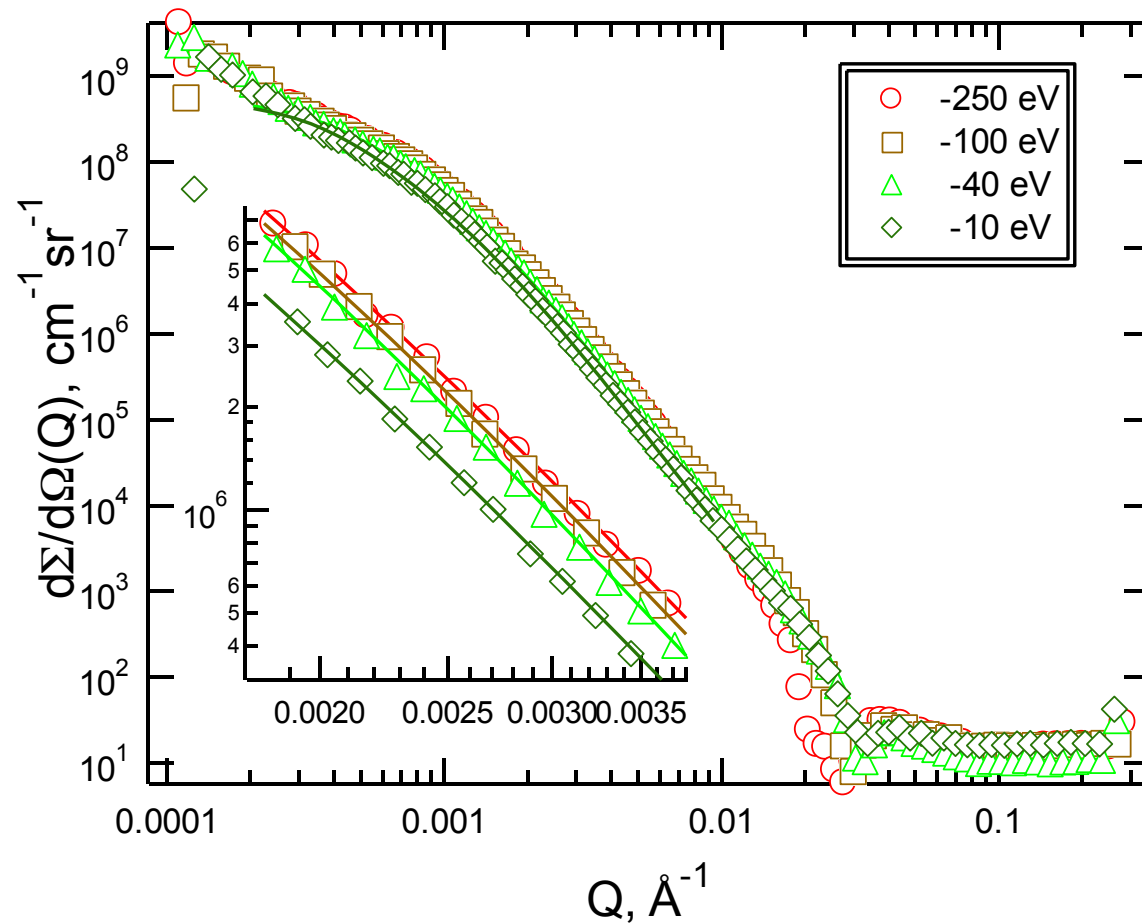


- commercial grade of gas-pressure sintered silicon nitride (designated SN88)
- β -Si₃N₄ grains
- major crystalline secondary phase after heat treatment is ytterbium disilicate, Yb₂Si₂O₇
- minor phases include residual Yb₄Si₂N₂O₇, Y₅Si₃NO₁₂, residual SiO₂ glass, and porosity

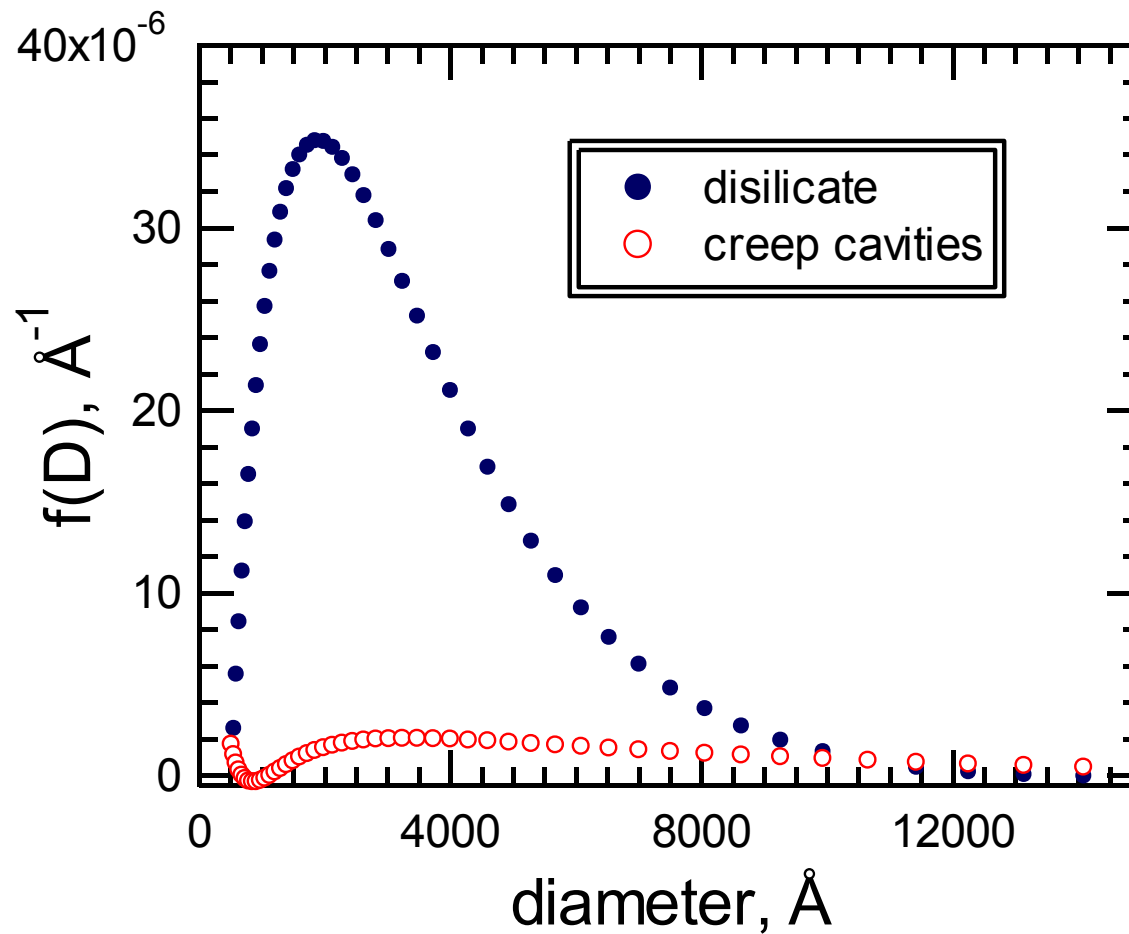
Silicon nitride SN-88 samples

- Five tensile creep tests
- Different test times: 30 s – 85 h
- 1400° C, 150 MPa load
- Tests interrupted and cooled under load
- A-USAXS samples ground and hand-polished
- Sample from undeformed grip, 180 μm
- Sample from gage parallel to stress axis, 100 μm

A-USAXS near the Yb L_{III} edge from SN-88 tensile creep sample, 50 h



Yb disilicate and tensile creep cavity size distributions from SN-88



Creep strain and cavitation in SN-88

J. Eur. Ceram. Soc. 22 [14-15] 2479-2487 (2002).

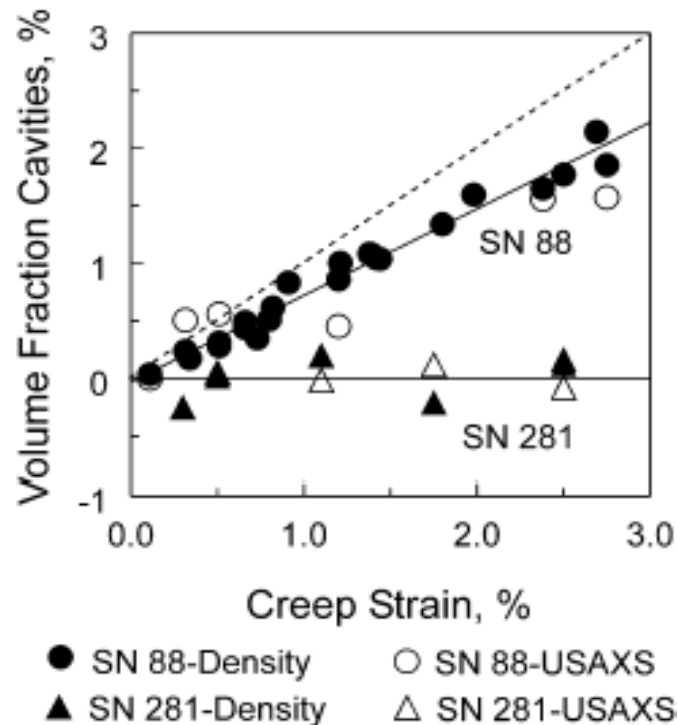


Fig. 6. A comparison of the dependencies between strain and volume fraction of cavities determined from USAXS and density change measurements in SN 281 and SN 88.^{16,30} The contribution of cavities to tensile strain in SN 281 is close to zero while it is around 70% in SN 88.

Conclusions: SN88 A-USAXS study

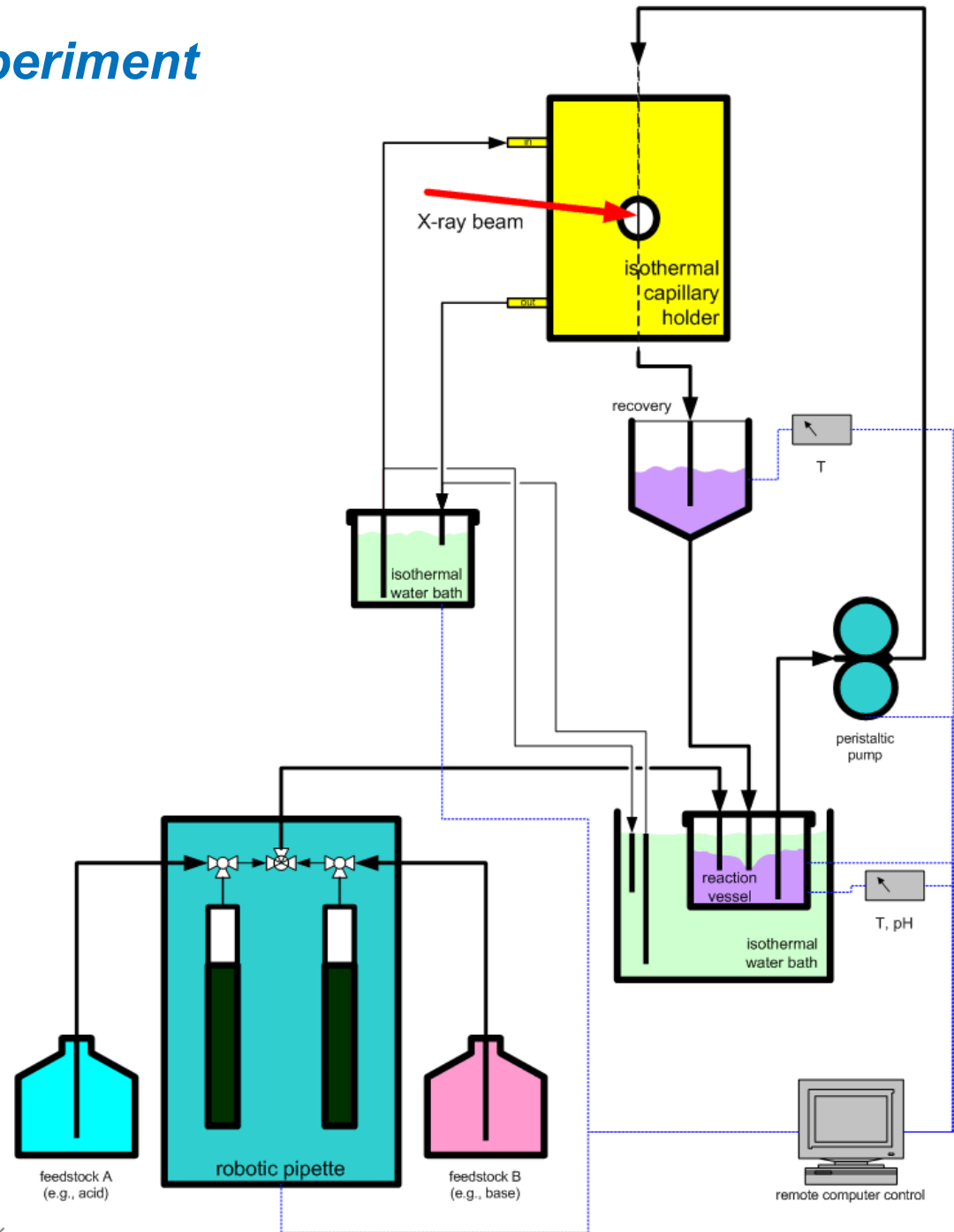
- A-USAXS used to determine simultaneously Yb disilicate and creep cavity size distributions in SN-88
- Yb disilicate and creep cavities were of comparable size
- V_v of Yb disilicate 5-8 times greater than V_v of creep cavities
- V_v of creep cavities proportional to tensile strain, slope = 1
- Good agreement with density change data
- Confirmation that cavitation is the main creep mechanism
- A-USAXS obtained statistically-significant measurements of Yb-rich secondary phase pockets during creep in the presence of a creep cavity population of similar dimensions

Time resolved SAXS

In situ ultrasmall-angle X-ray scattering study of solution-mediated precipitation of nanocrystalline ceria

Flow cell for this experiment

- isothermal experiments at 20, 25 and 35 °C
- reaction changes followed for up to 10 h
- periodic scans selected for modeling to represent observable reaction time line
- pH and temp recorded continuously



In situ ultrasmall-angle X-ray scattering study of solution-mediated precipitation of nanocrystalline ceria

A. J. Allen¹, V. A. Hackley¹, P. R. Jemian², J. Ilavsky², J. Raitano³ and S-W. Chan³

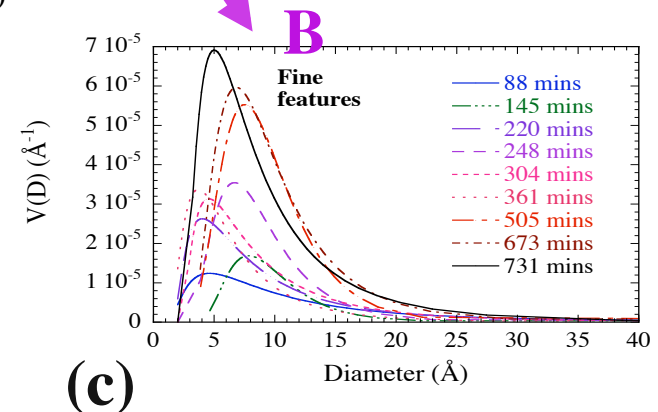
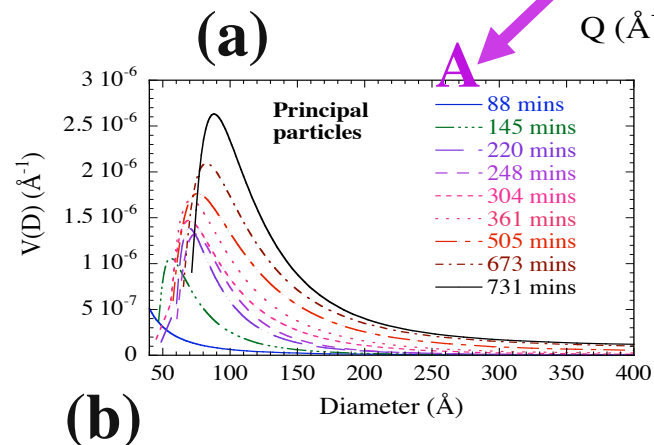
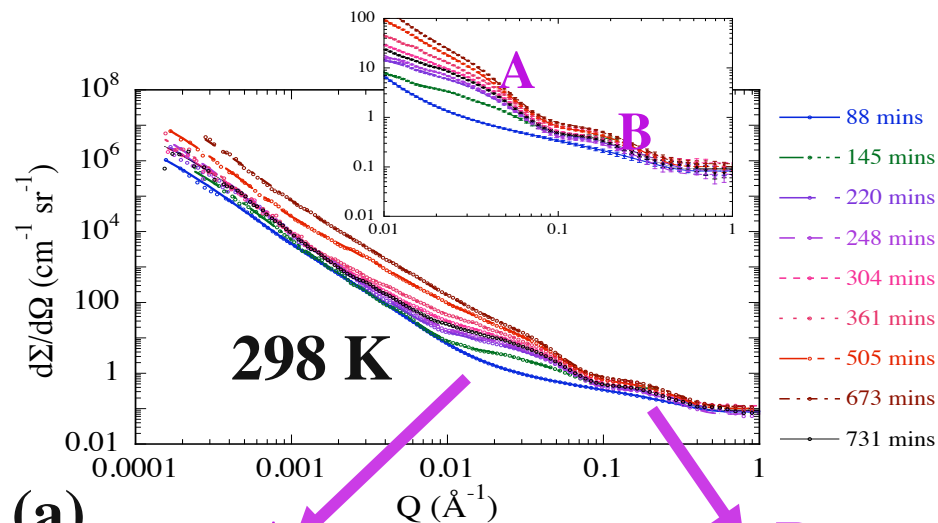
¹National Institute of Standards and Technology, Gaithersburg, MD 20899-8520

²Advanced Photon Source, Argonne National Laboratory, Argonne, IL 60439

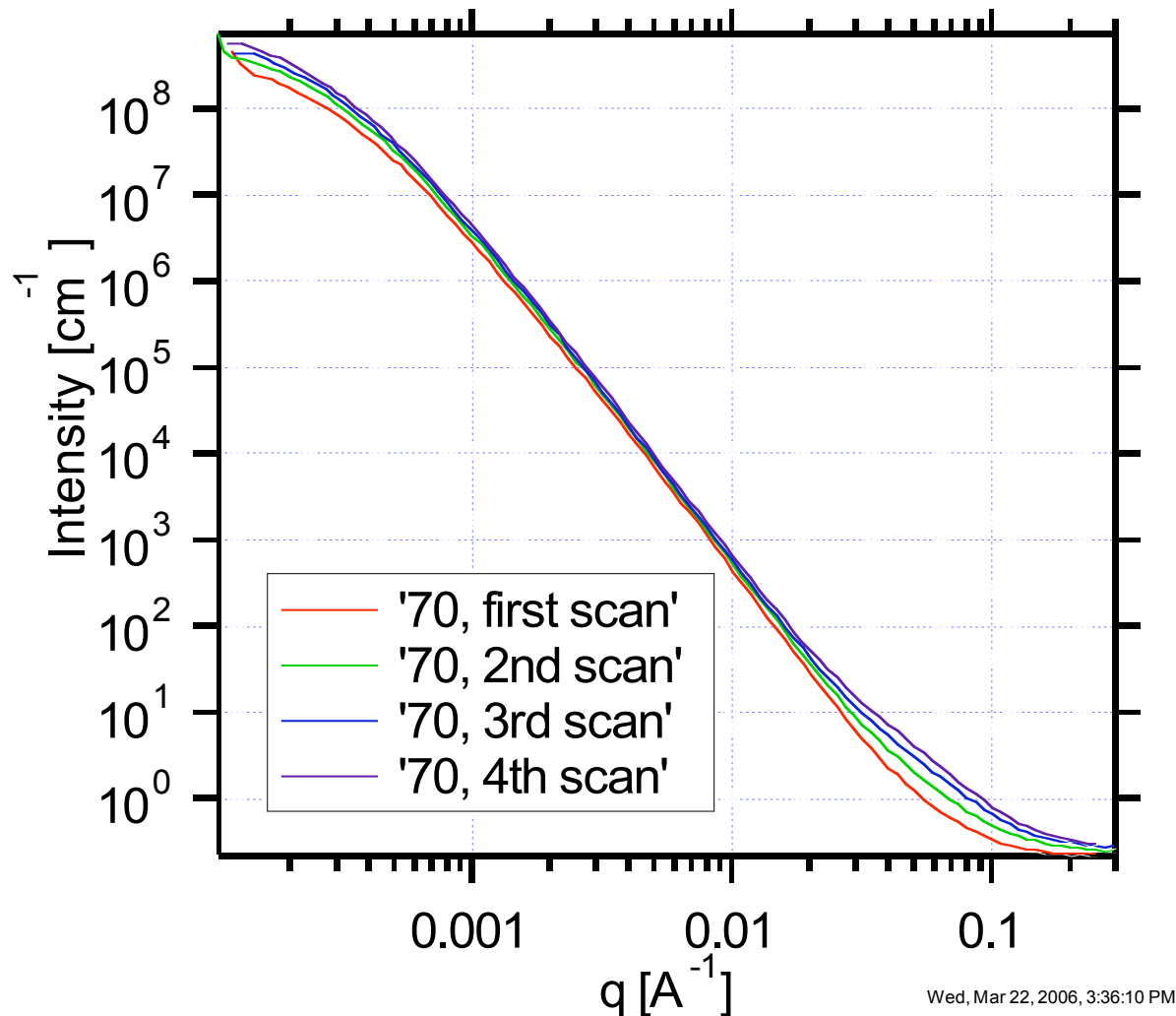
³Columbia University, New York, NY 10027

•Nano-CeO₂ has important potential applications:

3-way catalysts for vehicle emissions, SOFC electrolytes, gas sensors, optical coatings, CMP slurries, etc.

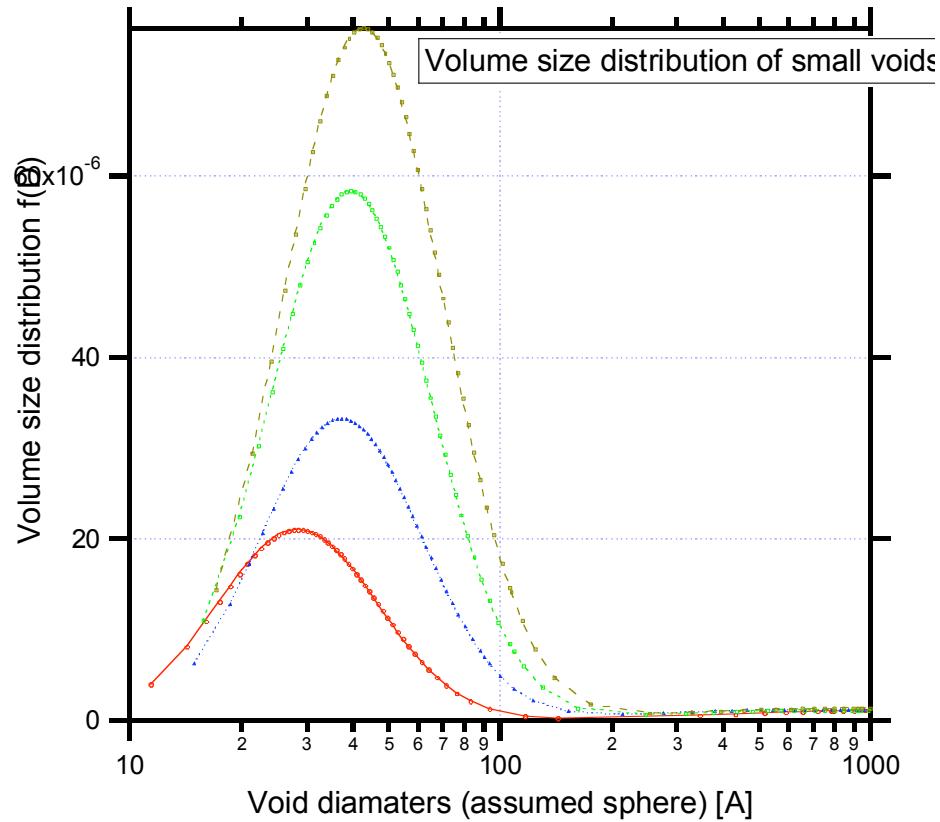


High explosives

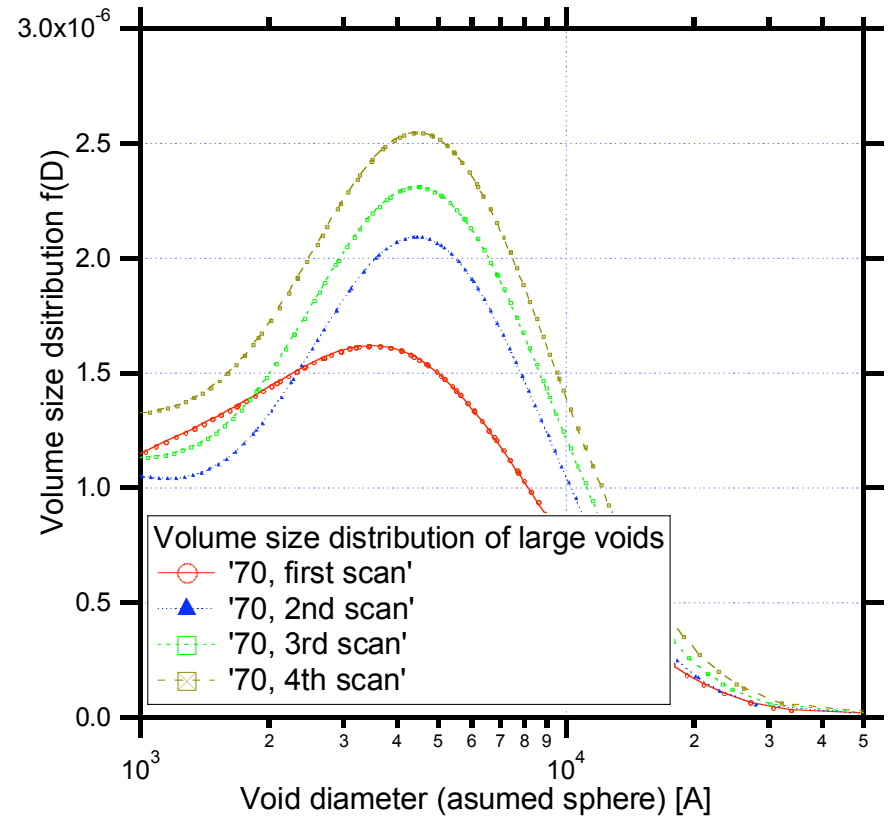


USAXS data from in situ measurements of highly insensitive energetic materials based on 1,3,5-triamino-2,4,6-trinitrobenzene (TATB). Various TATB formulations experience an irreversible volume growth event that is a function of both temperature and time, generally referred to as ratchet growth. This affects significantly the detonation velocity of these highly insensitive explosives. Of particular concern are the voids in the nanometer to micron size scale intrinsically associated with the detonation process. Such small porosity in bulk material is not easily investigated using various techniques, however, ultra small angle scattering (USAXS) technique is ideally suited for characterization of structure on this scale in energetic materials. Presented data are from in situ experiment, each scan represents one thermal cycle between -30C and 80C. Graph is from work performed by Trevor M. Willey, Tony van Buuren, and Jonathan R. I. Lee, LLNL.

High explosives



Small voids



Large voids

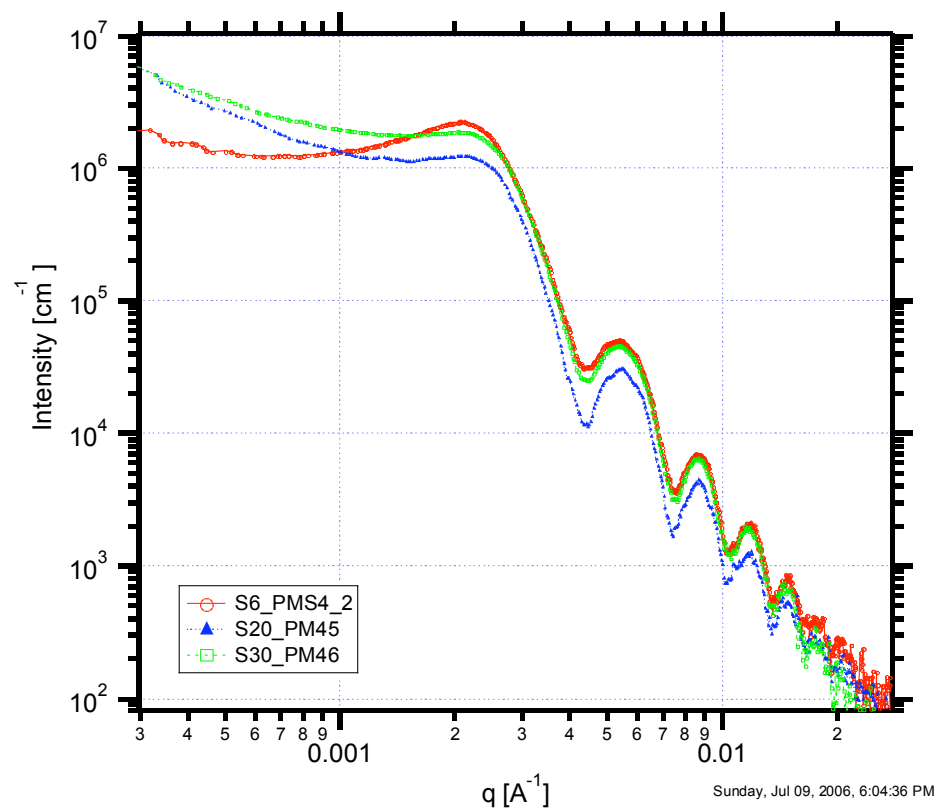
Quantitative results for large voids are very important for ratchet growth modeling efforts by LLNL. Nano voids were not known before...

Colloidal microstructures

- Use 2-D collimated USAXS to study structure of colloidal suspensions for spherical & anisotropic submicron particles.
 - High q resolution
 - Access to low q
 - Large q and intensity range
- Colloidal microstructure and macroscopic properties are closely linked.
- Simulations suggest physically and chemically anisotropic colloids assemble into unique microstructures, not obtained with spheres.^{1,2}
- USAXS on concentrated nonspherical colloids and spheres, shows nonspherical colloids form a rotator phase with translational but no orientational order, and as volume fraction, ϕ , is increased form an orientationally ordered crystal.

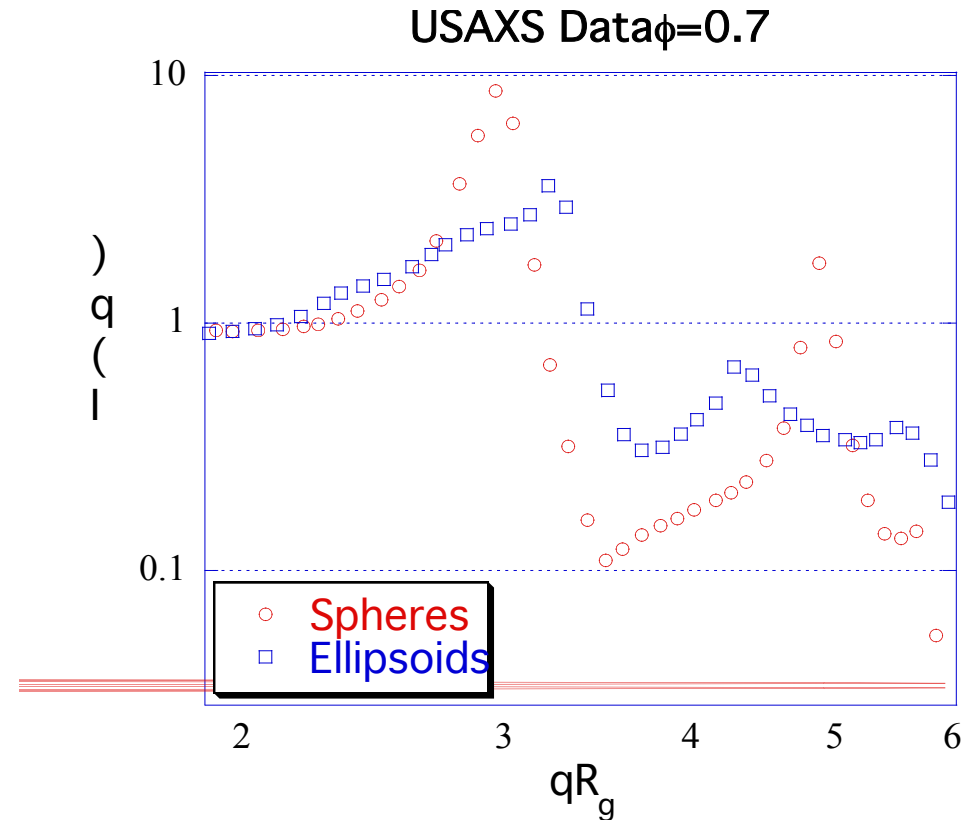
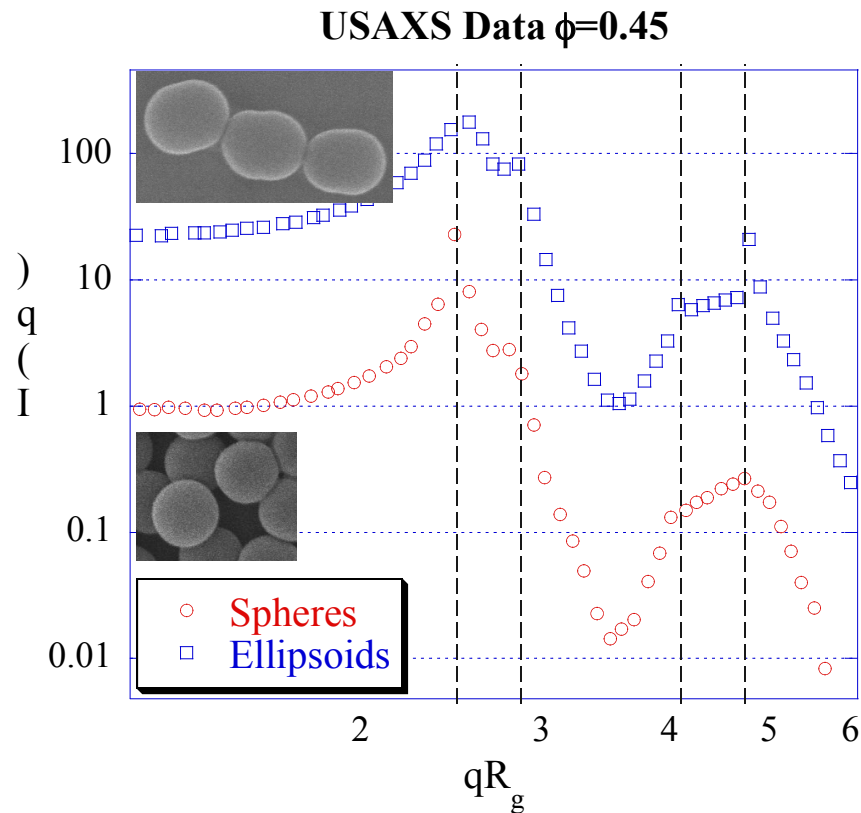
¹ Horsch, M. A. et al. *Phys. Rev. Lett.* **2005**, 95, (5), 056105.

² Vega, C.; Monson, P. A. *J. Chem. Phys.* **1997**, 107, (7), 2696-2697.



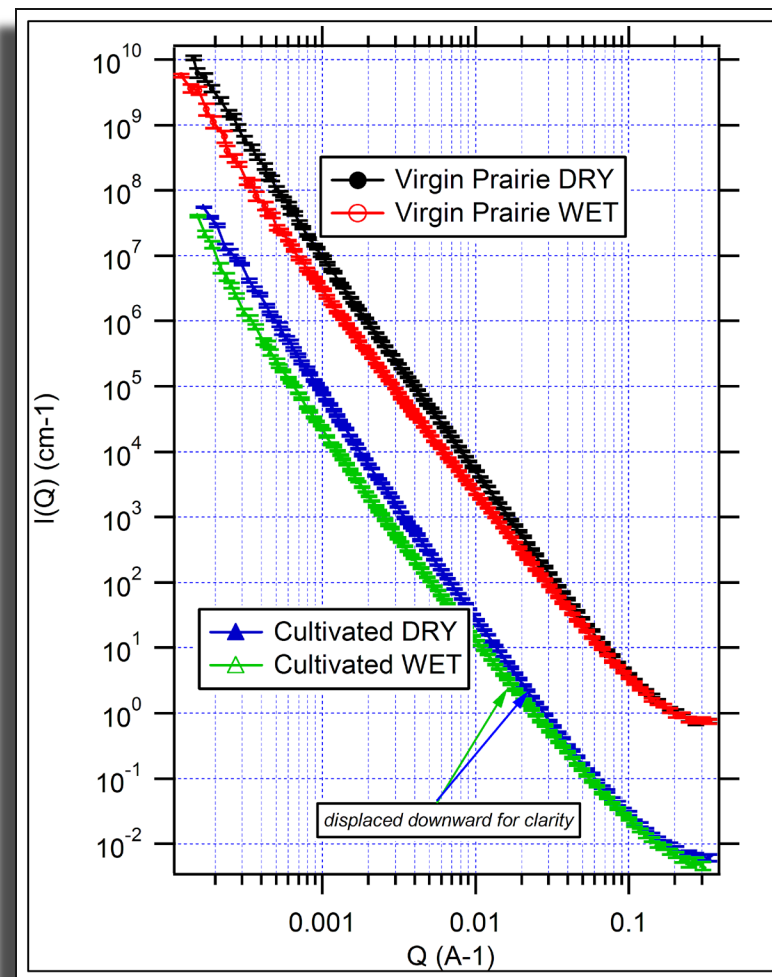
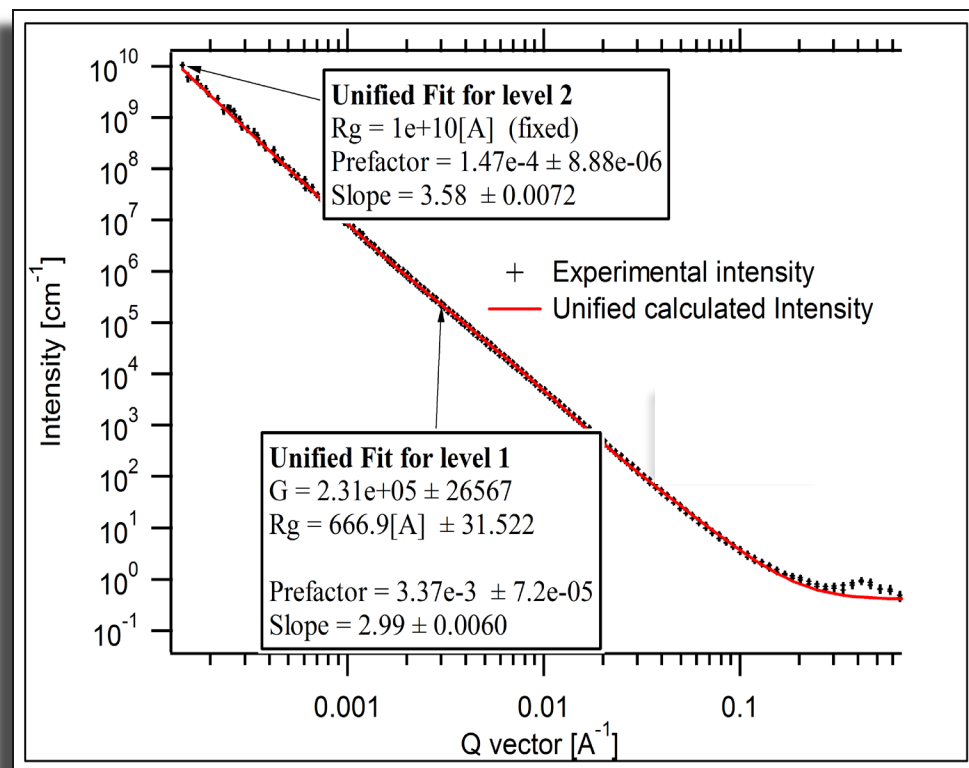
**Univ. of Illinois Urbana-Champaign group
(C. Zukoski, Eric Mock, et al.)**

Colloidal microstructures



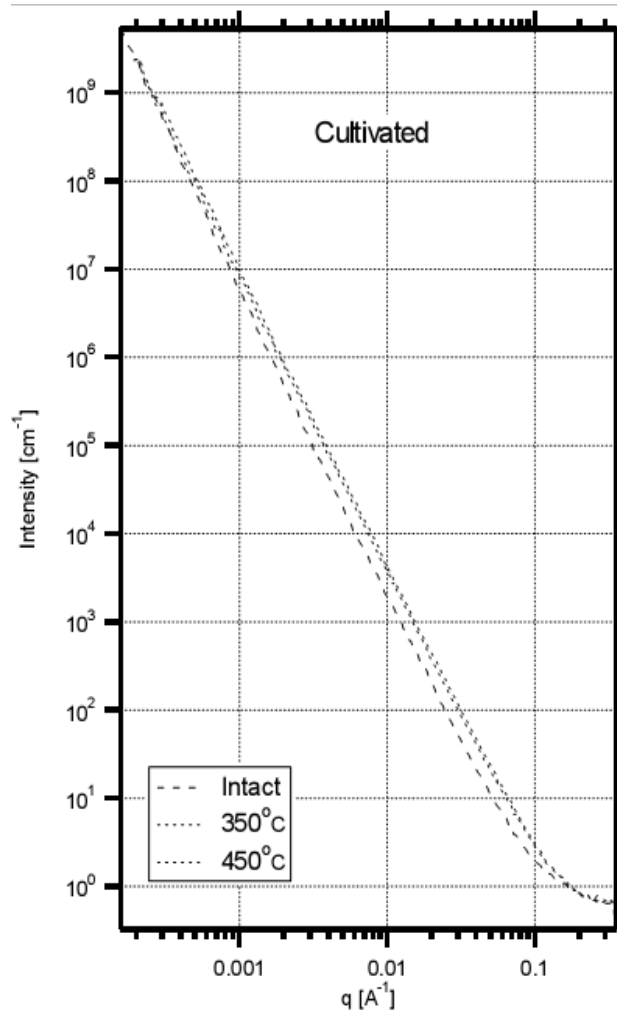
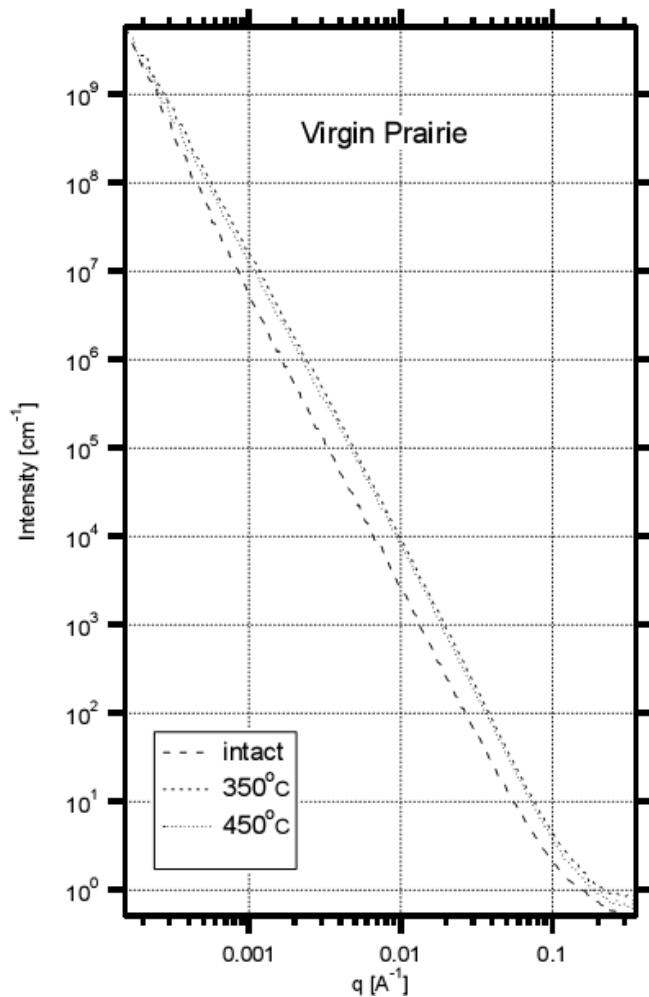
R_g is obtained using a Guinier analysis of the dilute suspension scattering. Fraction $\phi=0.45$ (note: particles are charged) results indicate that the ellipsoids are ordering into a crystal that is similar to structure of the spheres "rotator phase" where the particles will be disordered orientationally, but their centers of mass will be in a cubic arrangement like spheres. For $\phi=0.7$ the Bragg peaks are at different positions indicating that the system is forming a crystal where the particles are orientationally ordered. This may be the first case when these colloid phases were actually experimentally observed.

SAS from Soils – fractal scatterer over many decades



John McCarthy et al.

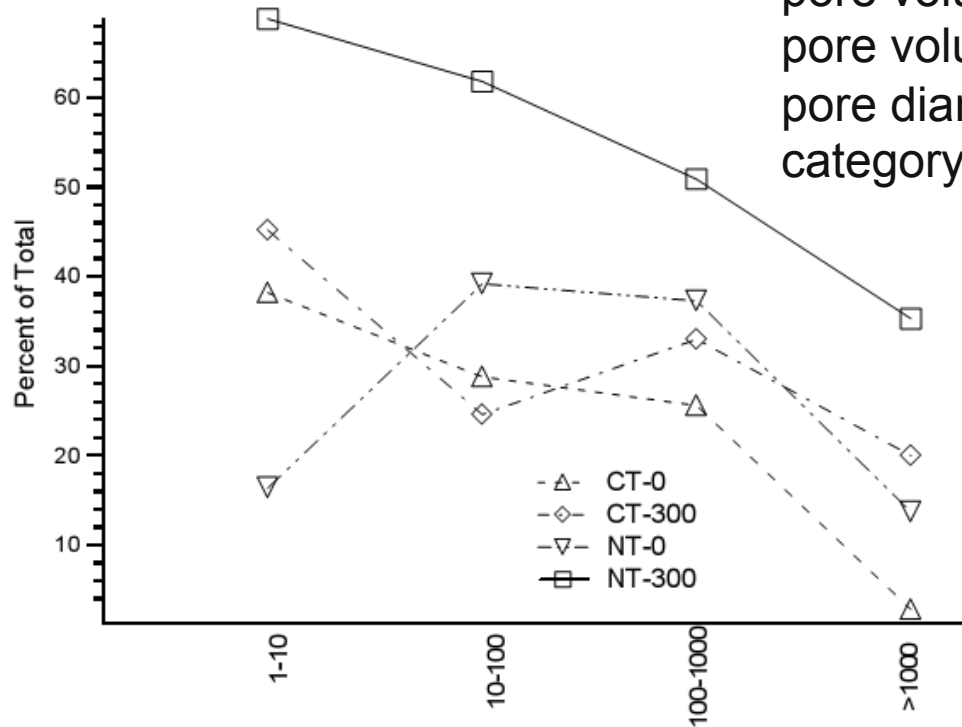
Soils – voids and organic matter structure



Prairie soils can contain significantly more organic matter than farmed (cultivated) soils. It is not known why, what the difference in organic matter arrangements are. By studying samples with organic matter and after burning off the organic matter over wide q /intensity range (including USANS) we were able to quantitatively find organic matter location.

Soils - results

Unique result: Relative abundance (as %) of the organic matter filled pore volume relative to the total pore volume within decade-wide pore diameter (in nm) size category.

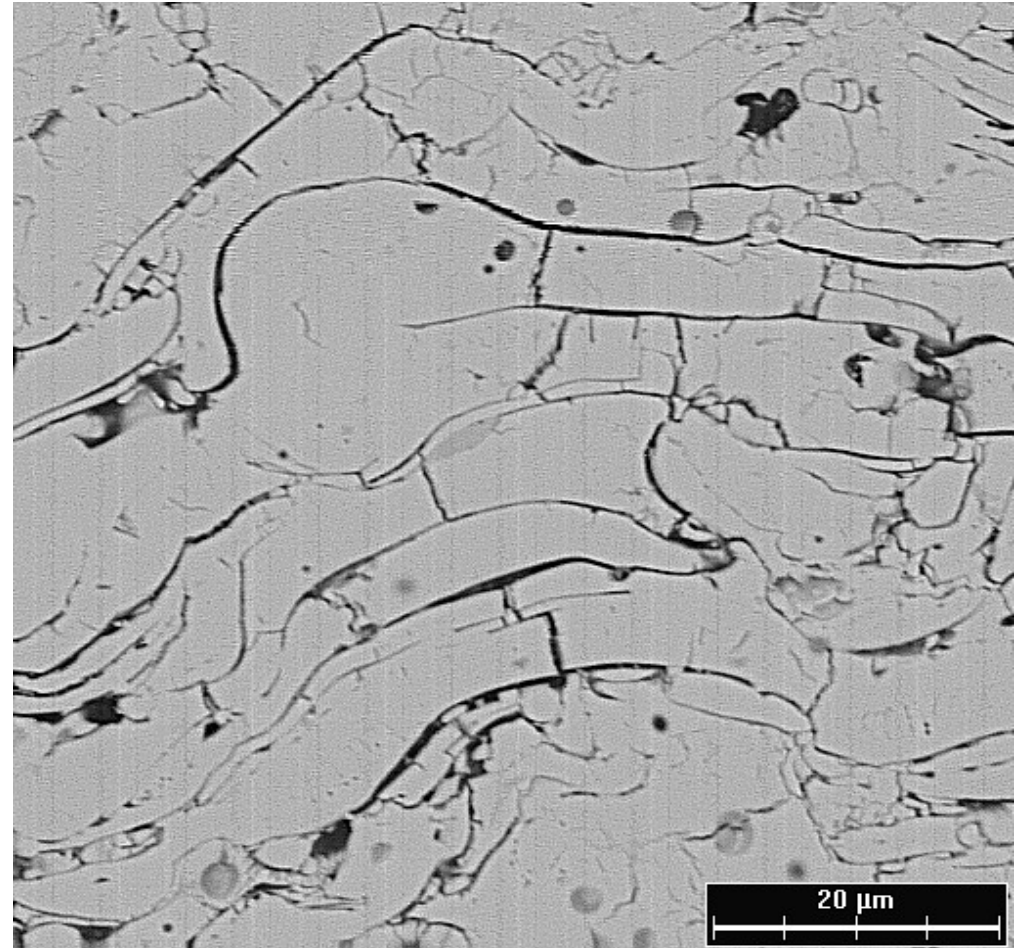
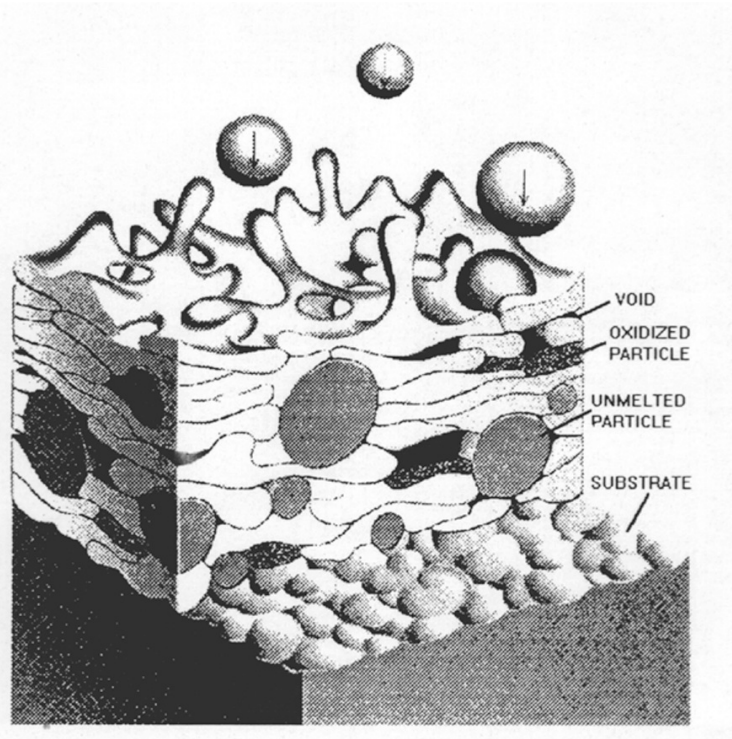


From: “Protection of Organic Carbon in Soil Microaggregates Occurs via Restructuring of Aggregate Porosity and Filling of Pores with Accumulating Organic Matter”, John F. McCarthy, Jan Ilavsky, Lawrence M. Mayer, Julie D. Jastrow, Edmund Perfect, and Jie Zhuang (submitted)

Anisotropic Small-angle scattering

- Porod (surface) scattering
- Multiple scattering
- Single scattering

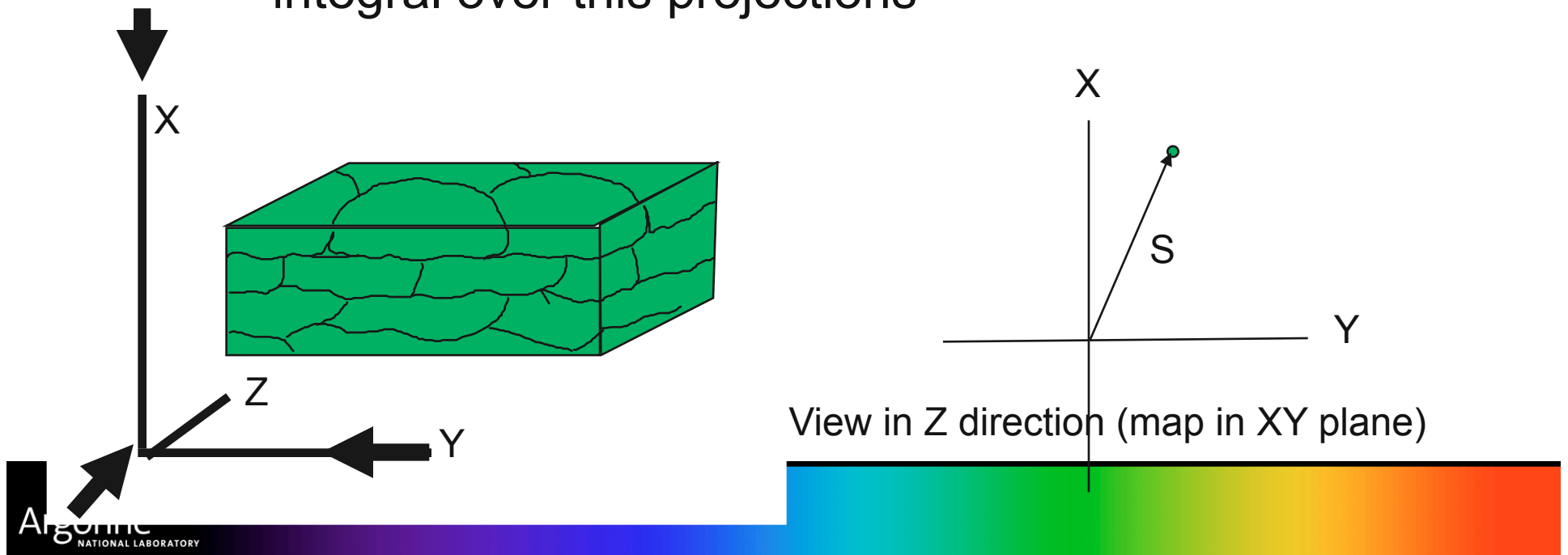
- Example: Plasma sprayed deposits



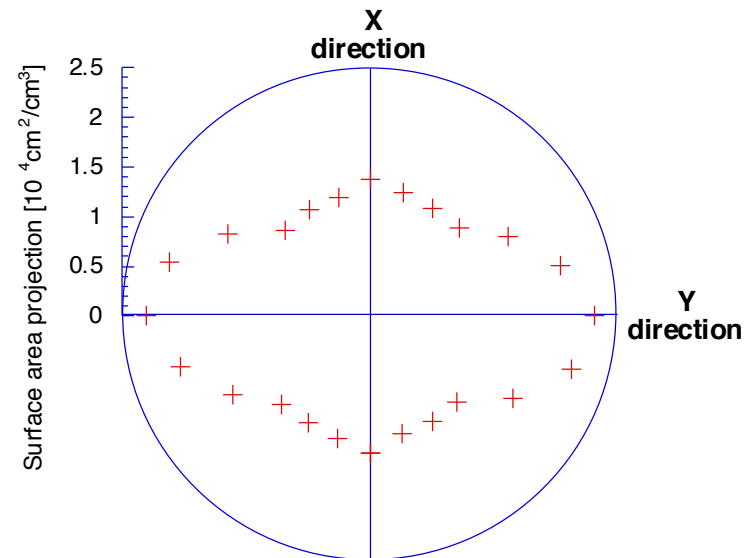
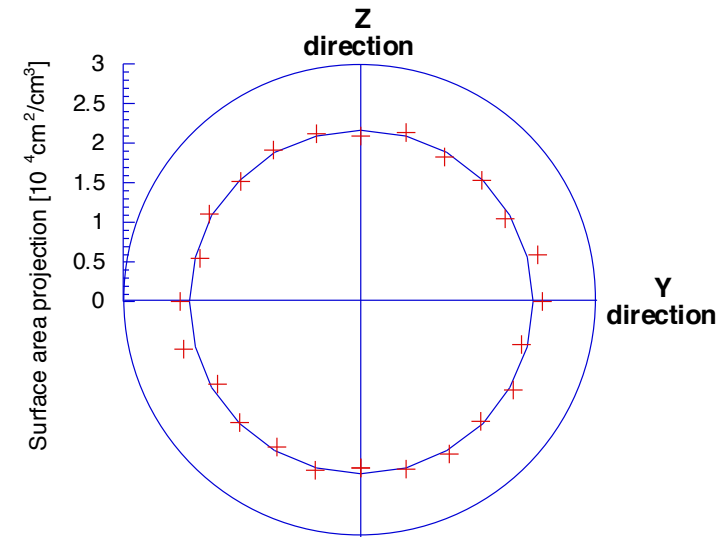
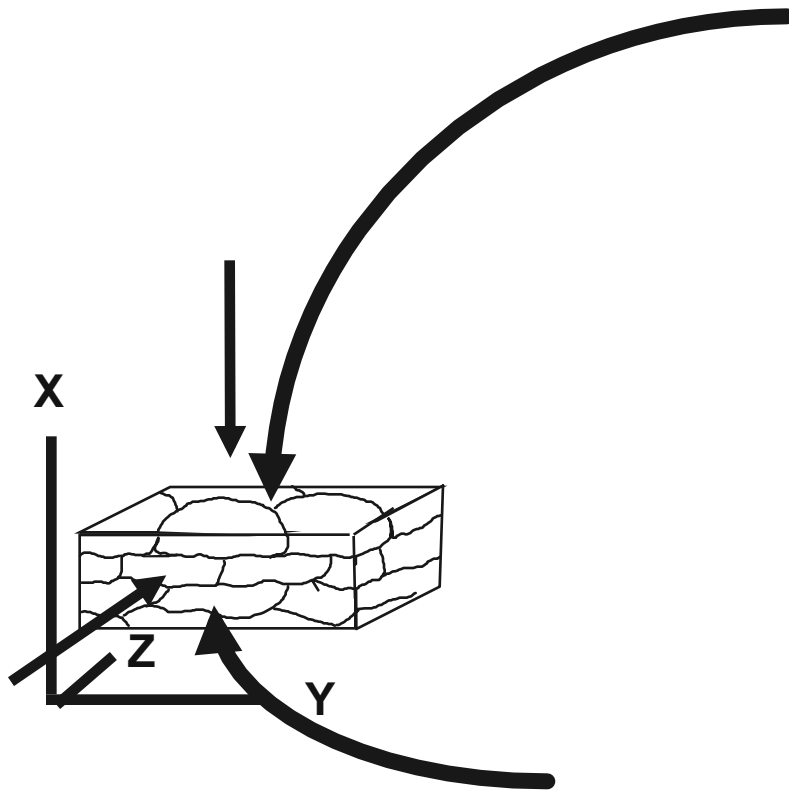
Anisotropic POROD scattering

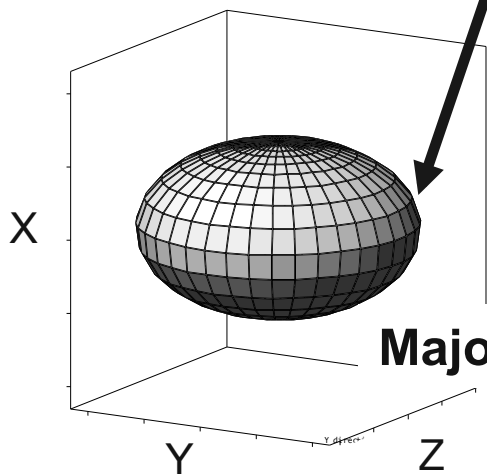
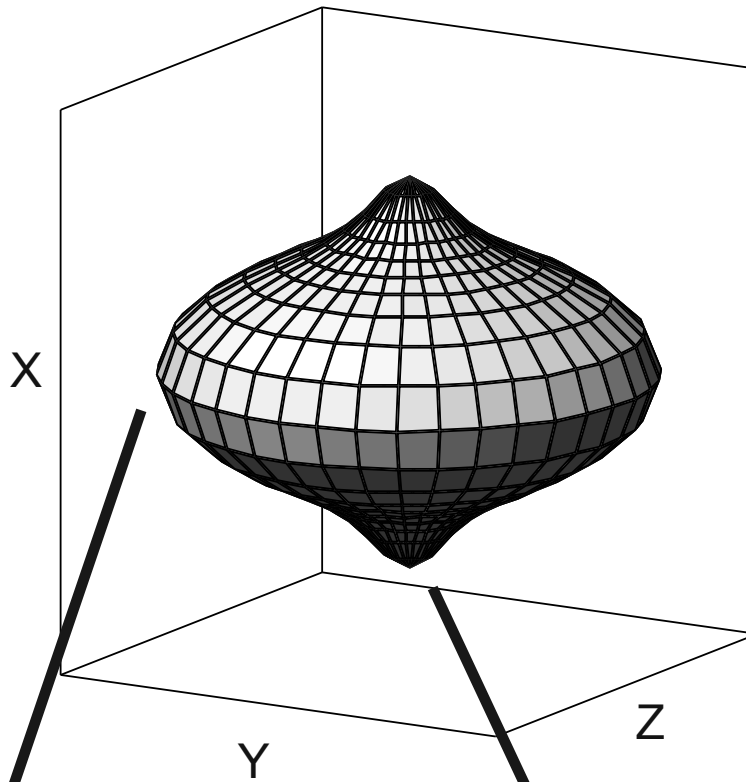
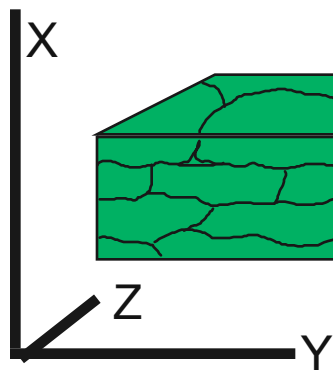
Specific surface area and its anisotropy

- The technique yields projections of the void surfaces in the plane perpendicular to the scattering vector direction - “surface maps”
 - *projected surface area = distance from origin*
 - *scattering vector orientation = direction in the graph*
- Real absolute surface area is the 3 dimensional integral over this projections

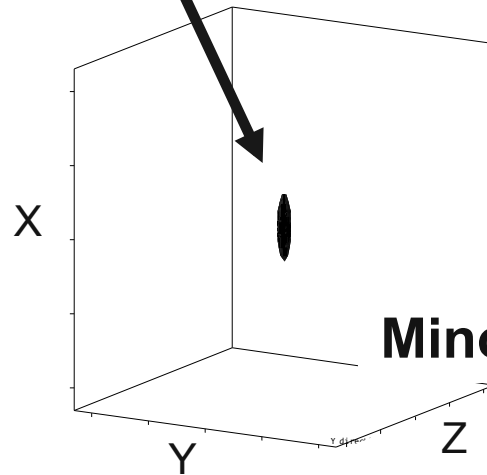


■ Surface area maps in different planes

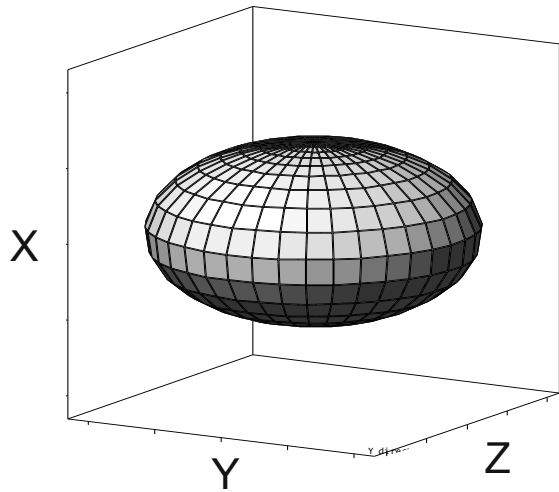




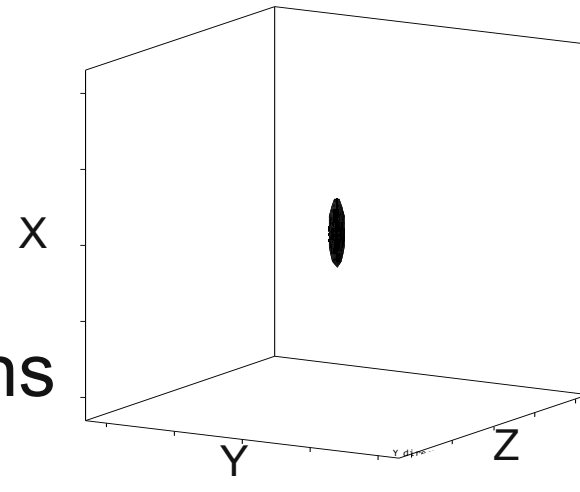
Major component



Minor component



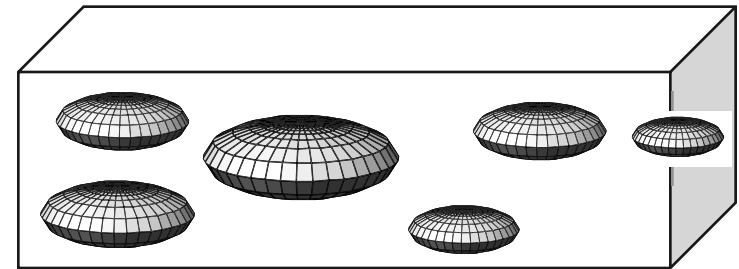
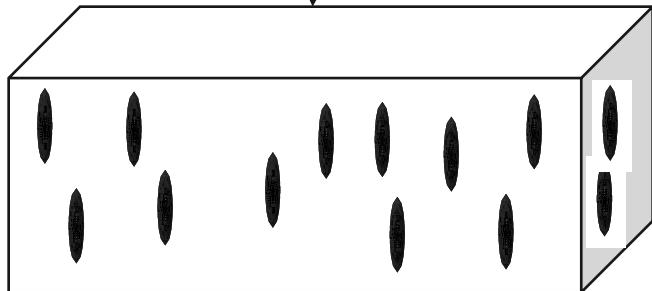
Surface
distributions



$\sim 1.7 \times 10^4 \text{ cm}^2 / \text{cm}^3$

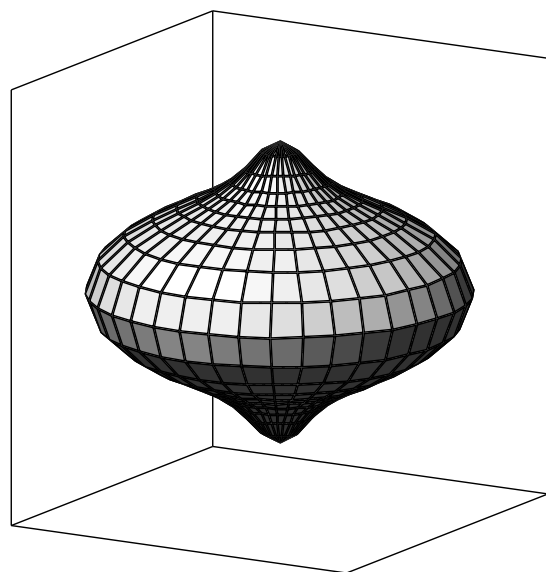
$\sim 0.3 \times 10^4 \text{ cm}^2 / \text{cm}^3$

Real space
(model
shapes)

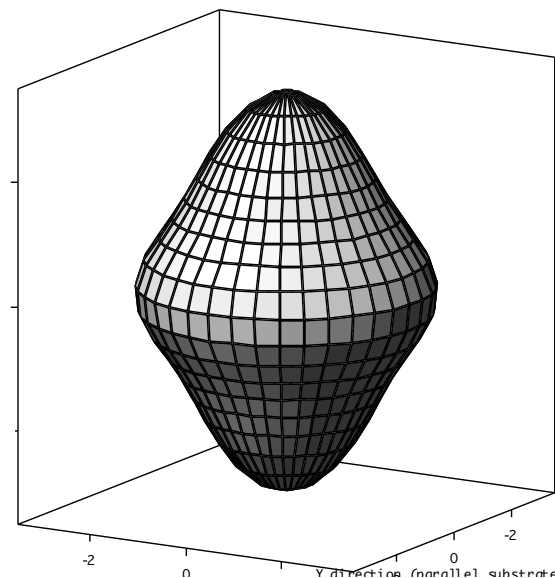


Apparent Porod distribution for Al_2O_3 and YSZ

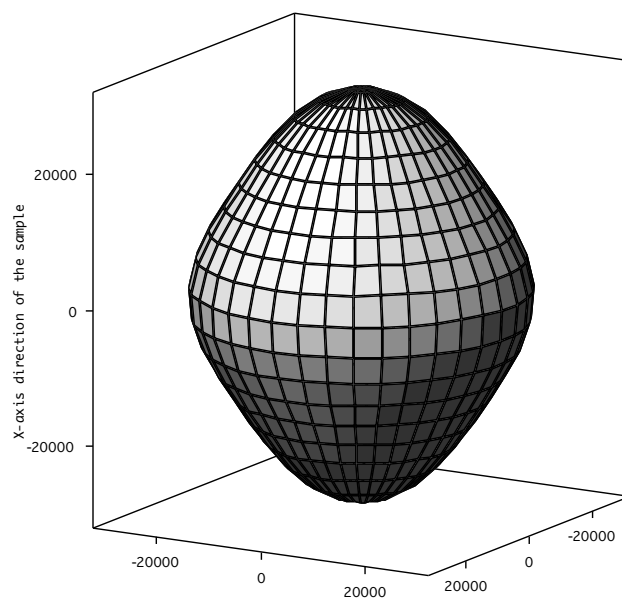
WSP alumina



APS alumina

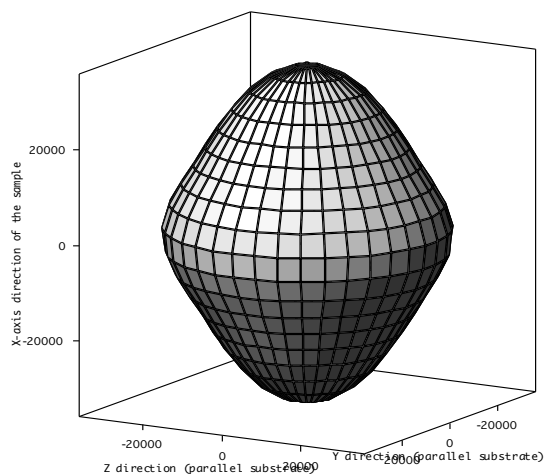


APS YSZ

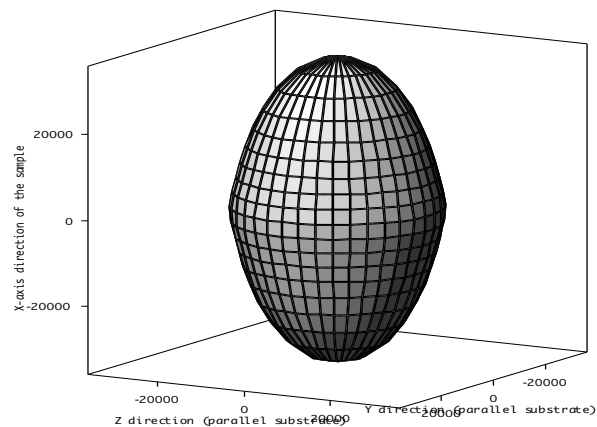


Surface characterization (Porod) Amdry sample

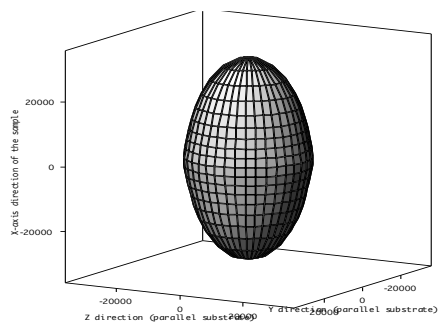
AS SPRAYED



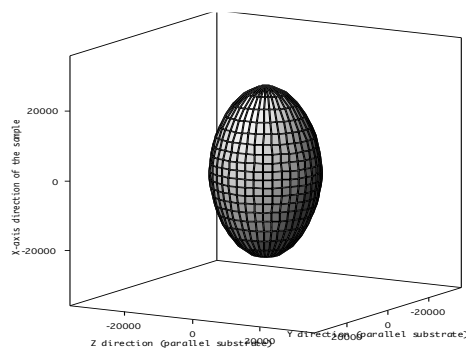
1100C/1h



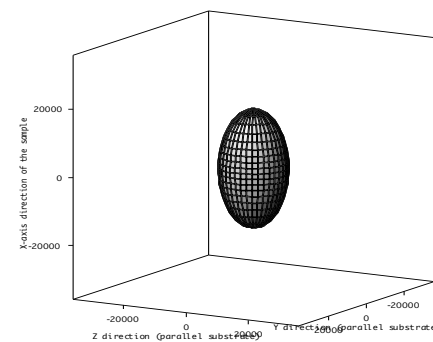
1200C/1h



1300C/1h



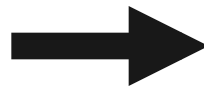
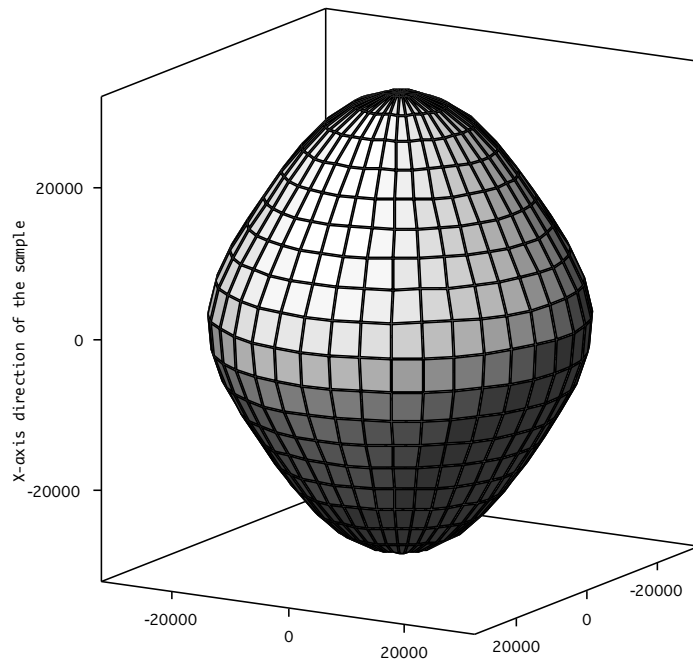
1400C/1h



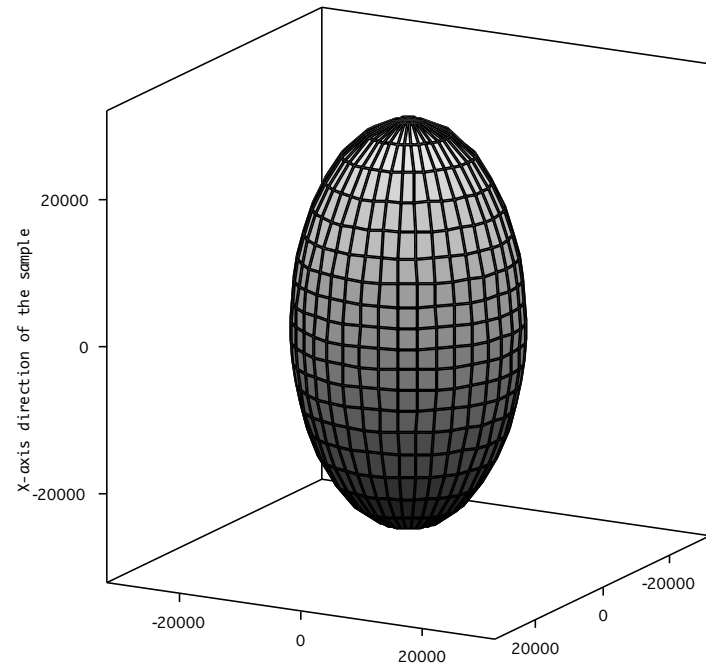
THERMAL SHOCKING & HEAT TREATMENT

~ in service microstructure change

AS SPRAYED

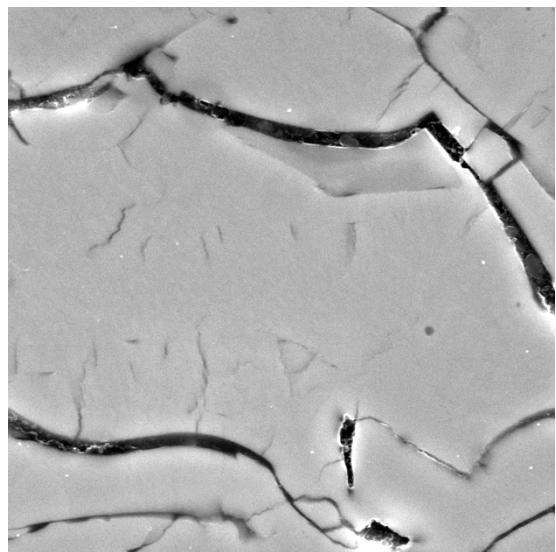


5 x 1100deg. C, 1/2 h,
air cooling

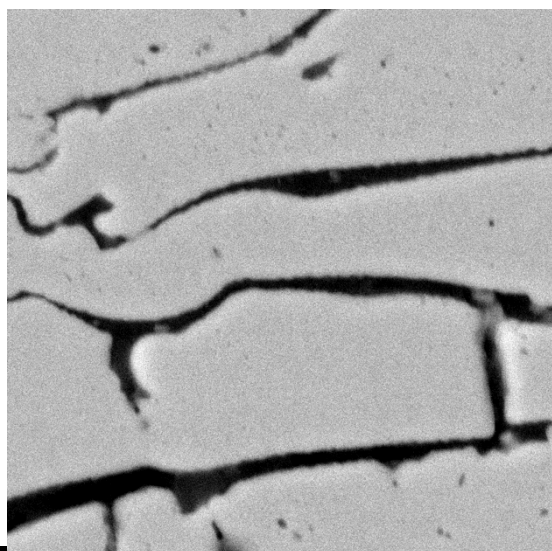
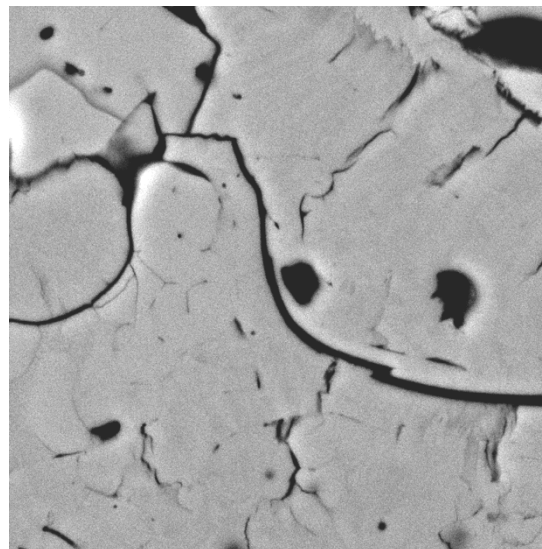


Microstructure comparison

Amdry as sprayed

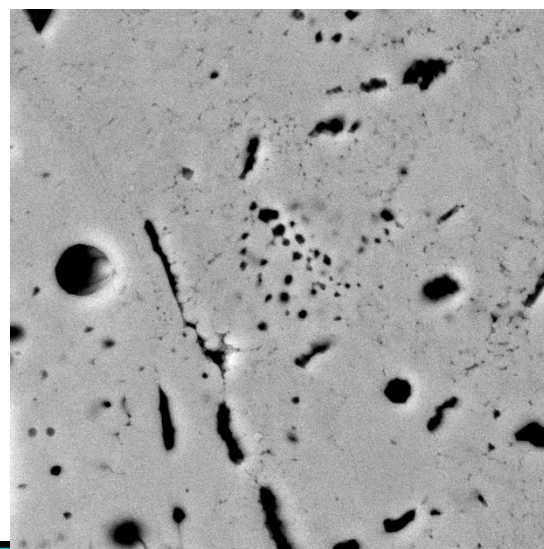


SX233 as sprayed



4 μm

1400C/1hour

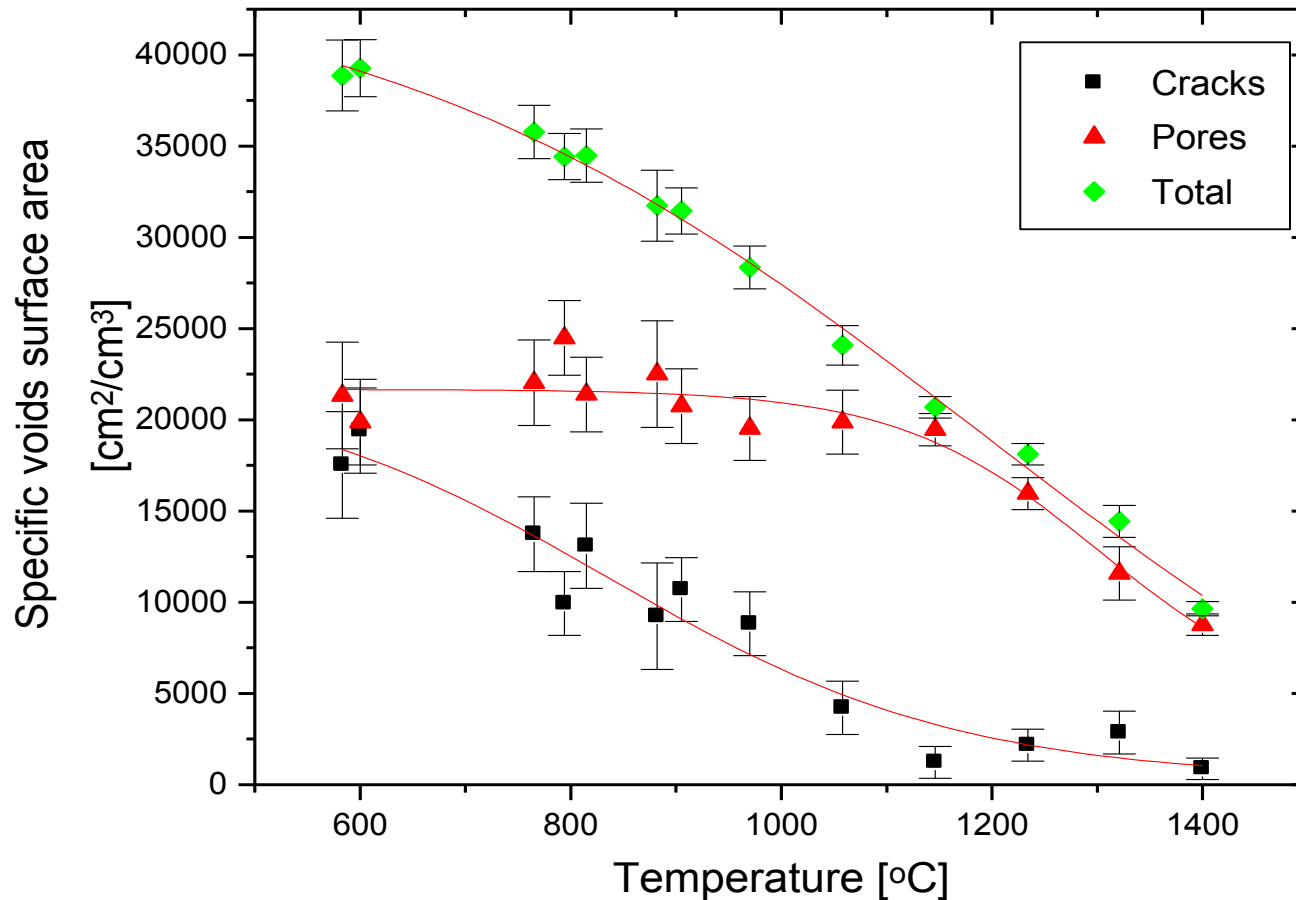


Unique experiment

In-Situ measurement

- Furnace in the sample position
 - up to 1700°C in controlled atmosphere
 - control temperature / time dependence
 - calibrated SANS spectra measured in 5 min to 30 min
- Two experiments:
 - Time dependence @ 1100°C (up to 19 hours)
 - Temperature dependence (heating rate 50°C/h up to 1400°C)
- YSZ sample (8 wt% Yttria in Zirconia)
 - Amdry 142 feedstock powder,
 - Plasma Technik PT F4 system at CTSR, SUNY Stony Brook

Temperature dependence *Specific surface area*

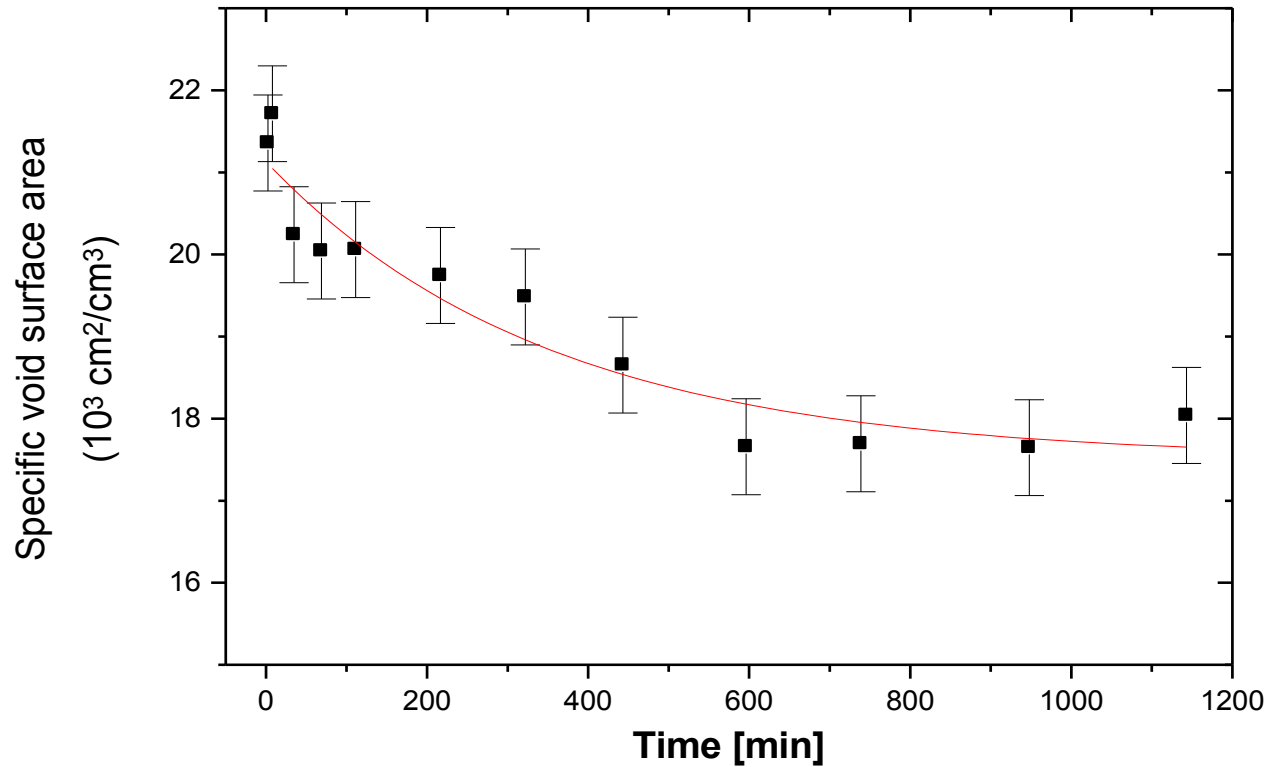


Note:

1. Cracks surface decreases at lower temperatures
2. Pore interlamellar surface decreases at higher temperatures
3. Total surface decreases continuously above 600°C.
(no change between as sprayed conditions and 600°C)

Time dependence Specific surface area

Measured at 1100°C



Note:

1. Total surface area decreases
2. No separation into void systems was possible.

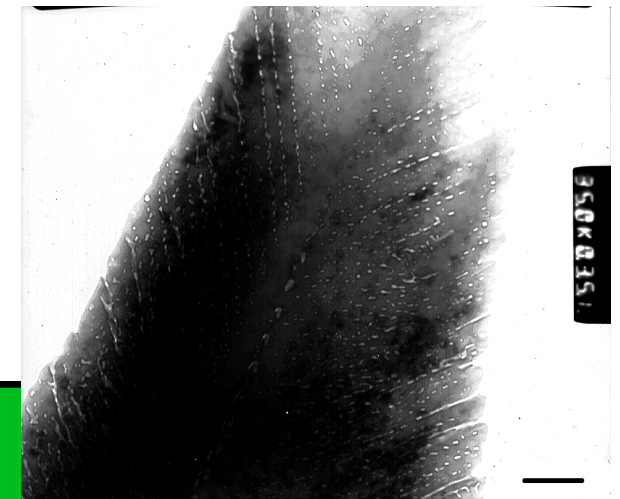
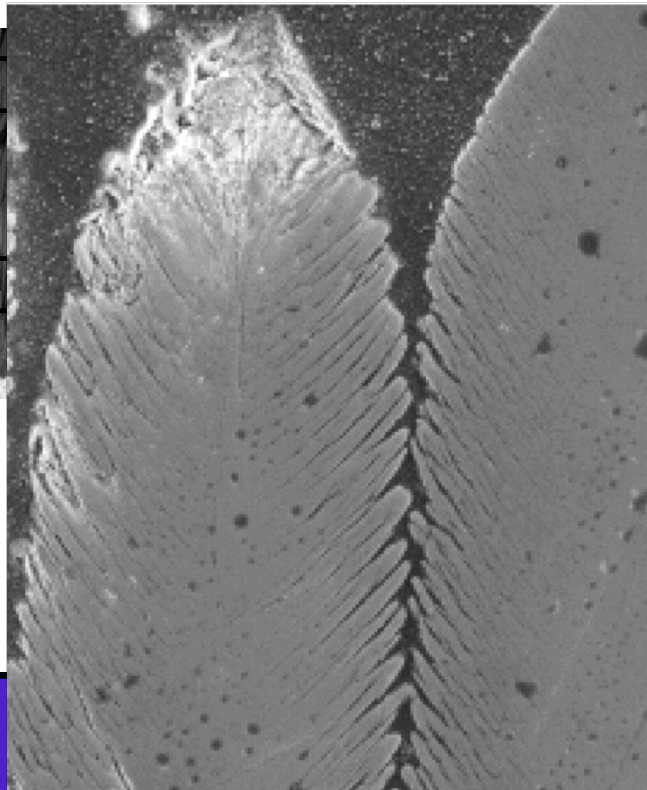
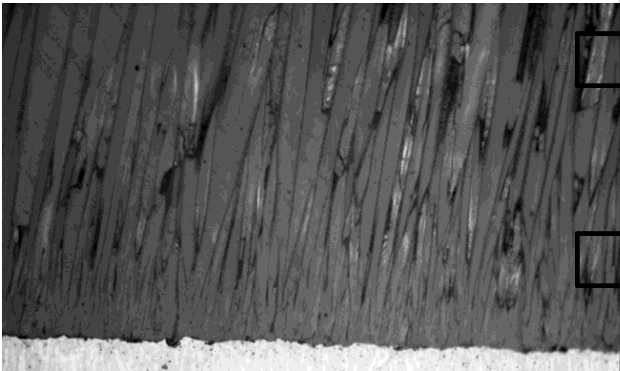
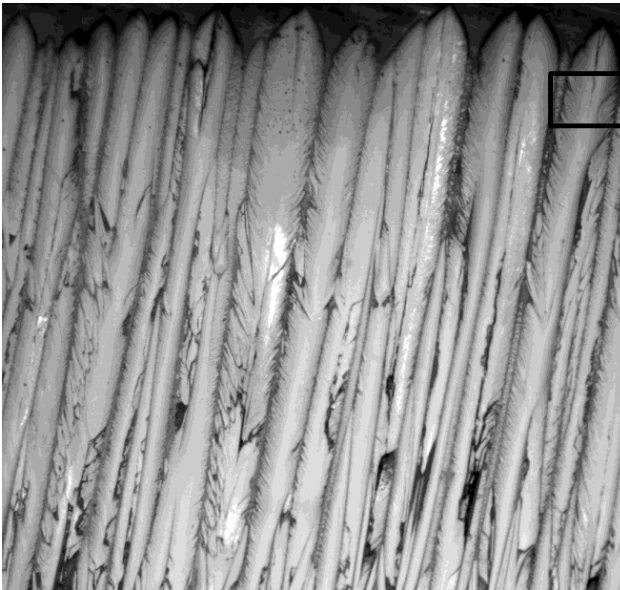
Anisotropic (USAXS) small-angle scattering

Example:

Electron-beam physically vapor deposited coatings

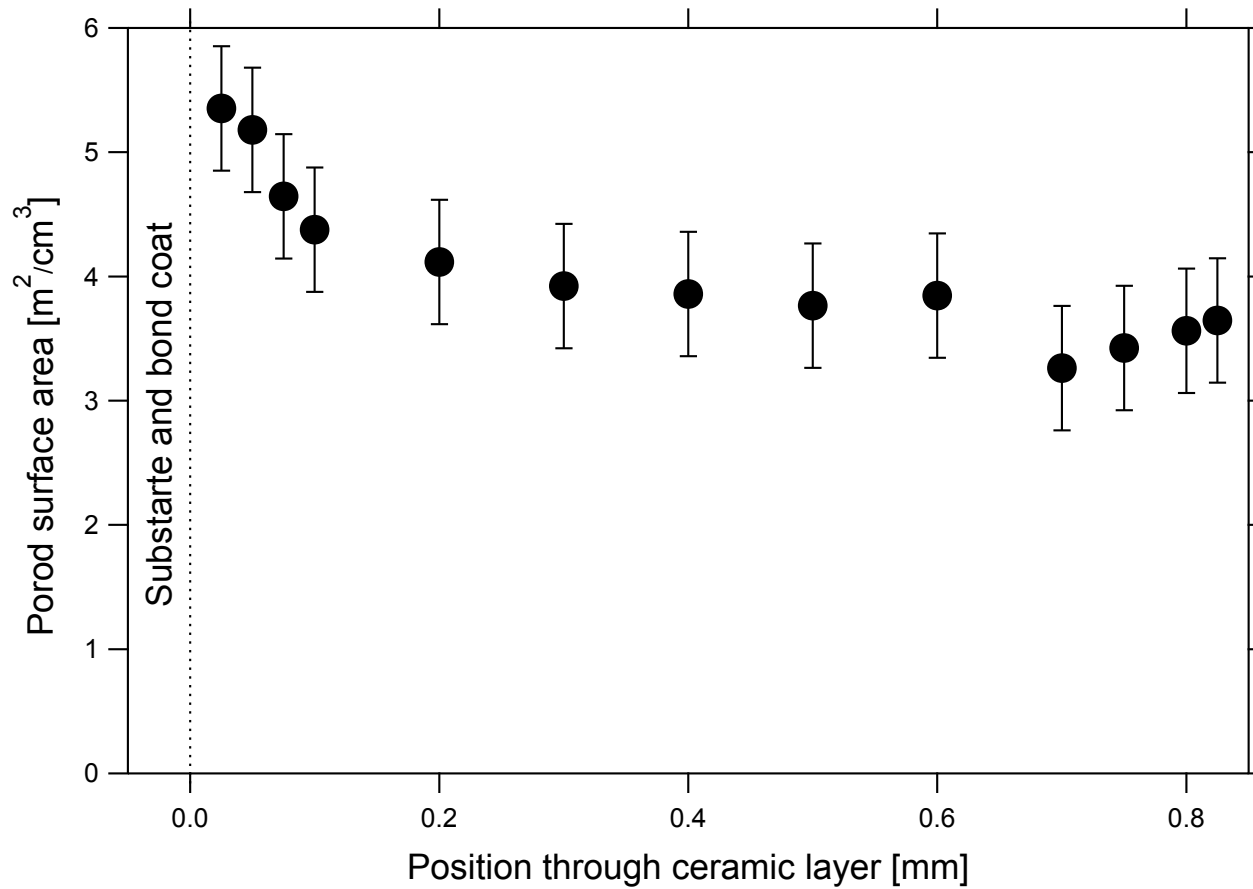
Example of microstructure of EBPVD YSZ thermal barrier coatings

- Columnar structure
- “Feather-like” pores within columns
- Change of microstructure through thickness
- Usual thickness about 400 μm , up to 1 mm
- In service changes – sintering and cracking during thermal cycling



HESAXS

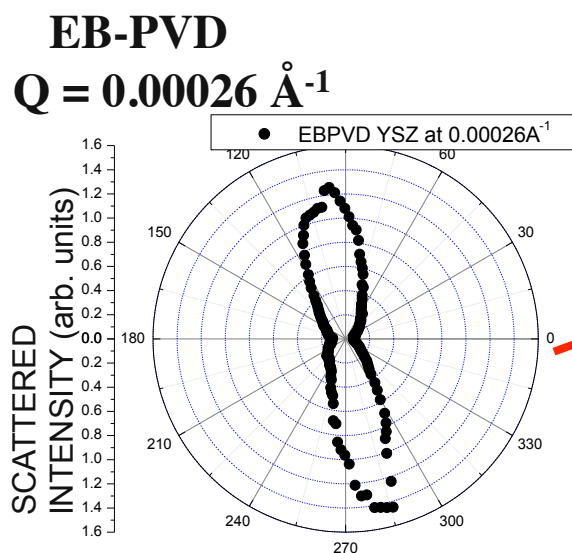
Through thickness porosity surface area variation



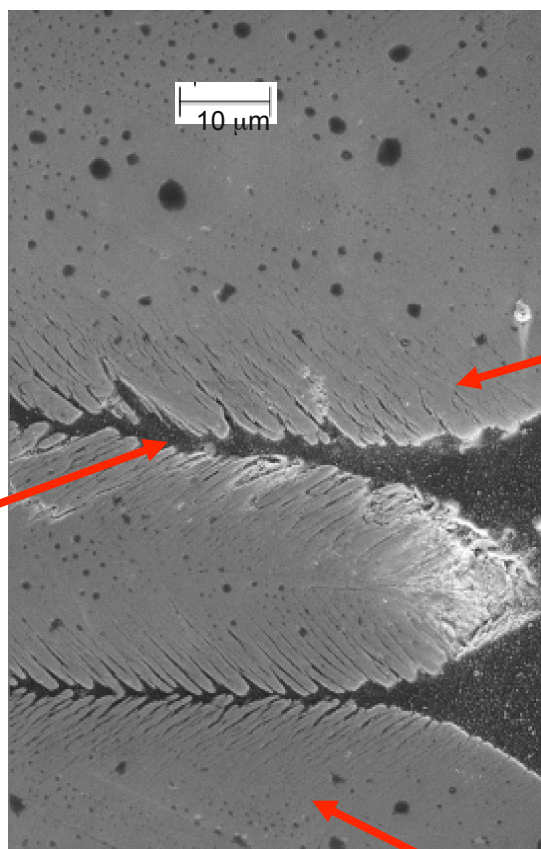
“Aniso SAS” model for USAXS

- USAXS provides wealth of data, not available from other SAS techniques. Especially 2D-collimated on anisotropic samples...
- Developed model for EBPVD coatings, which describes small angle scattering data from anisotropic particles, anisotropically oriented. Features:
 - Up to 5 populations of spheroids
 - Independent size, aspect ratio, contrast, orientation distribution
 - Dilute limit approximation
 - Simplified size distribution assigned to each population
 - Diffraction & refraction accounted for
 - Allows least square fitting of parameters
- Solution must satisfy USAXS data in all directions with reasonable quality

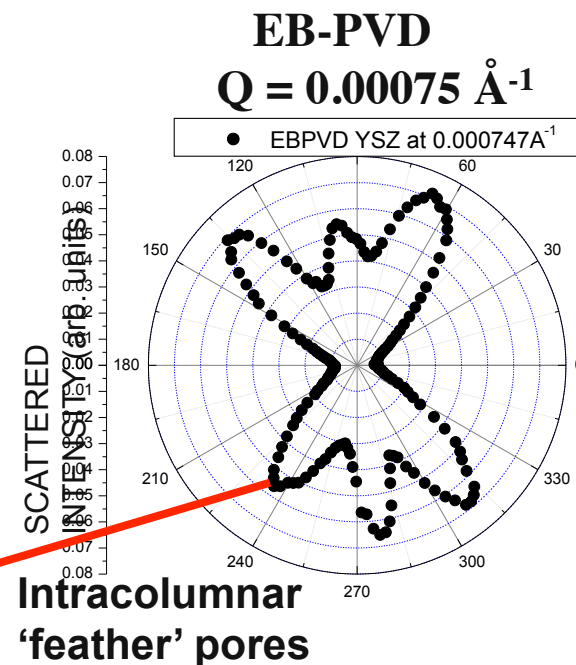
2D collimated USAXS anisotropy at fixed Q



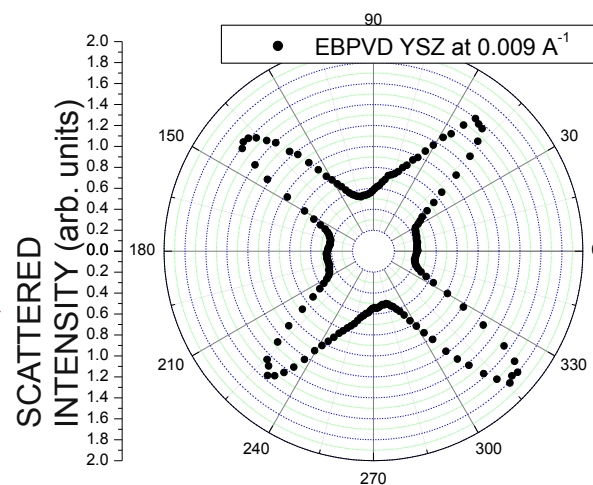
Intercolumnar pores



Intracolumnar Nanometer pores



EB-PVD
 $Q = 0.00902 \text{ \AA}^{-1}$



EB-PVD coatings provided by SUNY-SB via industrial collaboration with Chromalloy Gas Turbine Corporation .

SAS modeling results

TOTAL POROSITY: 22.56 %

(1) INTERCOLUMNAR PORES:

POROSITY: $6.1 \pm 0.6 \%$

<O.D.>: $722 \pm 7 \text{ nm}$

[Aspect Ratio = 0.110, 85° to substrate]

(2) COARSE 'FEATHER' PORES:

POROSITY: $3.9 \pm 0.4 \%$

<O.D.>: $191 \pm 20 \text{ nm}$

[Aspect Ratio = 0.068, 49° to substrate]

(3) FINE nm-PORES:

POROSITY: $3.8 \pm 0.4 \%$

<O.D.>: $33 \pm 4 \text{ nm}$

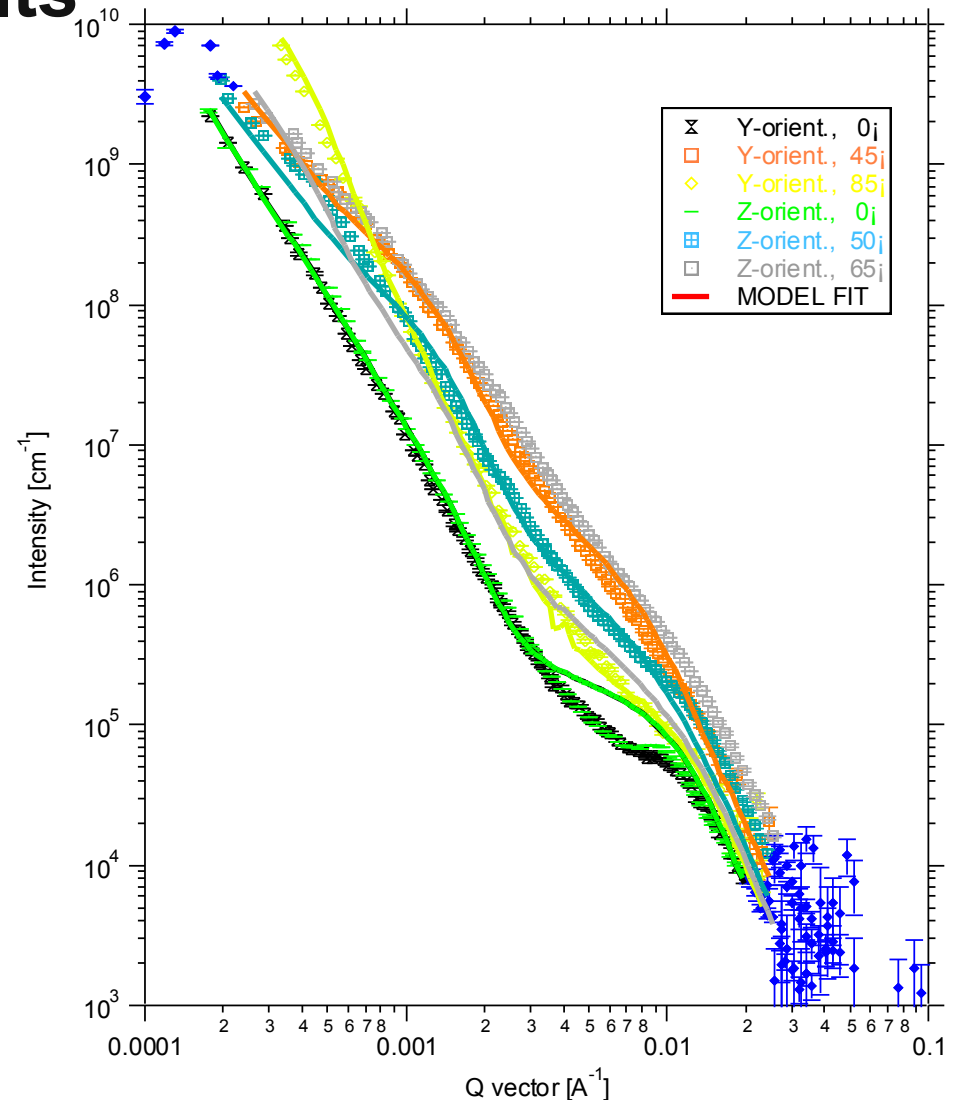
[Aspect Ratio = 0.050, 49° to substrate]

(4) GLOBULAR nm-PORES:

POROSITY: $8.7 \pm 0.9 \%$

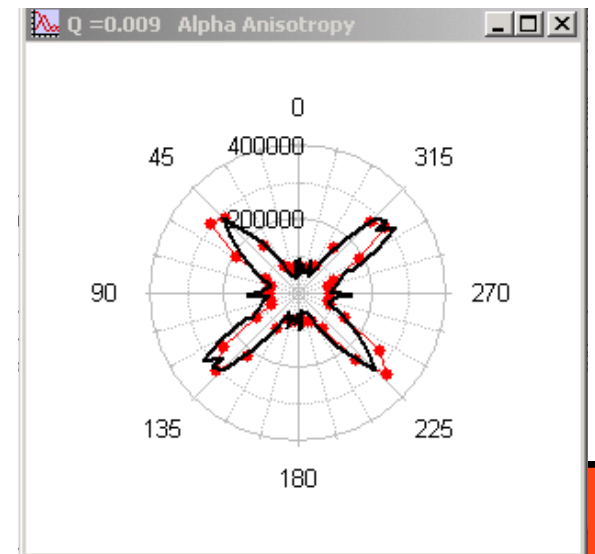
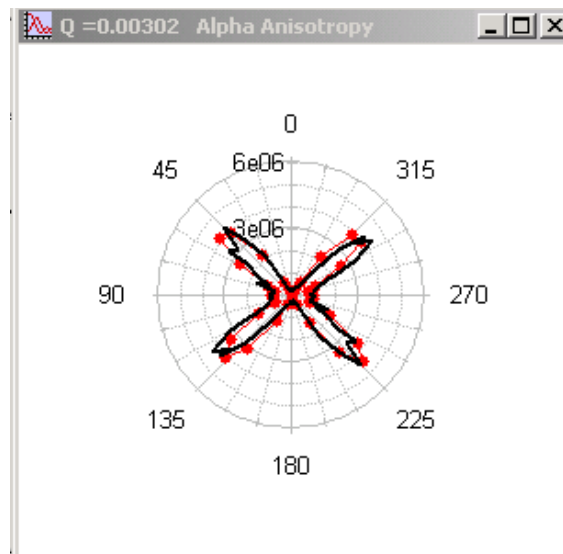
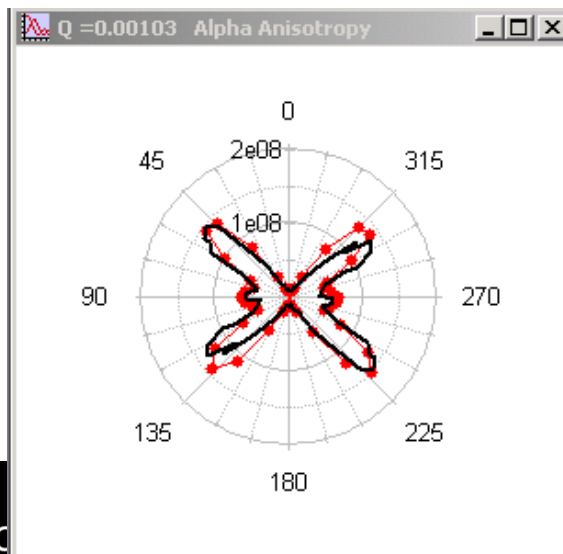
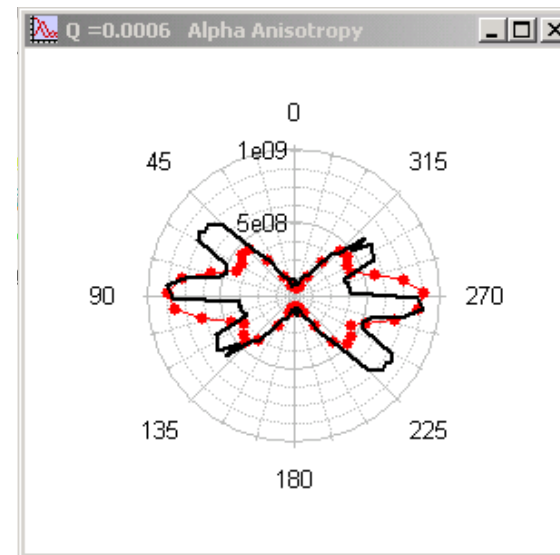
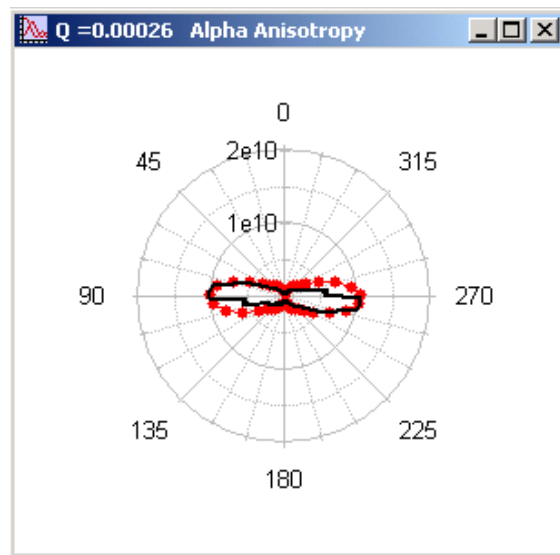
DIAMETER: $39 \pm 4 \text{ nm}$

[MEAN DIMENSIONS =
 $39.1 \times 39.1 \times 27.4 \text{ nm}$]



As-Deposited EBPVD Coating

Anisotropy modeling

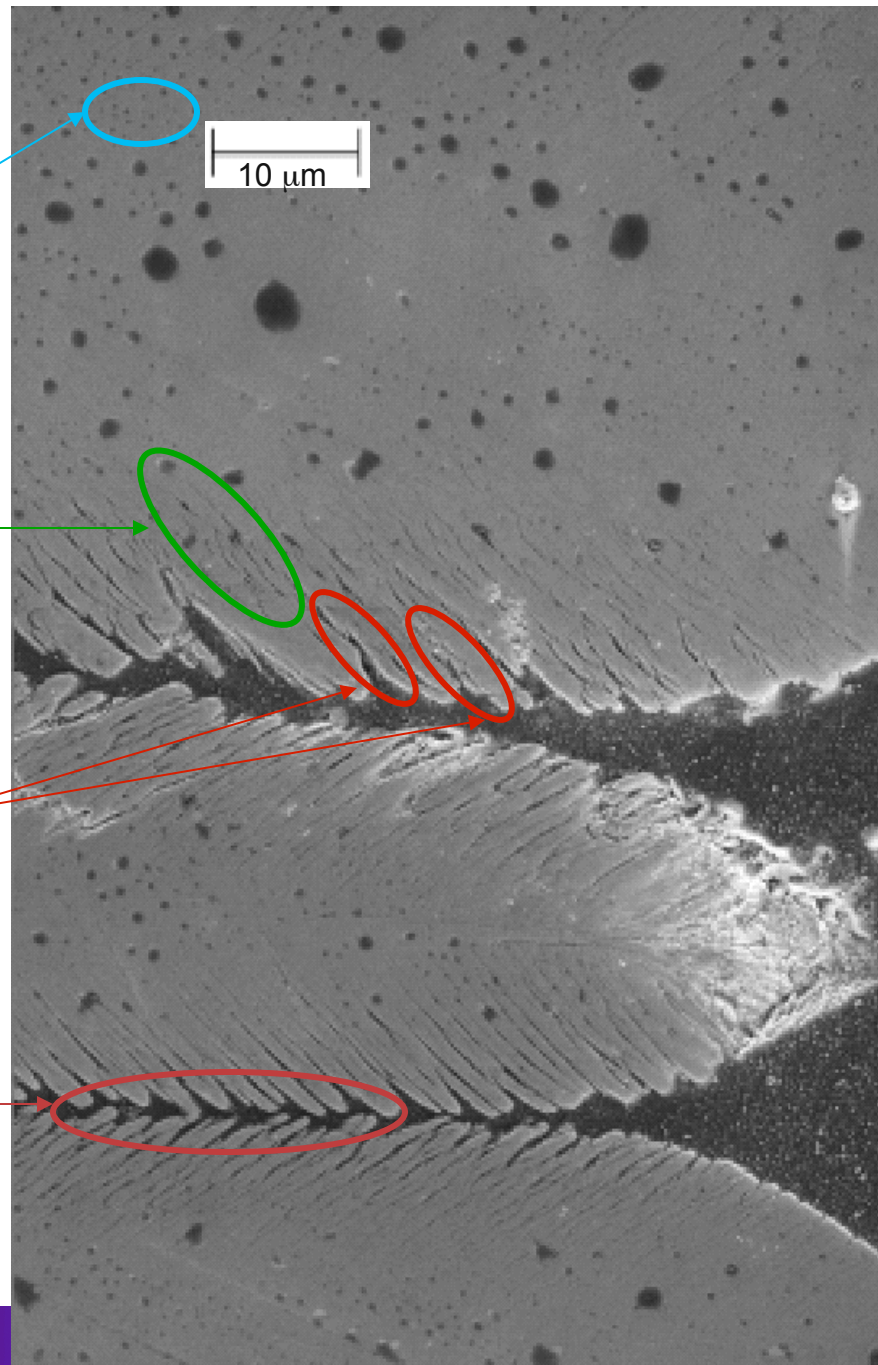


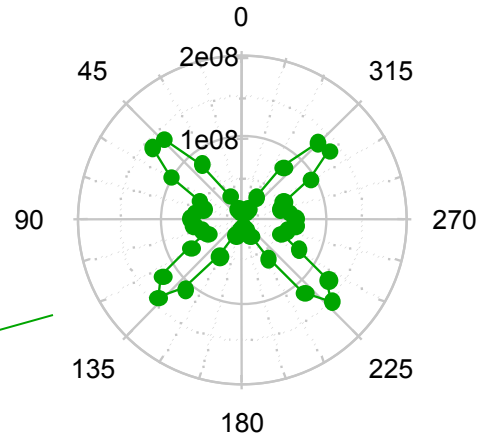
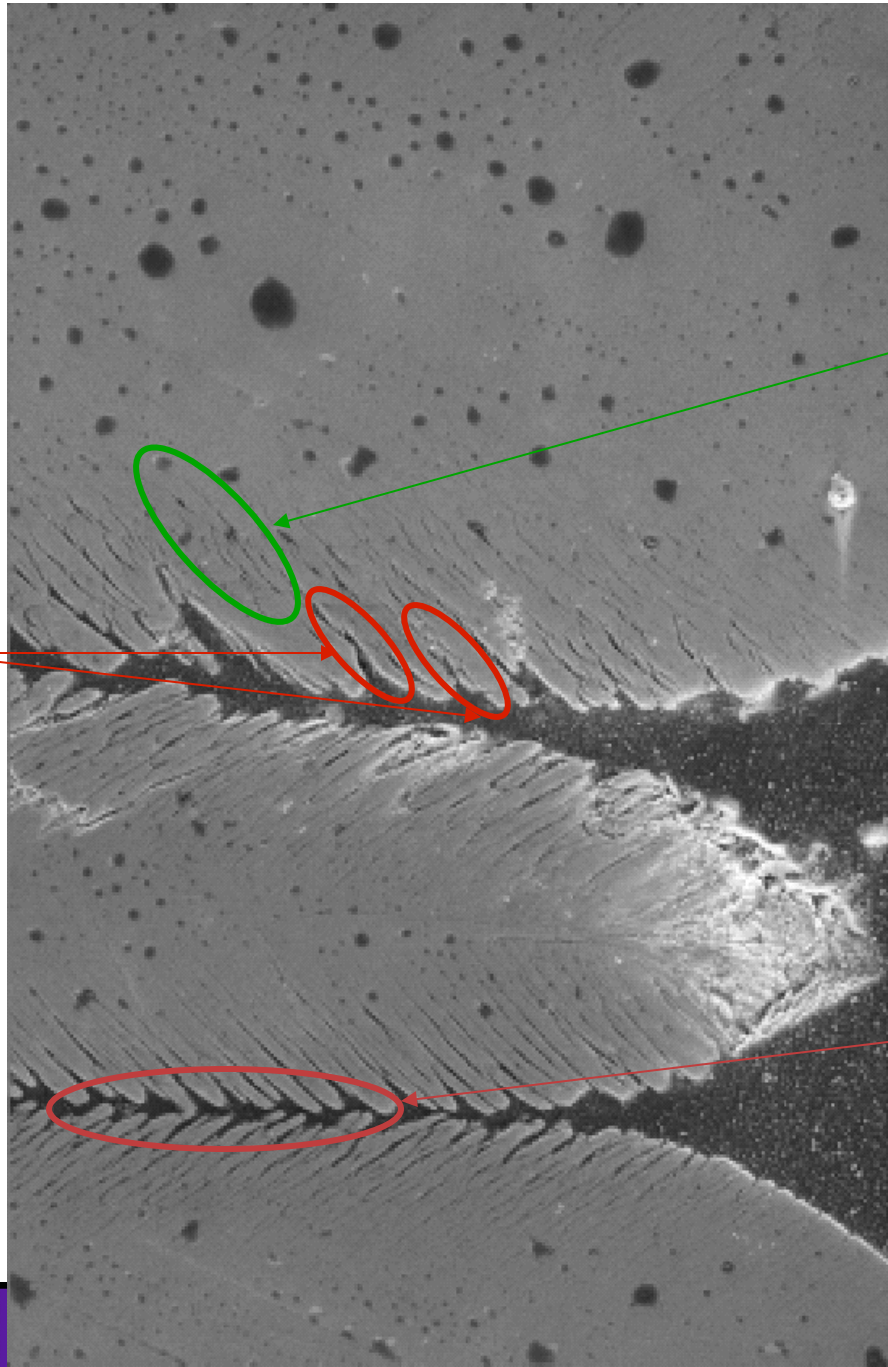
**Population 4:
Nano-
Globular
Voids**
<o.d.>=0.039 μ m
8.7%

**Population 3:
Fine
Intracolumnar
Voids**
<o.d.>=0.033 μ m
3.8%

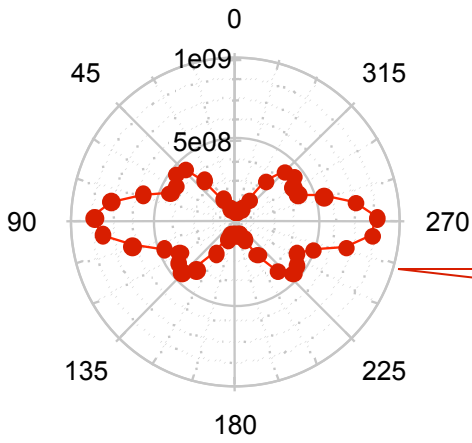
**Population 2:
Coarse
Intracolumnar
Voids**
<o.d.>=0.19 μ m
3.9%

**Population 1:
Intercolumnar
Voids**
<o.d.>=0.72 μ m
6.1%

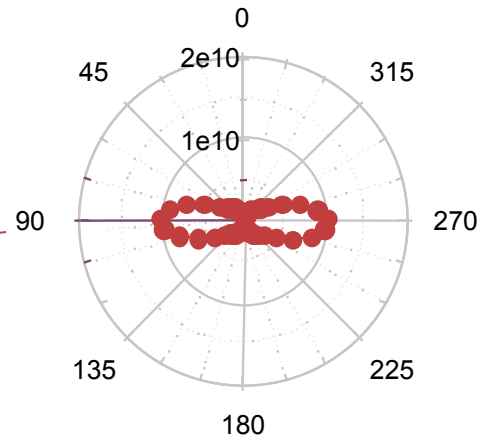




**<o.d.>=0.026
μm
2.1%**

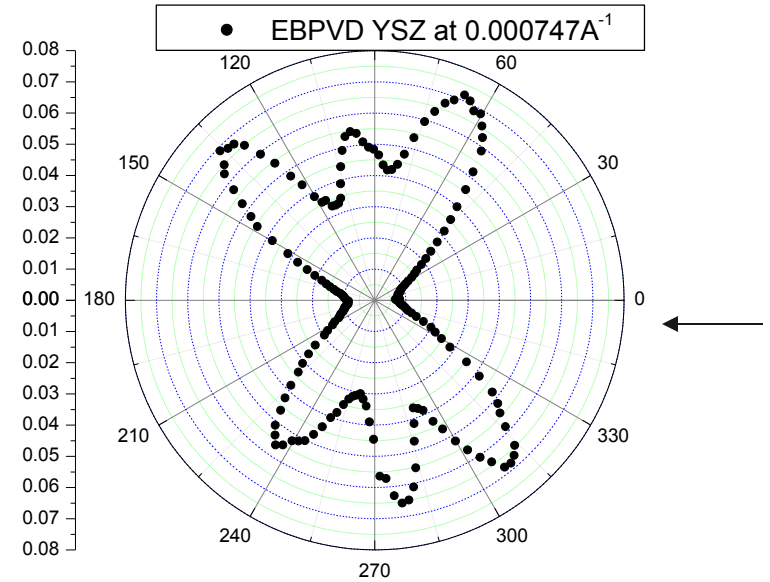
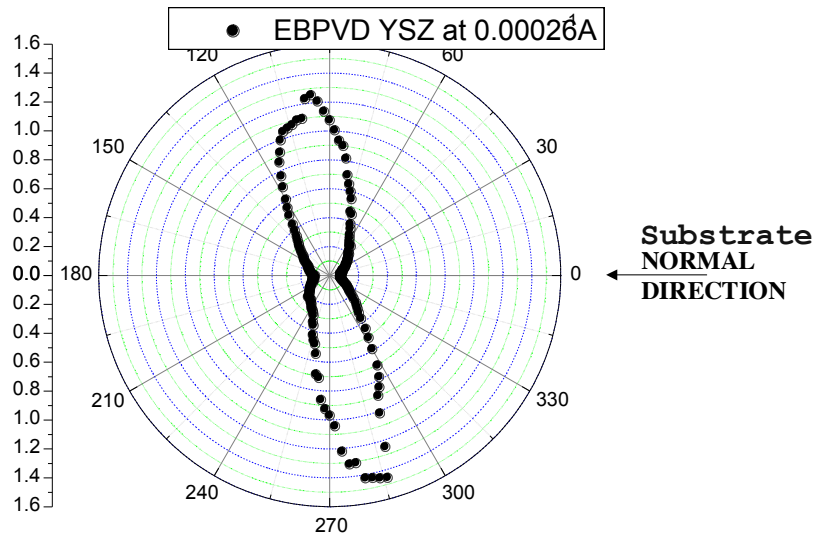


**<o.d.>=0.15 μm
2.8%**

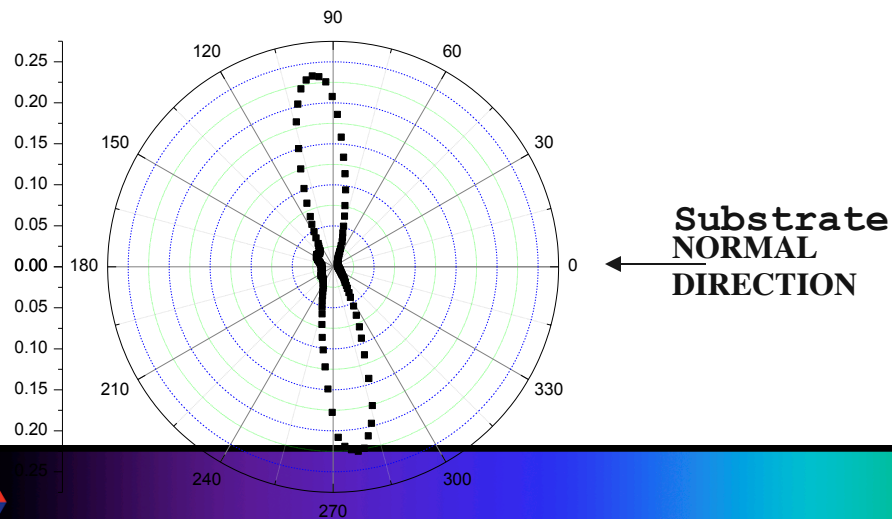


**<o.d.>=0.41
μm
5.3%**

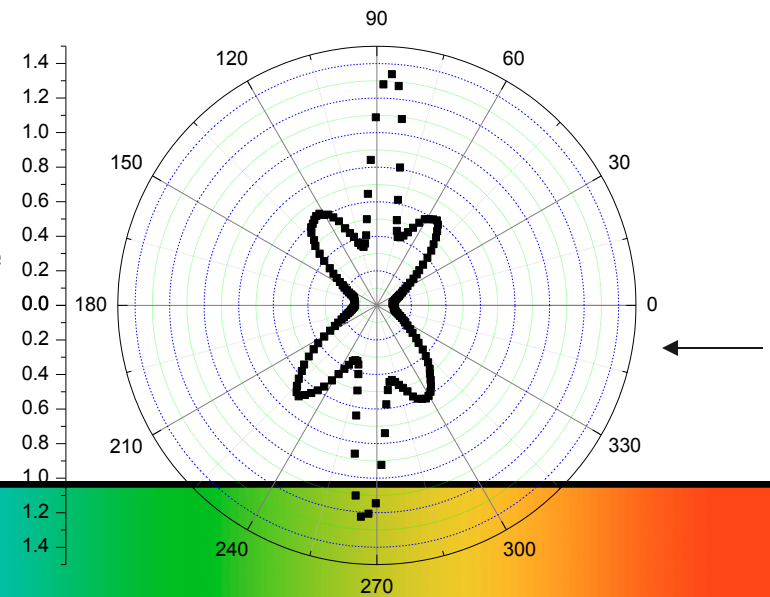
Thermally cycled microstructure shows evolution of different void components in EB-PVD Coatings



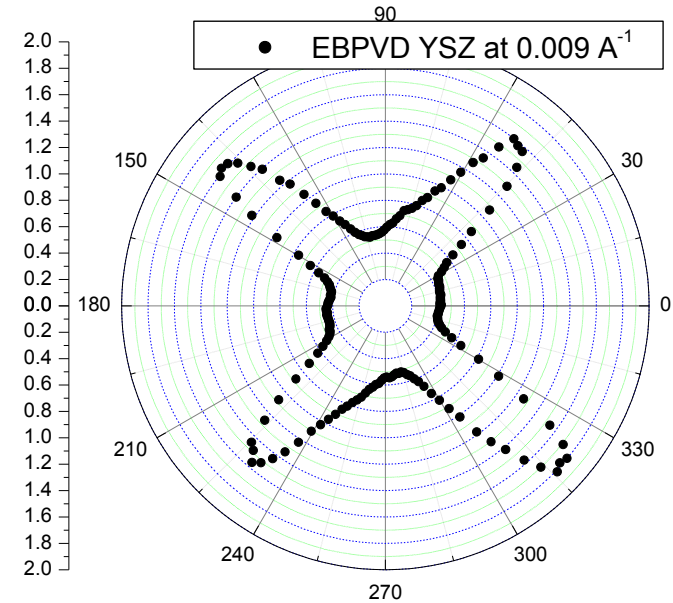
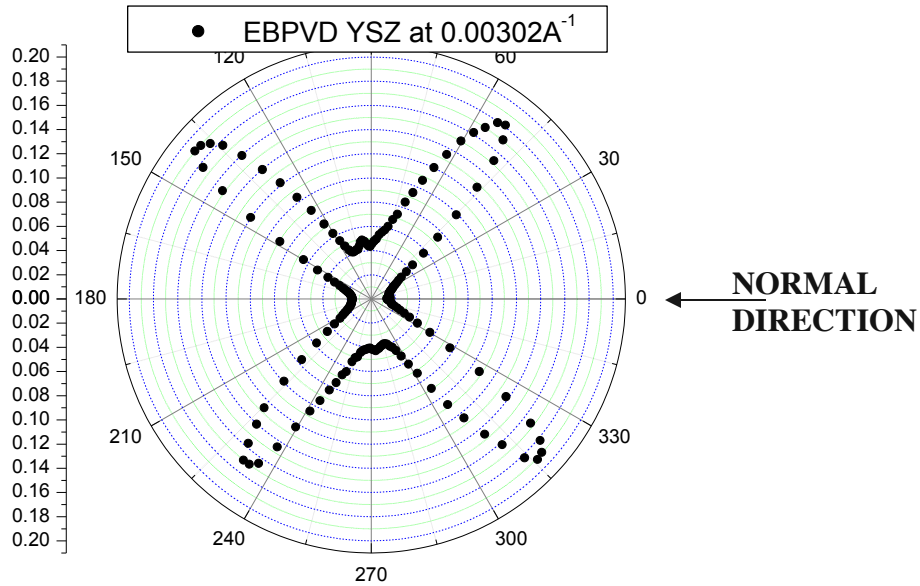
Thermally Cycled 0.00029\AA^{-1}



Thermally Cycled 0.000723\AA^{-1}

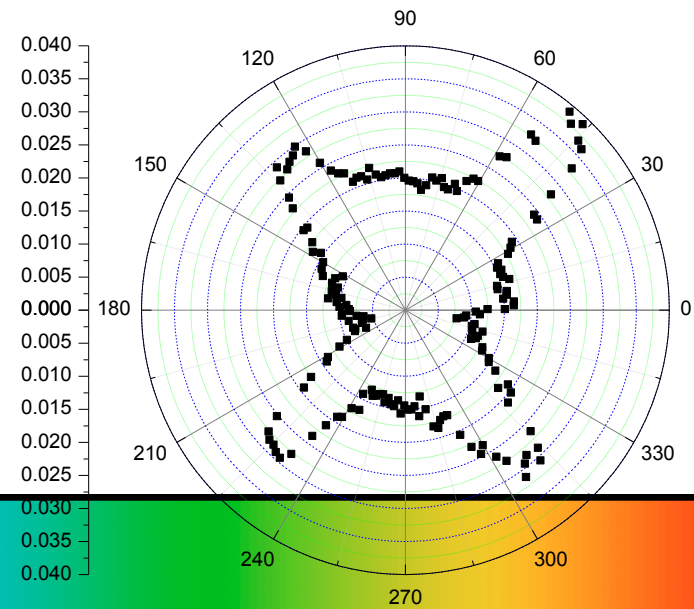
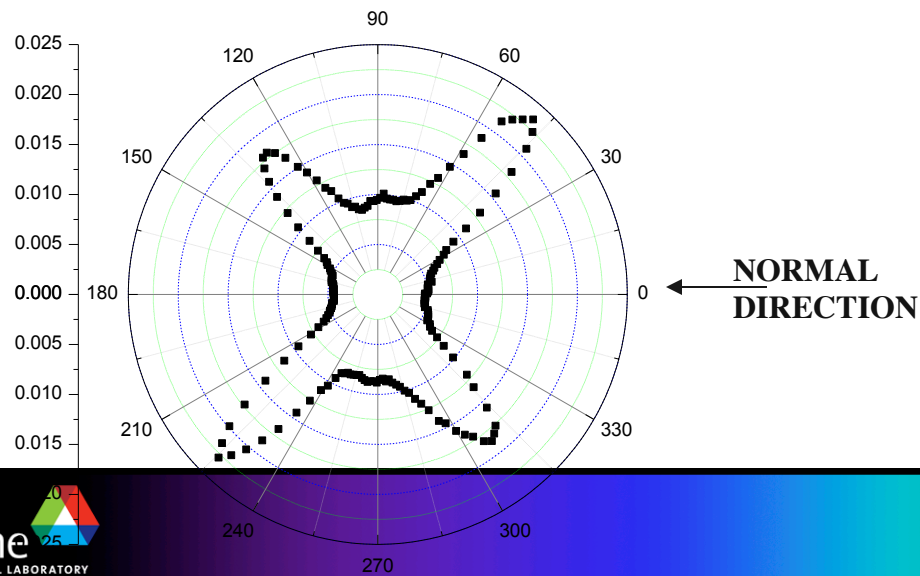


Thermally cycled microstructure shows evolution of void components



Thermally Cycled 0.00302 A^{-1}

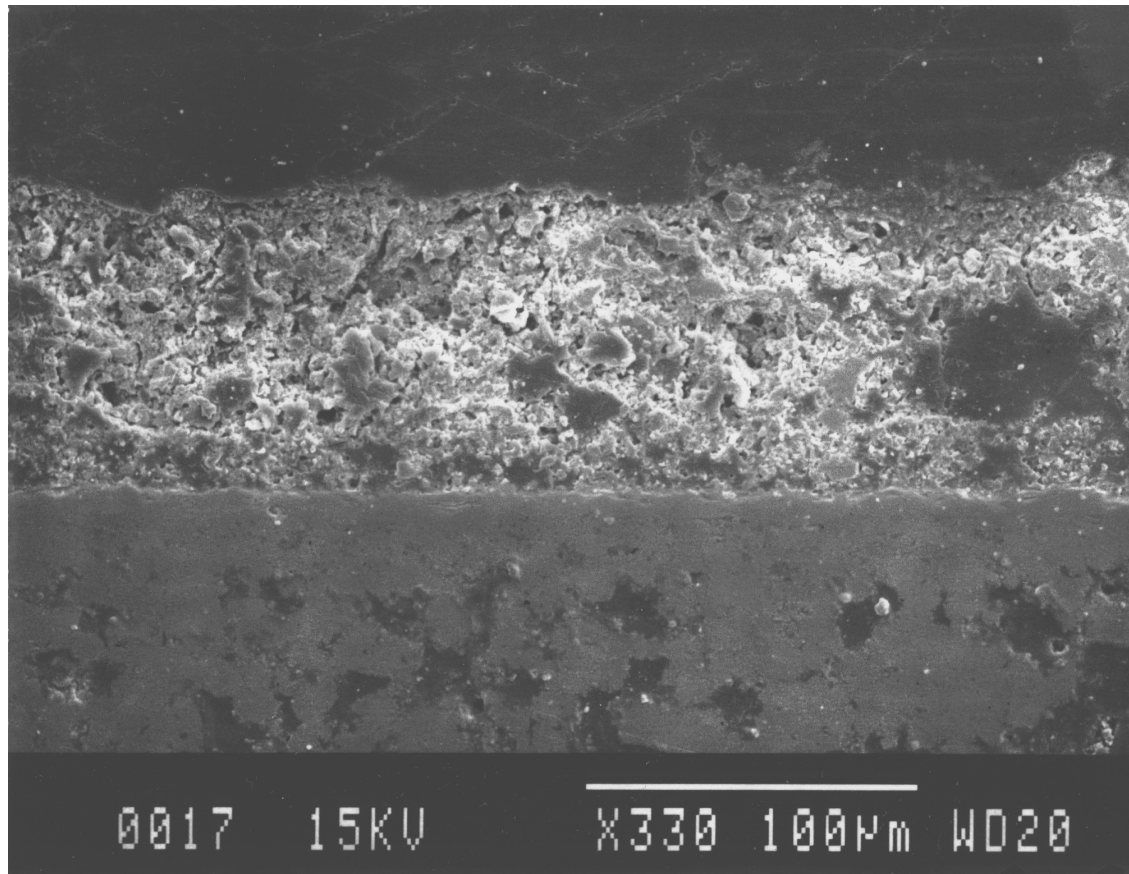
Thermally Cycled 0.00914 A^{-1}



Local area SAXS

Solid oxide fuel cells

Solid oxide fuel cell microstructures

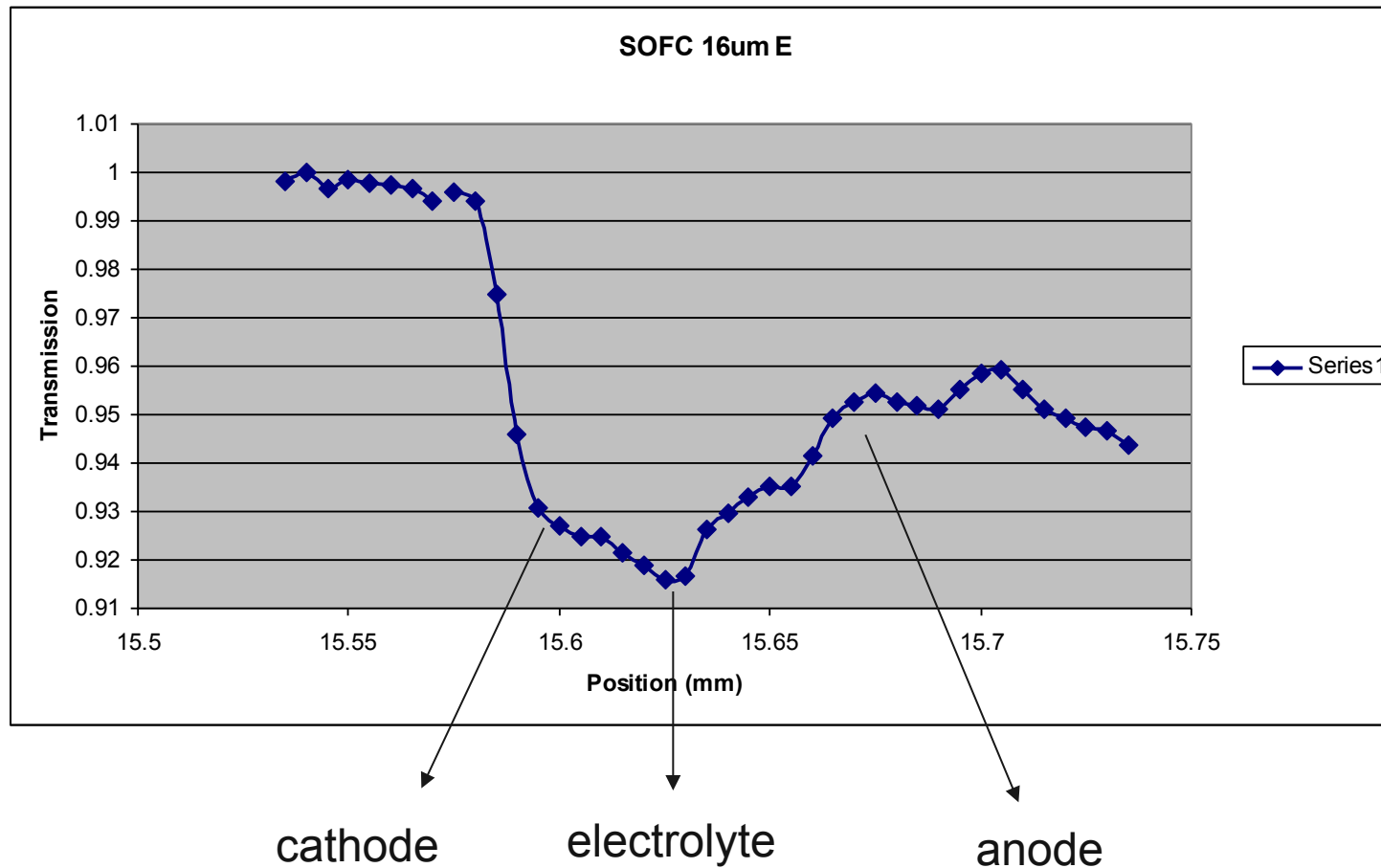


Layered structure

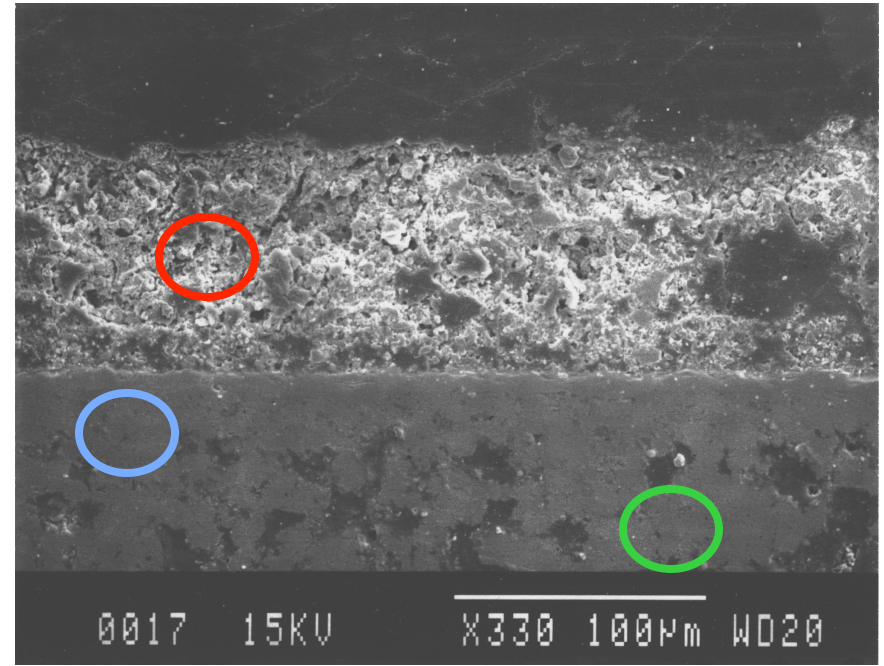
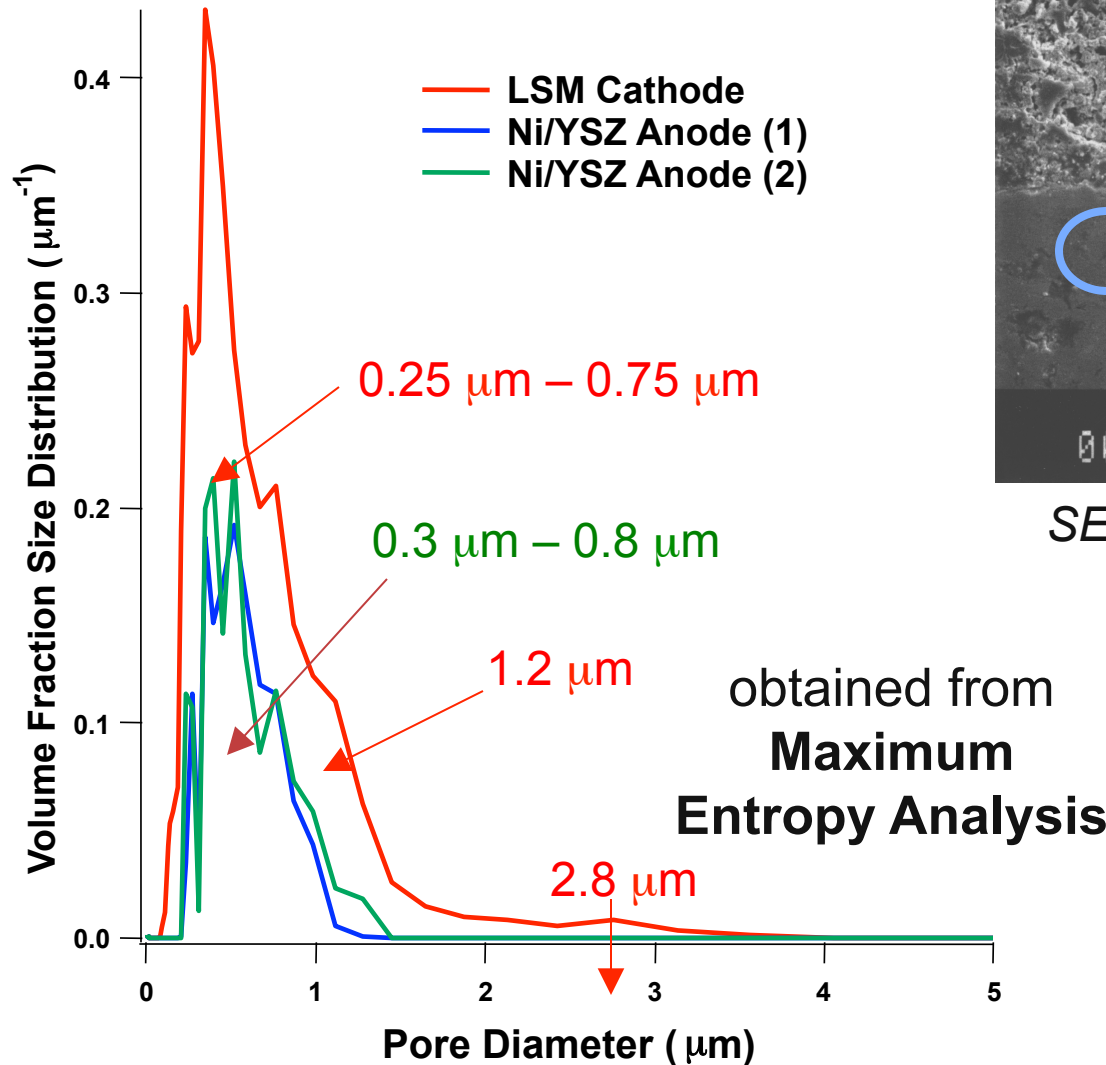
- Top (cathode) porous and fragile
- Thin layer of electrolyte
- Lower (anode) layer - porous

HESAXS - transmission

- Various Fuel cell materials available
- This one has 16 micron electrolyte
- Transmission results with 5 μm spatial probe:



Void Size Distributions 2-D collimated USAXS



SEM micrograph near interfaces.

Volume Fractions (%):

Cathode: 24.6

Anode (1): 10.0

Anode (2): 10.5

Surface Areas ($\text{m}^2 \text{cm}^{-3}$):

Cathode: 3.39 ± 0.01

Anode (1): 1.06 ± 0.01

Anode (2): 1.20 ± 0.01

Small Angle X-Ray Scattering From Nanoporous Biocarbon

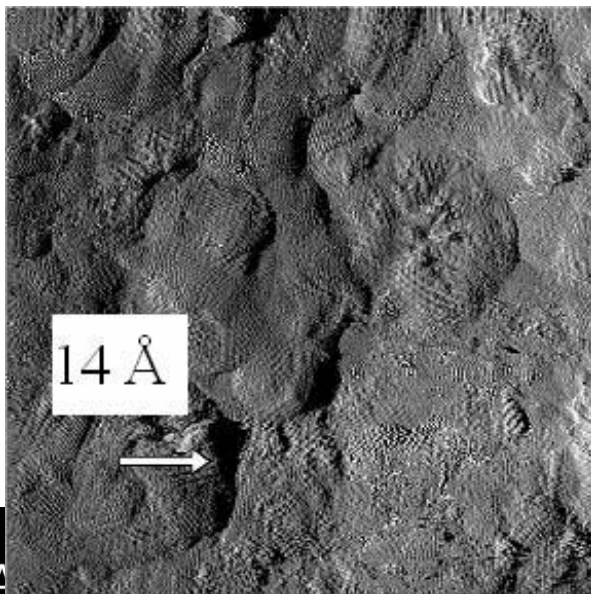
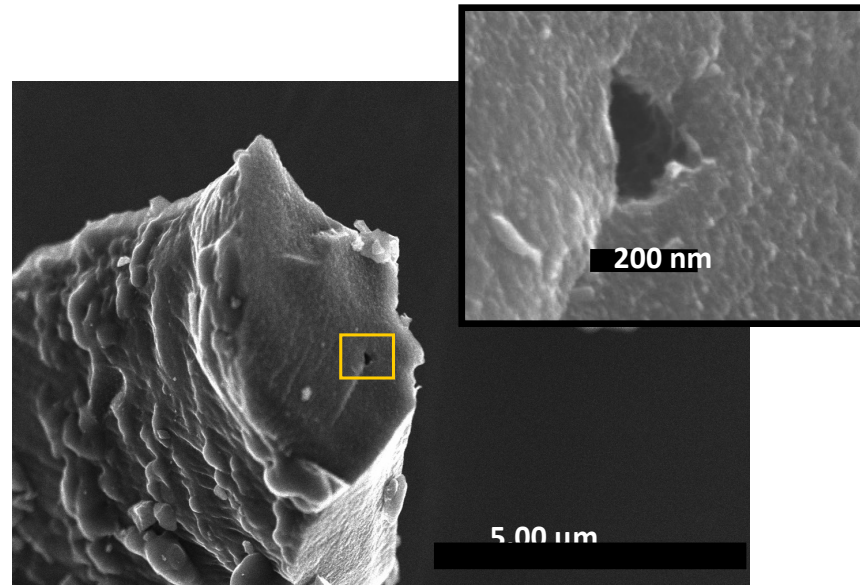
Mikael Wood, Jacob Burress, Jeff Pobst, Sarah Carter, Peter Pfeifer, and Carlos Wexler

Department of Physics and Astronomy, University of Missouri-Columbia



ALL-CRAFT

•As a member of the Alliance for Collaborative Research in Alternative Fuel Technology (ALL-CRAFT) our research group studies the properties of powdered and monolithic nanoporous biocarbon produced from waste corn cob, with the goal of achieving the 2010 DOE gravimetric and volumetric targets for vehicular hydrogen (H_2) and methane (CH_4) storage.



- Pore structure of carbon analyzed via Small Angle X-ray Scattering (SAXS), nitrogen and methane adsorption, and Scanning Electron Microscopy (SEM)
- ALL-CRAFT is based on the 2002 discovery by Pfeifer *et al.* of carbons crisscrossed by a nearly space-filling network of channels 1.5 nm wide.

Gas Storage

	77K, 47 bar	300K, 47 bar
S-33/k Hiden	7.9 mass%	1.2 mass%
S-33/k Pfeifer	7.3 – 9.1 mass%	1.0 -1.2 mass%
S-33/k Parilla	~8 mass%	1.4 – 1.6 mass%
AX-21 [®] (*)	5.1 mass%	.6 mass%
MOF-177 (**)	~10 mass%	2.4 mass%

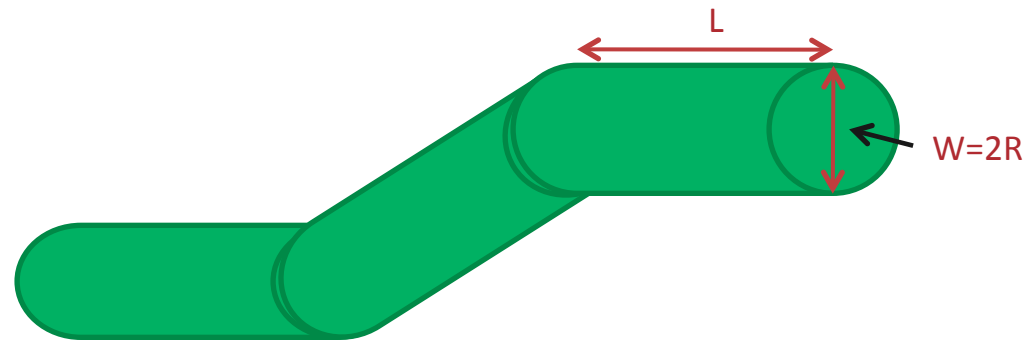
Hydrogen Uptake

Methane Uptake

•As can be seen our uptake values are quite good. We are one of the best performers for hydrogen storage and we have achieved the DOE's target for methane storage.

	ALL-CRAFT Best Performance S-33/k	ANG DOE Target
M/M	230-239 g/kg	N/A
M/V	115-119 g/L	118 g/L
V/V	176-182 L/L	180 L/L

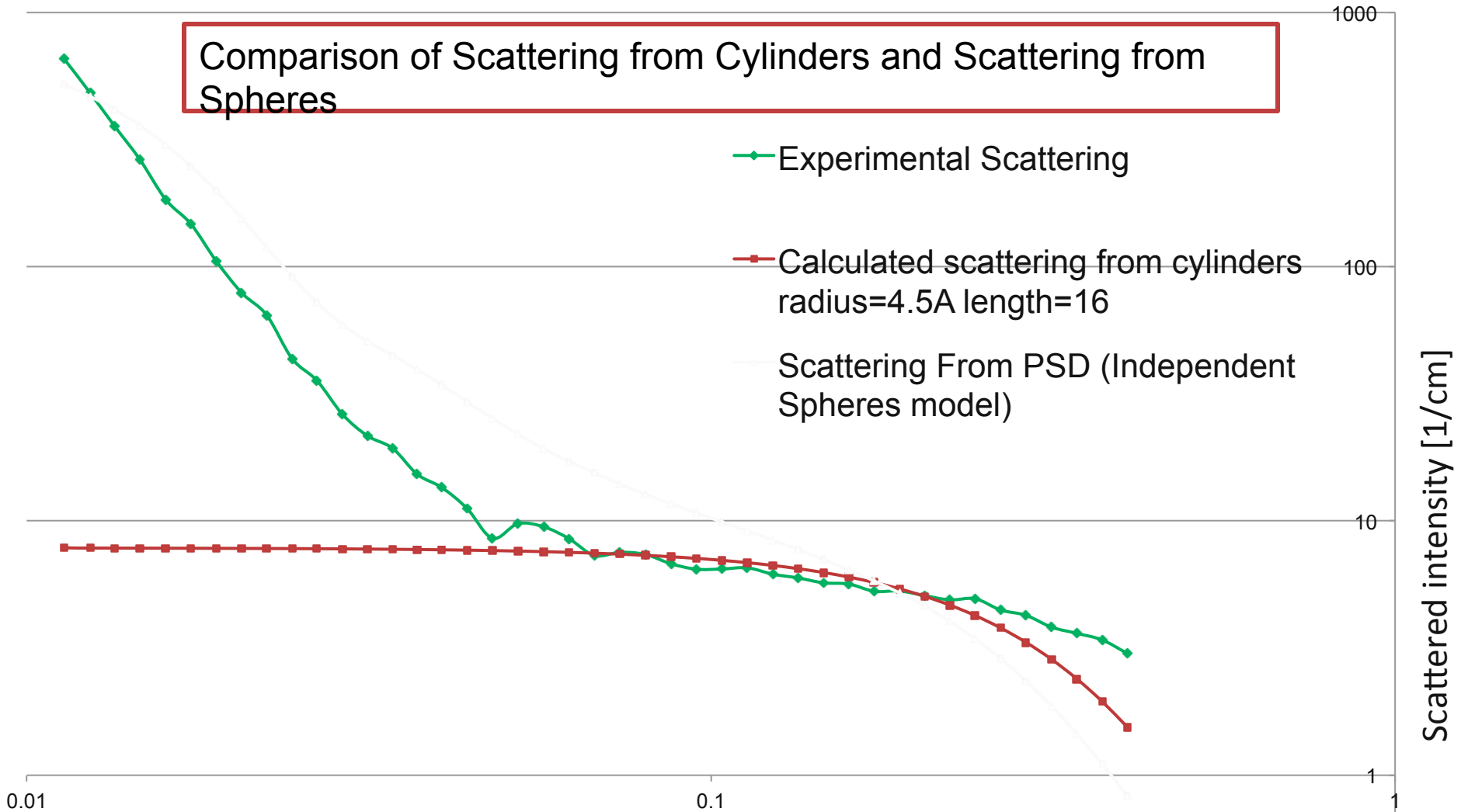
Two Phase Approximation: Single Cylinders



•We now wish to examine the scattering from cylindrical pores. The figure above illustrates (roughly) what we imagine to be happening in our pore space. As we have seen spherical pores are not always a good model for what is happening in our pore space. One reason for this is that spheres have only one characteristic length scale, the radius of the sphere. If instead we imagine our pores to be cylindrical we can attempt to find a characteristic length over which pores of a given radius persist (the so called “persistence length”). For now we will consider scattering from independent cylinders. That is to say, we will ignore the interference term between cylinders. Later we will qualitatively look at the interference term and its implications.

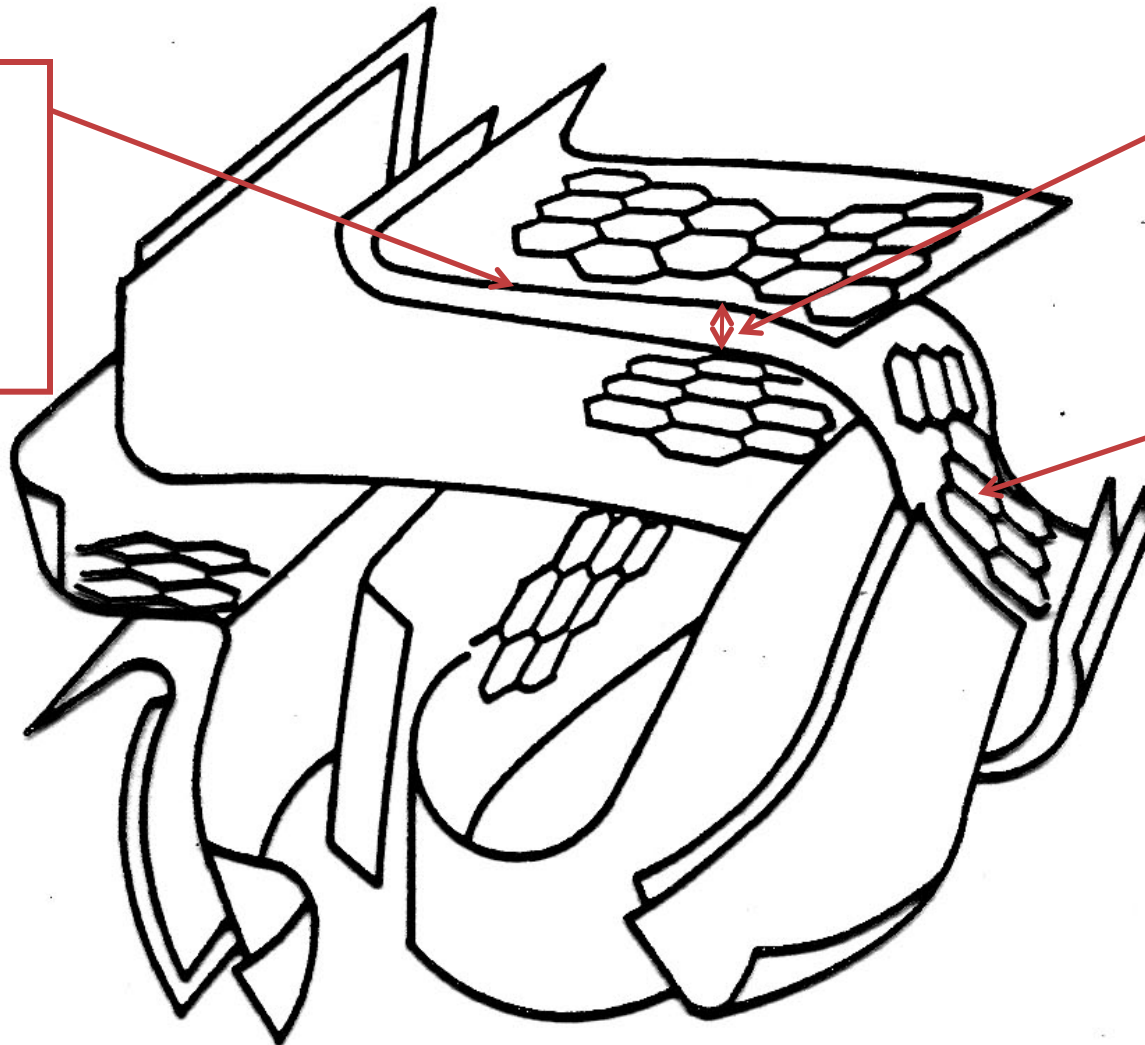
Comparison of Scattering from Cylinders and Scattering from Spheres

- Experimental Scattering
- Calculated scattering from cylinders
radius=4.5Å length=16
- Scattering From PSD (Independent Spheres model)



Structure of Activated Carbon

Graphitic layer edge. This is where dopants can bind to provide further gas storage.



Pore

Graphitic Layer

Outline

- Small-Angle Scattering Primer
- Quantitative Small-Angle Scattering
- Instrumentation
- Examples
- Summary

Wrap up

- SAS investigations measure nanoscale microstructure
- Many different materials of technological importance can be investigated
- Contrast variation methods possible
- Statistically significant results
- Unique results not obtainable by other methods
- Complementary methods increase the information content which can be realized from a quantitative SAS investigation



Resources

■ Organizations

- IUCr SAS <http://www.iucr.org/iucr-top/iucr/csas.html>
- ANL SAS SIG <http://small-angle.anl.gov>
- USAXS <http://usaxs.aps.anl.gov>

■ References

- *Small-Angle Scattering of X-rays*, André Guinier and Gérard Fournet, John Wiley & Sons, New York, 1955
- *Small-Angle X-ray Scattering*, H. Brumberger, Gordon and Breach, Syracuse University, 1965
- *Small-Angle X-ray Scattering*, Otto Glatter and O. Kratky, Academic Press, London, 1982
- *Neutron, X-ray and Light Scattering: Introduction to an Investigative Tool for Colloidal and Polymeric Systems*, European Workshop on Neutron, X-ray and Light Scattering as an Investigative Tool for Colloidal and Polymeric Systems, edited by Peter Lindner and Thomas Zemb, Bombannes, France, 1990 (North-Holland, Amsterdam)
- *Modern Aspects of Small-Angle Scattering*, NATO Advanced Study Institute on Modern Aspects of Small-Angle Scattering, Vol. C451, edited by Harry Brumberger, Como, Italy, 1993 (Kluwer Academic Publishers, Dordrecht)
- **Ryong-Joon Roe, Methods of X-ray and neutron scattering in Polymer science**